NASA/TM-2003-212441

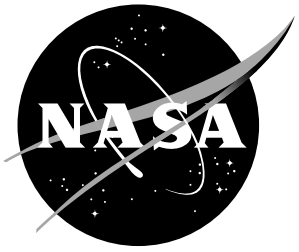

Structured Uncertainty Bound Determination From Data for Control and Performance Validation

Kyong B. Lim
Langley Research Center, Hampton, Virginia

August 2003

The NASA STI Program Office ... in Profile

Since its founding, NASA has been dedicated to the advancement of aeronautics and space science. The NASA Scientific and Technical Information (STI) Program Office plays a key part in helping NASA maintain this important role.

The NASA STI Program Office is operated by Langley Research Center, the lead center for NASA's scientific and technical information. The NASA STI Program Office provides access to the NASA STI Database, the largest collection of aeronautical and space science STI in the world. The Program Office is also NASA's institutional mechanism for disseminating the results of its research and development activities. These results are published by NASA in the NASA STI Report Series, which includes the following report types:

- TECHNICAL PUBLICATION. Reports of completed research or a major significant phase of research that present the results of NASA programs and include extensive data or theoretical analysis. Includes compilations of significant scientific and technical data and information deemed to be of continuing reference value. NASA counterpart of peer-reviewed formal professional papers, but having less stringent limitations on manuscript length and extent of graphic presentations.
- TECHNICAL MEMORANDUM. Scientific and technical findings that are preliminary or of specialized interest, e.g., quick release reports, working papers, and bibliographies that contain minimal annotation. Does not contain extensive analysis.
- CONTRACTOR REPORT. Scientific and technical findings by NASA-sponsored contractors and grantees.
- CONFERENCE PUBLICATION. Collected papers from scientific and technical conferences, symposia, seminars, or other meetings sponsored or co-sponsored by NASA.
- SPECIAL PUBLICATION. Scientific, technical, or historical information from NASA programs, projects, and missions, often concerned with subjects having substantial public interest.
- TECHNICAL TRANSLATION. English-language translations of foreign scientific and technical material pertinent to NASA's mission.

Specialized services that complement the STI Program Office's diverse offerings include creating custom thesauri, building customized databases, organizing and publishing research results... even providing videos.

For more information about the NASA STI Program Office, see the following:

- Access the NASA STI Program Home Page at ***http://www.sti.nasa.gov***
- E-mail your question via the Internet to help@sti.nasa.gov
- Fax your question to the NASA STI Help Desk at (301) 621–0134
- Phone the NASA STI Help Desk at (301) 621–0390
- Write to:
  NASA STI Help Desk
  NASA Center for AeroSpace Information
  7121 Standard Drive
  Hanover, MD 21076–1320

NASA/TM-2003-212441

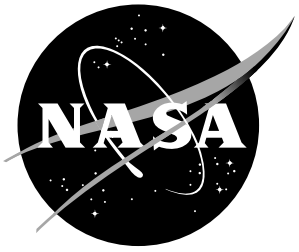

Structured Uncertainty Bound Determination From Data for Control and Performance Validation

Kyong B. Lim
Langley Research Center, Hampton, Virginia

National Aeronautics and
Space Administration

Langley Research Center
Hampton, Virginia 23681-2199

August 2003

Acknowledgment

Most of the simulation and experiment on the Ducted fan and the basic UBID toolbox development has been carried out while the author was visiting the Control and Dynamical Systems group at California Institute of Technology under an Intergovernmental Personnel Act between California Institute of Technology and NASA Langley Research Center. The gracious support by the host, Professor John Doyle, is greatly appreciated, and Professor Richard Murray for access to the Ducted fan testbed. The author would also like to thank Dr. David Bayard of Jet Propulsion Laboratory for the advice offered concerning closed loop system identification, Marc Trotoux for conducting many of the experiments and simulations on the Ducted fan, and his colleagues Dr. David Cox for his help during the final toolbox development phase and Dr. Daniel Moerder for the sustained moral support, both at NASA Langley Research Center.

Available from:

NASA Center for AeroSpace Information (CASI)
7121 Standard Drive
Hanover, MD 21076–1320
(301) 621–0390

National Technical Information Service (NTIS)
5285 Port Royal Road
Springfield, VA 22161–2171
(703) 605–6000

Contents

Abstract

This report attempts to document the broad scope of issues that must be satisfactorily resolved before one can expect to methodically obtain, with a reasonable confidence, a near-optimal robust closed loop performance in physical applications. These include elements of signal processing, noise identification, system identification, model validation, and uncertainty modeling. Based on a recently developed methodology involving a parameterization of all model validating uncertainty sets for a given LFT structure and noise allowance, a new software, Uncertainty Bound Identification (UBID) toolbox, which conveniently executes model validation tests and determine uncertainty bounds from data, has been designed and is currently available. This toolbox also serves to benchmark the current state-of-the-art in uncertainty bound determination and in turn facilitate benchmarking of robust control technology. It is hoped that a convenient new toolbox will encourage extensive application of this baseline methodology and toolbox so that researchers can build on it to make robust control a truly useful tool. To help clarify the methodology and use of the new software, two tutorial examples are provided. The first involves the uncertainty characterization of a flexible structure dynamics, and the second example involves a closed loop performance validation of a ducted fan based on an uncertainty bound from data. These examples also help describe the many factors and assumptions that determine the degree of success in applying robust control theory to practical problems. The results demonstrate the highly non-unique nature of model validating set of uncertainties, which require only matching predicted to measured input and output data, and hence almost any internal model structure is possible. The results on the effects of erroneous or non-existent uncertainty structure indicates that model validation conditions satisfy easily but often gives unpredictable uncertainty norm bounds, due to differing uncertainty structures.

1 Motivation

1.1 Robust control theory, a promise

In robust control theory of the μ variety (for example, see [1], [2]), uncertainties in a mathematical model representation of a physical system are addressed by considering a bounded set of models. A widely accepted representation of a bounded set of input-output models for general, multivariable, linear, time-invariant (LTI) system is the linear fractional transformation (LFT) representation

$$\begin{pmatrix} e \\ y \end{pmatrix} = \mathcal{F}_u(P_o(W), \Delta_u) \begin{pmatrix} r \\ u \end{pmatrix}, \ \Delta_W := W\Delta_u \in \mathcal{D}_W$$

Figure 1 shows the standard LFT connections of an uncertainty model, Δ_u, augmented nominal plant, P_o, and controller, K. The component uncertainty sizes are denoted by the block-diagonal uncertainty weight matrix, W, which corresponds in structure to the unity norm-bounded block-diagonal structured uncertainty set

$$\mathcal{D}_B := \{\Delta_u := \{\text{diag}[\delta_1 I_{n_1}, \ldots, \delta_r I_{n_r}, \Delta_1, \ldots, \Delta_F] : \delta_i, \ \Delta_j \in \mathcal{RH}_\infty\}, \|\Delta_u\|_\infty \leq 1\}$$

With the above notions of LFT's and uncertainty structure, a set of plant models can then be represented as

$$\mathcal{P}_\Delta := \{\mathcal{F}_u(P_o(W), \Delta_u), \ \Delta_u \in \mathcal{D}_B\}$$

and the notion of robustness can be defined such that if a characteristic holds for every plant $P \in \mathcal{P}_\Delta$, then controller K is said to be "robust". As an example, "robust performance" characteristics include both internal stability and a minimum performance level. The amazing thing about μ robustness theory is that nominal performance (NP), robust stability (RS), and robust performance (RP) requirements for the general LFT system shown in Figure 1

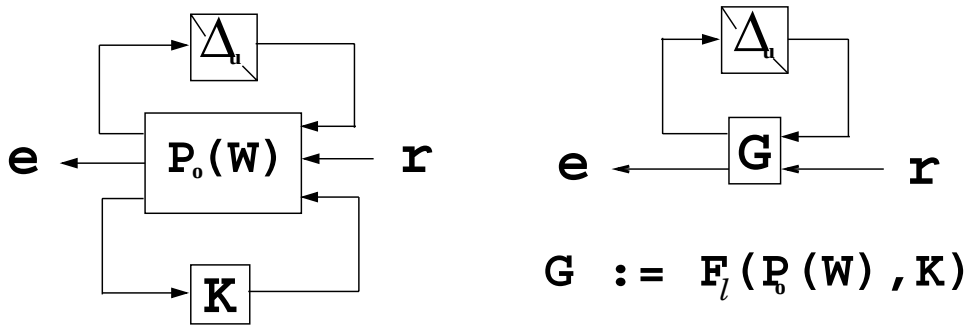

Figure 1: Standard LFT uncertainty-plant-controller representation.

can be succinctly quantified by the following μ conditions:

$$\begin{array}{lcll} \text{NP} & \Leftrightarrow & \text{NS} + \|G_{22}\|_\infty < 1 & \Leftrightarrow \quad \bar{\sigma}(G_{22}) = \mu_{\Delta_p}(G_{22}) < 1, \ \forall\omega \\ \text{RS} & \Leftrightarrow & \text{NS} + F_u(G,\Delta) \text{ stable}, \forall\Delta \in B_\Delta & \Leftrightarrow \quad \mu_{\Delta_u}(G_{11}(W)) < 1, \ \forall\omega \\ \text{RP} & \Leftrightarrow & \text{RS} + \|F_u(G,\Delta)\|_\infty < 1, \forall\Delta \in B_\Delta & \Leftrightarrow \quad \mu_\Delta(G(W)) < 1, \ \forall\omega \end{array}$$

where

$$\mu_\Delta(G) := \frac{1}{\min_{\Delta\in\mathcal{D}} \{\bar{\sigma}(\Delta) \mid \det(I - G\Delta) = 0\}}$$

and

$$\Delta := \begin{bmatrix} \Delta_u & \\ & \Delta_p \end{bmatrix} \in \mathcal{D}, \quad \Delta_p \text{ unstructured, complex, performance block}$$

The point here is that robust control theory is very elegent and computationally reliable [3] but depends heavy on the uncertainty structure and weight, W. Notice that the assumed uncertainty structure and weight is implicit in the augmented nominal plant and its LFT interconnectons.

1.2 Robustness dependence on uncertainty model

Even after almost two decades of well established theory, there is a persistent gap across robust control theory and technology. This means that its usefulness to practical systems is limited and is painfully evident from simulation studies of simple toy models to applications on more realistic systems, some of which is illustrated in this study. Figure 2 hints at why this may be so - a priori knowledge of a physical application is imperfect and there are limitations to measurements.[1]

Interestingly the exploitation of a given uncertainty model, with explicit assumptions on the system structure, is the key advantage in robust control as well as its main predicament in applications. With a given uncertainty model, robustness analysis can address what-if questions such as worst case response which can be used as a means to tradeoff system robustness with performance. Furthermore, with a given uncertainty model, robust control synthesis can build-in robustness with respect to this uncertainty model. In the end however, the *physical* significance of these analysis and synthesis results depends on the relevance of the given uncertianty model with respect to the physical system in question.

[1] A plausible historical explanation for this state appears to be that while feedback control was originally motivated by physical applications, control theory apparently evolved in its own sphere very often without the distractions caused by physical realities and a myriad of peculiar characteristics in physical systems. Modeling is not the primary concern of control systems theorists, which makes new control theories more and more difficult to apply.

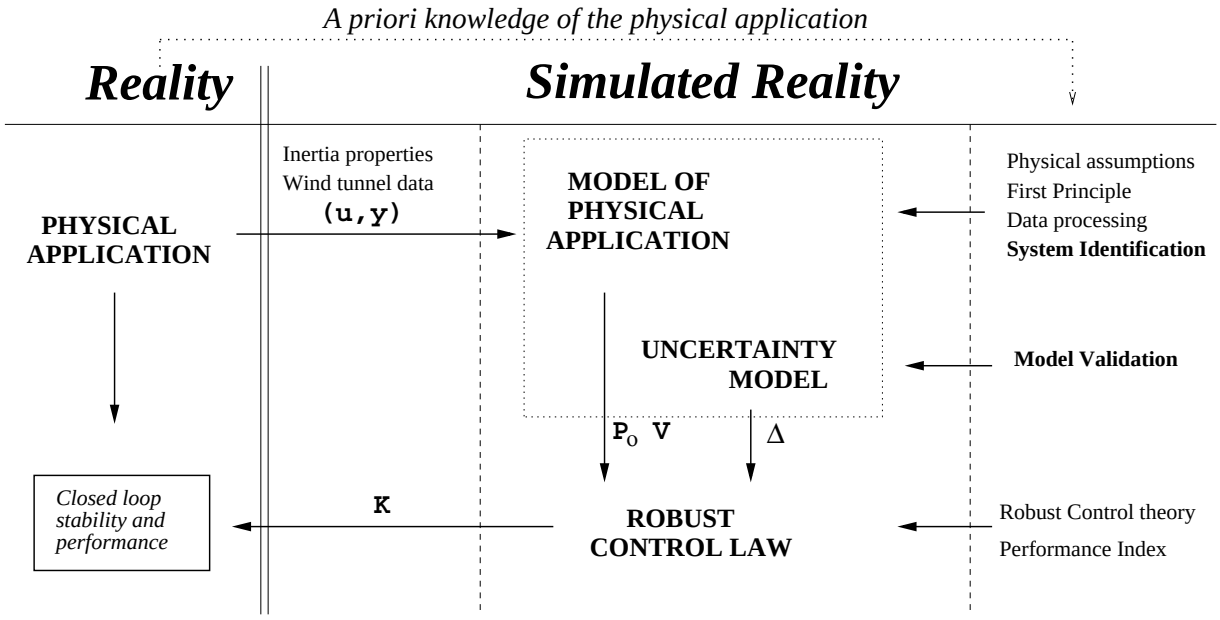

Figure 2: Factors contributing to robust control law performance in real problems.

These reasons motivate the goal and the particular approach reported here. Namely, we seek to improve the usefulness of robust control by constructing uncertainty model bounds based on both a priori information and test data, the latter which is usually not used due to the lack of a sensible methodology.

2 Structured uncertainty bound determination from data

2.1 Assumptions on signals and systems

In dealing with signals for model validation, sufficient care must be given to prevent inadvertent errors. For example, we may not necessarily want to apply tapered time windows for input and output signals to improve their spectral spreading and leakage as commonly done in spectral analysis, at the expense of spectral distortions in the predicted output. In general, we have to avoid nonperiodicity in the signals because it can lead to significant errors when used in predicting output DFT's, as described in the following subsections. Hence, implementing experiments that produce periodicity in the input and output signals appear necessary in a proper application of model validation tests based on matching predicted output spectra to measurements based on time-limited samples. However, if a periodic time sample cannot be attained, the nonperidicity induced errors can be mitigated to some degree by applying tapered time windows with a nominal level of spectral distortions. In addition, to develop theory with some level of rigor, simplifying assumptions on the system are also required, although not more limiting than μ theory in robust control.

2.1.1 Model of physical system and signals

Consider a given physical system modeled as a linear transfer function matrix, G, with inputs and outputs denoted by u and y respectively and driven by unknown exogenous disturbances denoted by d as shown in Figure 3. Our interest is of course the model validation (or invalidation) of the system model, G, using a judicious set of inputs and measured outputs from an unknown "true" plant model, G_{true} . Assume discrete time signals so that hereon we

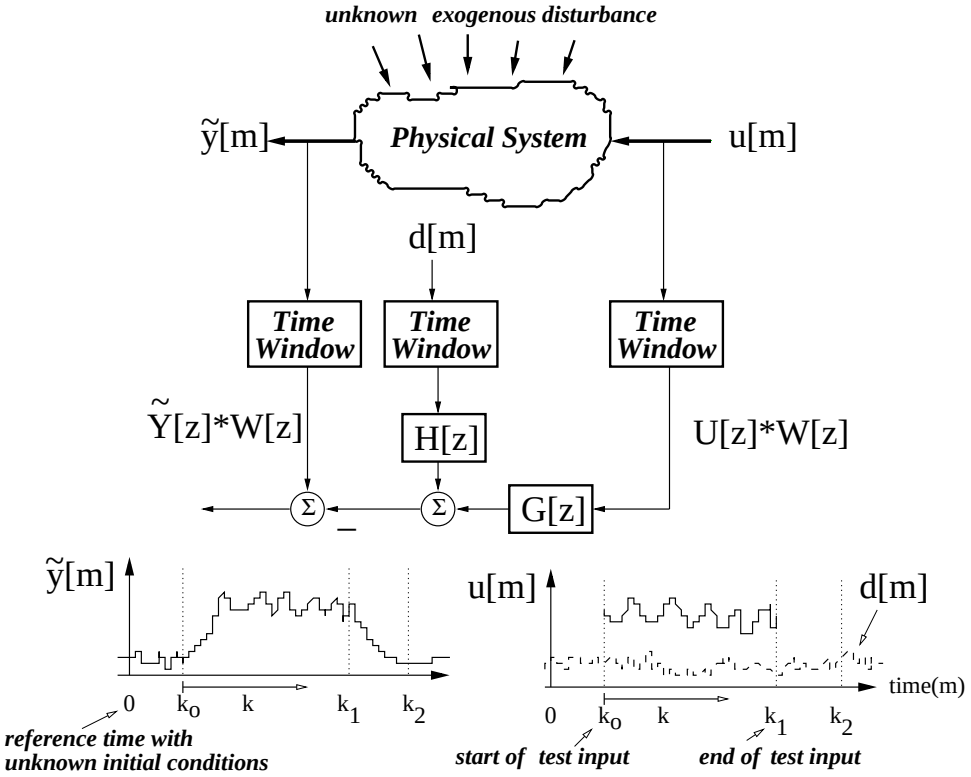

Figure 3: Schematic of signals collected for model validation

denote, for example, the input $u[m] := u(t = m\tau)$ to mean the input at time $t = m\tau$ where τ denotes the sampling time and m is an integer index denoting time. While the unknown exogenous disturbance signals, d, are *everlasting*, the test input, u, starts at time k_o and ends at k_1. The interval from k_1 to k_2 marks the transition from the end of forced response to beginning of zero input steady-state response. For more details on signals and systems, see for example [4].

Suppose the system is modeled as an n-th order state-space, linear, discrete time-invariant, and asymptotically stable so that its j-th eigenvalue denoted by γ_j satisfies

$$\text{Assumption 1:} \quad |\gamma_j| < 1, \quad j = 1, \ldots, n$$

with its output at time $m := k_o + k$, given by

$$y[m] = \underbrace{\sum_{j=1}^{n} c_j \gamma_j^m}_{zero\ input\ response} + u[m] * g[m] + d[m] * h[m] \tag{1}$$

where $\{c_j, j = 1, \ldots, n\}$ denote constants dependent on generally unknown initial conditions at time $m = 0$, "$*$" denotes convolution operation, and $g[m]$, $h[m]$ denote pulse responses of models for the physical system and noise filter respectively. Assuming these models are causal,

$$\text{Assumption 2:} \quad g[m] = 0, \quad h[m] = 0, \quad \forall m < 0$$

and the convolution terms in equation 1 reduce to, for example

$$u[m] * g[m] := \sum_{l=-\infty}^{\infty} u[l]g[m-l] = \sum_{l=-\infty}^{m} u[l]g[m-l] \tag{2}$$

To deal with the unknown initial conditions, we assume that the corresponding reference time for the asymptotically stable system is sufficiently far back relative to time k_o such that its zero input response component at time $m \geq k_o$ is insignificant. Specifically, given an $\epsilon > 0$, we assume that there exists a positive integer $\underline{k}$ such that if $k_o \geq \underline{k}$, then $|\sum_{j=1}^{n} c_j \gamma_j^m| < \epsilon$, $\forall m \geq k_o$. Simply put,

$$\text{Assumption 3:} \quad \sum_{j=1}^{n} c_j \gamma_j^m \approx 0, \quad m \geq k_o$$

For convenience, the reference time point is shifted forward by k_o and hereon for simplicity, with assumptions 1 to 3, the output equation 1 is reduced to

$$y[k] = u[k] * g[k] + d[k] * h[k], \quad k \geq 0 \tag{3}$$

2.1.2 Model validation using time-limited data

For model validation in the frequency domain, based on input and output data sequence which are of N-points duration (corresponding to a rectangular time window in Figure 3)

$$\{y\}^N = \{y[0], \ldots, y[N-1]\}, \quad \{u\}^N = \{u[0], \ldots, u[N-1]\}$$

consider the z-transform of equation 3

$$Y[z] = G[z]U[z] + H[z]D[z] \tag{4}$$

where

$$Y[z] := \sum_{k=-\infty}^{\infty} y[k]z^{-k}$$

and similarly for $U[z]$ and $D[z]$ while $G[z]$ and $H[z]$ denote transfer function matrices whose frequency response functions are defined on $z = e^{i\omega\tau}$. With time-limited data, we cannot compute the necessary z-transforms in equation 4 which motivates us to rewrite as

$$\begin{aligned} Y[z] &= \sum_{k=-\infty}^{-1} y[k]z^{-k} + \sum_{k=0}^{N-1} y[k]z^{-k} + \sum_{k=N}^{\infty} y[k]z^{-k} \\ &= G[z]\left(\sum_{k=-\infty}^{-1} u[k]z^{-k} + \sum_{k=0}^{N-1} u[k]z^{-k} + \sum_{k=N}^{\infty} u[k]z^{-k}\right) + H[z]D[z] \end{aligned}$$

The above relation rewritten only at discrete set of frequency points evenly spaced on the unit circle in the z-plane is

$$Y_N[z_r] = G[z_r]U_N[z_r] + R_N[z_r] + \frac{1}{\sqrt{N}}H[z_r]D[z_r], \quad z_r = e^{i\frac{2\pi}{N}r}, r = 0, \ldots, N-1 \tag{5}$$

where Discrete Fourier Transforms of samples $\{y\}^N$ and $\{u\}^N$ are given by[2]

$$Y_N[z_r] := \frac{1}{\sqrt{N}}\sum_{k=0}^{N-1} y[k]z_r^{-k}, \quad U_N[z_r] := \frac{1}{\sqrt{N}}\sum_{k=0}^{N-1} u[k]z_r^{-k}$$

and the mostly unknown residual

$$R_N[z_r] := \frac{1}{\sqrt{N}}\left\{-\sum_{k=-\infty}^{-1} y[k]z_r^{-k} - \sum_{k=N}^{\infty} y[k]z_r^{-k} + G[z_r]\left(\sum_{k=-\infty}^{-1} u[k]z_r^{-k} + \sum_{k=N}^{\infty} u[k]z_r^{-k}\right)\right\}$$

is due to time-limited input-output data. Ignoring for the moment the effect of unknown exogenous disturbances and noise, $\frac{1}{\sqrt{N}}H[z_r]D[z_r]$, an upper bound on the residual can be written in terms of the worst case input signal and a measure of system gain as [5]

$$|R_N[z_r]| \leq \frac{2}{\sqrt{N}}\|u\|_\infty \sum_{k=0}^{\infty} k|g[k]|$$

Since the DFT of an N-point sample is equivalent to the Fourier Transform of the corresponding everlasting N-periodic signal, this means that the residue consists of the difference between an N-periodic output constructed from measured output, and the calculated output from a given discrete-time filter driven by an N-periodic input constructed from measured input. Of course without a priori knowledge of the given measured signals, there is no reason

[2] In MATLAB-Signal Processing Toolbox, the scale factor $\frac{1}{N}$ is used in the DFT calculation (rather than $\frac{1}{\sqrt{N}}$ implied by our DFT and inverse DFT definitions) and a unity scale factor in the inverse DFT expression.

to assume that the constructed N-periodic sample is representative of a nonexistent periodic input-output response of the physical system. Also, this residual holds for a generally unavailable "true" model (the given discrete-time filter) which produced the sample time records, hence, additional model error terms must be included subsequently for a model validation test.

If the measured input and output signals are truly N-periodic, then

$$\text{Assumption 4:} \quad R_N[z_r] = 0, \forall r$$

A time-limited signal, for instance $\{y\}^N$, can be seen as the product of everlasting time signals, y, with a rectangular window function, w of width N, i.e.

$$y_N[k] := y[k]w[k], \;\; k = -\infty, \ldots, \infty; \quad Y_N[z] := Y[z] * W[z]$$

where $\{y_N\} := \{\ldots, 0, \{y\}^N, 0, \ldots,\}$ is the everlasting time signal which contains the time-limited signal. In spectral estimation problems tapered time windows are often used to mitigate spectral spreading and leakage caused by the rectangular window function which can be seen as a convolution with a sinc spectrum. Basically, the tapering works because the signal spectra in some bandwidth of interest is minimally distorted unlike at other frequencies.

In contrast to the spectral estimation/analysis problem, we are interested in accurately characterizing the predicted output error defined by (see Figure 3)

$$E[z_r] := \tilde{Y}_N[z_r] - Y_N[z_r], \quad r = 0, \ldots, N-1 \tag{6}$$

where

$$\begin{aligned}
\tilde{Y}_N[z_r] &:= \mathcal{Z}(\tilde{y}[k]w[k]) = \tilde{Y}[z_r] * W[z_r] = (\tilde{G}[z_r]U[z_r] + \text{ Noise}) * W[z_r] \\
Y_N[z_r] &:= G[z_r]\mathcal{Z}(u[k]w[k]) + \frac{1}{\sqrt{N}}H[z_r]D_N[z_r] = G[z_r](U[z_r] * W[z_r]) + \frac{1}{\sqrt{N}}H[z_r]D_N[z_r]
\end{aligned}$$

The term $\tilde{Y}_N[z_r]$ denotes the z-transform, denoted by $\mathcal{Z}(\cdot)$, of windowed measured outputs evaluated at z_r while the term $Y_N[z_k]$ denotes the predicted outputs based on assumption 4, i.e. $R_N[z_r] = 0$ in equation 5. The predicted output error given by equation (6) with N-periodic assumption reduces to

$$E[z_r] = (\tilde{G}[z_r]U[z_r]) * W[z_r] - G[z_r](U[z_r] * W[z_r]) + \text{ Noise Terms}, \quad r = 0, \ldots, N-1 \tag{7}$$

so that even for the true model, i.e., $G[z] = \tilde{G}[z]$, and excluding noise effects, the above predicted output error will not be zero; only a rectangular window will indicate a zero predicted output error for the true model. Intuitively, it matters whether the time windowing is applied at the input to the plant or at its output. This means that tapered windows should be used sparingly in model validation for preconditioning signals (for example to force periodicity or even mitigate aliasing).

In the context of conducting model validation experiments, we can try to satisfy the N-periodic assumption by either (i) literally implementing an N-periodic test input or (ii) implementing a test input sequence that will produce a rest-to-rest N-point sample, for instance by beginning an N-point sample such that the zero input response from earlier time is negligible and by including at the tail end of the sample the decaying output response (due to zero input) until steady state. In either case, the experiment must be designed such as to allow a certain prescribed periodicity in a measurement sample, without using tapered windows. The effects of unknown exogenous signal terms are difficult to account for and is dealt with by prescribing noise/disturbance allowances in the periodogram of the appropriate signals based on a priori knowledge of say their estimated spectra.

2.1.3 Example

In this section we illustrate possible errors in the predicted output even if the model to be validated is the true model which generated the signals. Suppose the true system is a lightly-damped second-order discrete time plant defined by $\texttt{G[z]} = \texttt{zp2sys}(\ [-1,-1],\ [.9+\texttt{j}*.4, .9-\texttt{j}*.4], 1)$ with sampling time $\tau = .1$ sec. Figure 4 shows the Bode plot of the true plant and simulated input and output time records imbedded with a low level of additive output noise. The test input chosen is simply a random number sequence having a uniform distribution,

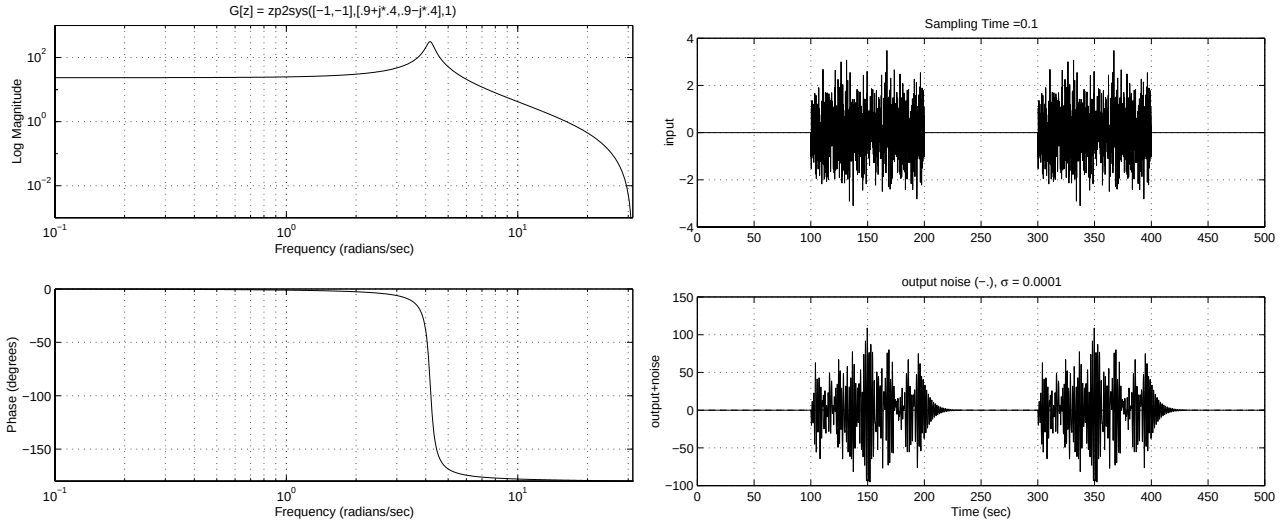

Figure 4: Frequency response of $G[z]$ (left), simulated input/output data with low noise (right).

zero-mean with unit standard deviation generated by $\texttt{inp} = [\texttt{zeros}(1000,1); \texttt{randn}(1000,1); \texttt{zeros}(1000,1); \texttt{randn}(1000,1); \texttt{zeros}(1000,1)]$, independently for each case. Similarly, the assumed output noise considered are generated by uniformly random time sequences having zero mean and with two different levels of standard deviations, $\sigma = 10^{-4}$ to represent low noise case and $\sigma = 10^{-1}$ for high noise cases. Starting at rest, it is assumed that the input is periodic over exactly 2000 points (or 200 seconds) of which the latter half consists of zero input to let the system decay to near zero state before the next period begins. Of course in principle, it does not matter where the 2000 points begins and ends for periodicity but it must be *exactly* 2000 points, else, the errors can be huge. For this reason, in applications, it helps to select the end timepoints of a sample such that the measured output do not end abruptly at both ends.

Table 1 show cases under which the predicted output errors are computed with variations in output noise levels, signal periodicity, and window function. In all cases, the true model, which was used in generating the simulated signals, is used in computing the predicted output errors with only additive output noise - obviously to examine potential hazards without even worrying about model or parametric errors.

The top two figures in Figure 5 shows the input and output time records and the corresponding predicted output error for low noise, periodic Cases LPR and LPH. The only difference between these two cases is that the latter case uses a tapered time window. In both cases the time samples are chosen to be perfectly periodic over 2000 points, starting from point 1001 and ending with point 3000. A sufficient time interval of 100 seconds with zero input occurs at the latter half of these samples to satisfy periodicity with negligible zero input response from the past. The third subfigure for each case show the spectra magnitudes $|Y_N[z_r]|$ (solid line), $|G[z_r]U_N[z_r]|$ (dash-dot line), $|Y_N[z_r] - G[z_r]U_N[z_r]|$ (dash line), and $|D_N[z_r]|$ (dotted line) while the noise filter $H[z_r]$ is assumed to be unity. In all cases

Case	Noise Level, σ	Periodicity(point range)	Time Window
LPR	10^{-4}	Periodic(1001-3000)	Rectangular
LPH	10^{-4}	Periodic(1001-3000)	Hanning
LNR	10^{-4}	Non-periodic(1001-3700)	Rectangular
LNH	10^{-4}	Non-periodic(1001-3700)	Hanning
HPR	10^{-1}	Periodic(1001-3000)	Rectangular
HPH	10^{-1}	Periodic(1001-3000)	Hanning
HNR	10^{-1}	Non-periodic(1001-3700)	Rectangular
HNH	10^{-1}	Non-periodic(1001-3700)	Hanning

Table 1: Cases simulated for predicted output errors.

considered, the spectra magnitudes $|Y_N[z_r]|$ and $|G[z_r]U_N[z_r]|$ appears to overlap in the logarithmic scaled figures and yet their corresponding predicted output errors (dash line) are not insignificant.

The spectra magnitude plots for Case LPR shows that the predicted output error is totally due the output noise (the dash and the dotted lines overlap). However, if the periodic samples are Hanning windowed as in Case LPH, the predicted output error increases significantly relative to the output noise spectra floor. Furthermore, as indicated in the previous figures the frequency shape of this increase is dependent on the plant transfer function, i.e. dependent on the frequency convolution of Hanning function with plant transfer function.

The bottom two subfigures in Figure 5 corresponds to Cases LNR and LNH which illustrates the consequence of violating periodicity assumptions in the signals. This particular nonperiodic time samples start from point 1001 and ends at point 3700. The predicted output error for Case LNR is due to the nonperiodicity of the signals used in computing the DFT's and is significantly larger than the predicted output error in Case LPH which is primarily due to tapered window at the input for a periodic signal. With the application of the Hanning window to the nonperiodic signals in Case LNH, the predicted output error is significantly reduced when compared to the rectangular windowed nonperiodic Case LNR, but still the error peak near 4 rad/sec did not improve. Interestingly, the predicted output error level in Case LNH is comparable to Case LPH, whose errors are due to the generally nonequivalent frequency convolution at the input and the output for a general window function. This is likely due to the fact that applying the Hanning window on the nonperiodic signals in Case LNH makes it somewhat periodic, but still the error due to nonequivalence of the frequency convolution at the input and output remains, similar to Case LPH.

To illustrate the effect of high output noise level, Figure 6 show Cases HPR, HPH, HNR, and HNH. Similar to the ideal Case LPR but with a higher output noise floor, Case HPR shows that the predicted output error equals the increased noise floor. The predicted output errors in Case HPH shows the combined effects of the input/output Hanning windowing (comparable to Case LPH) and the higher noise floor (comparable to Case HPR) so that at low frequencies, the noise floor dominates the predicted output error while near plant resonance the Hanning window induced frequency convolution error dominates. The effects of using nonperiodic signals in Cases HNR and HNH is analogous to the low noise cases, namely, a large predicted output error is incurred by the nonperiodicity (Case HNR) and is subsequently improved by Hanning windowing (Case HNH) - of course subject to the limitation imposed by the higher output noise floor.

In summary, this example demonstrates that even with no model errors, significant errors in the predicted output can result due to the effects of nonperiodicity, windowing, and noise. If the signals are known to be nearly periodic, rectangular windowing appears to reduce the predicted output errors, however with nonperiodic signals including any signals with high known levels of noise, as in the Ducted fan example to be discussed later, tapered windowing

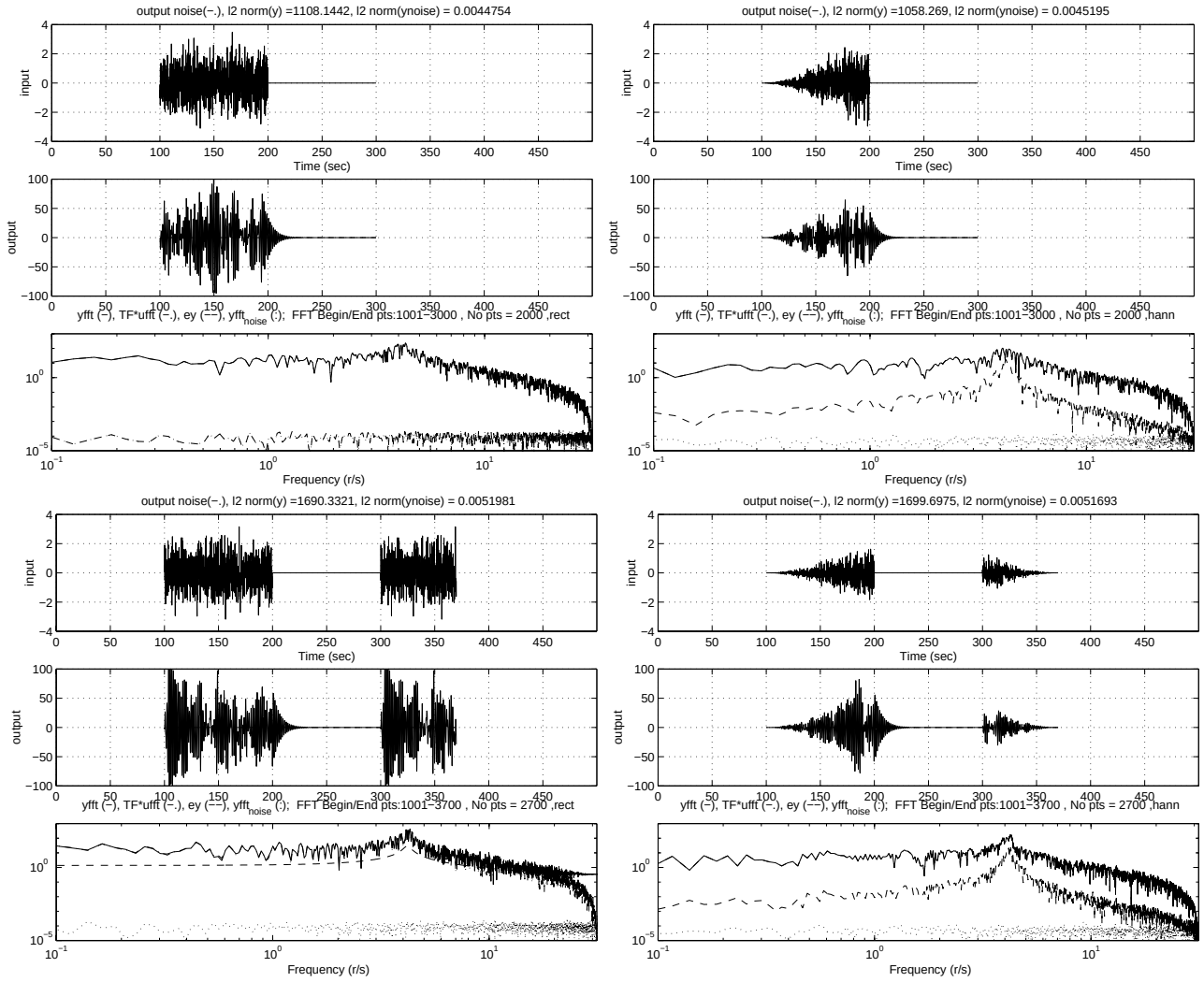

Figure 5: Cases LPR (top left), LPH (top right), LNR (bottom left), LNH (bottom right): Input/output records and predicted output error.

appears more suitable. Of course in actual applications, the added complication of model errors is inevitable. So, in model validation for robust control, we utilize the uncertainty structure and plant set associated with robust control to match the measured output with any one predicted output amongst a given set of models.

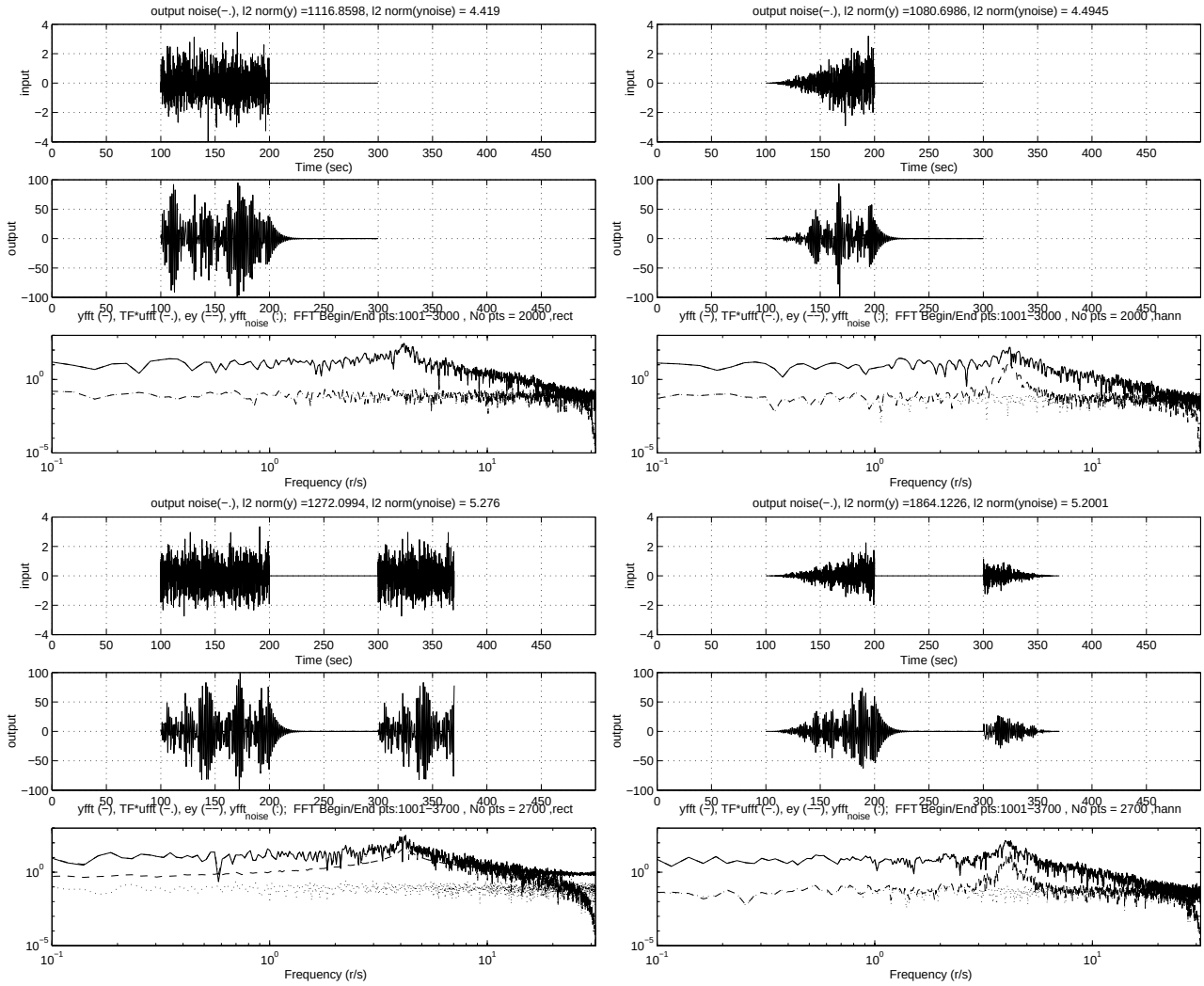

Figure 6: Cases HPR (top left), HPH (top right), HNR (bottom left), HNH (bottom right): Input/output records and predicted output error.

2.2 Model validation framework

We begin with making Assumptions 1 to 4 to restrict the class of signals and systems under consideration. Motivated by multivariable robust control theory (see for example [1]), we also limit the model structure to those that can be represented by LFT connections. The basic model validation question involves determining whether a particular plant model, belonging to a given set of plant models, and a particular exogenous signal, belonging to an unknown but bounded set of exogenous signals, could have produced a given pair of measured input and output signals. Going beyond this basic question, we also show how reasonable uncertainty bounds can be constructed for use in robust control or performance validation.

Figure 7 shows the basic LFT framework and its canonical form for model validation. Notice that for a closed loop system model validation where r and K are assumed known,

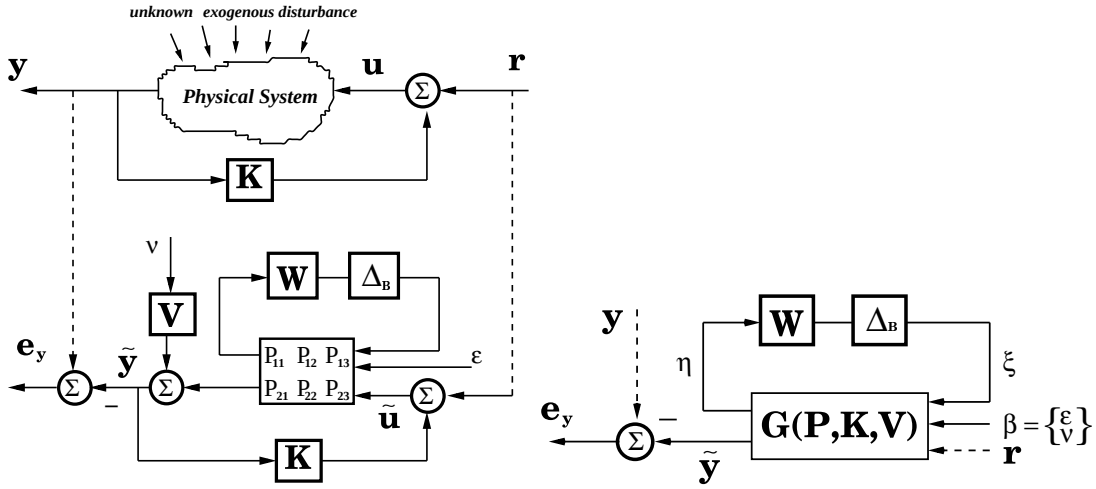

Figure 7: Model validation framework and canonical form.

$e_u := \tilde{u} - u = 0$ if $e_y = 0$ so that only the output error need to be considered. Given measurements of the output, y, command input, r, an augmented nominal plant and disturbance filter, P, controller, K, output noise filter, V, and a set of bounded structured uncertainty, $\mathcal{D}_W$, the set of plant (robust control design models)

$$\mathcal{P}_W := \{\mathcal{F}_u(P, \Delta), \Delta \in \mathcal{D}_W\}$$

is said to be a model validating set if at each frequency ($\omega_k = \frac{2\pi k}{\tau N}, k = 0, \ldots, N-1$) it contains an uncertainty model $\Delta \in \mathcal{D}_W$ such that there exists exogenous disturbance signals, ϵ and ν with $\|\beta\| \leq 1$ for which

$$y = \mathcal{F}_u(G(P, K, V), \Delta) \left\{ \begin{array}{c} \epsilon \\ \nu \\ r \end{array} \right\}$$

and

$$\begin{array}{rcl} \mathcal{D} & := & \{\Delta \in C^{m\times n} : \Delta = \mathrm{diag}(\delta_1 I_{m_1}, \ldots, \delta_r I_{m_r}, \Delta_{r+1}, \ldots, \Delta_\tau), \delta_i \in F_i, \Delta_k \in C^{m_k \times n_k}\} \\ W & := & \mathrm{diag}\,(w_1 I_1, \ldots, w_\tau I_\tau) \\ \mathcal{D}_W & := & \{\Delta \in \mathcal{D} : \Delta = W\Delta_B\} \\ \Delta_B & := & \{\Delta \in \mathcal{D} : \bar{\sigma}(\Delta) \leq 1\} \end{array}$$

With Assumptions 1 to 4, the set of signals y, r, η, ν, are viewed as the DFT's of their respective time-limited samples while systems, P, K, V, G, W, are viewed as transfer function

matrices evaluated at the same uniformly spaced frequencies up to Nyquist frequency. The symbol $\mathcal{F}_u$ denotes an upper LFT structure and $G(P, K, V)$ denotes the augmented closed loop transfer function matrix containing both noise and disturbance filters. Notice that we do not require $\Delta \in \mathcal{RH}_\infty$ so that stability and causality of the perturbation are not required, only that it is norm bounded. The terms δ_i, $i = 1, \ldots, r$, denote repeated scalar uncertainties which in general can depend on frequency in contrast to parametric uncertainties which are implicitly assumed to be unknown constants.

This question was first posed in [7] and they have shown that the validation test can be formulated analogous to a skewed-μ or alternately as a quadratic optimization problem. For the "most commonly applied cases: additive and input or output multiplicative" [8] it has been shown (and in time domain [9]) that the validation test takes the form of a convex feasibility problem when the fictitious signal η do not depend on ξ. More recently, [10] has shown that by choosing a plant uncertainty model based on coprime factorizations of the nominal plant and known controller, all closed loop transfer functions can be made affine in the coprime factor uncertainties so that the convexity of the validation test can be preserved through enforcing $G(P, K, V)_{11} = 0$. In dealing with closed loop validation in [10], the noise model enters as an additive output outside the loop and hence only G_{11} is relevant. On the other hand, in the work reported in [9], an open loop model validation problem with additive output noise is considered so that only P_{11} is relevant. However, it is not clear what the level of conservatism is on this particular form of plant uncertainty structure especially since no additional user specified uncertainty structure can be accomodated nor is necessary.

A key problem arises if one wishes to test a more general uncertainty structure for model validation beyond the "most commonly applied cases: additive and input or output multiplicative" (as mentioned in [8]), namely, the loss of convexity in the feasibility problem. This means that from a numerical implementation standpoint, the validation test is effectively a sufficient condition. Furthermore, if the validation test is passed for a particular plant set, there exists an infinity of other sets which will also be validating, irrespective of its convexity. In our view, this non-uniqueness diminishes the significance of a validation result for a particular set.

For these reasons, we take an alternate view of the model validation problem, as described in more detail in the next section. Instead of trying to validate a specific set with respect to given data by asking "Is $\mathcal{D}_W$ model (in)validating?" we ask instead "Does a model validating set $\mathcal{D}_W$ exist?" The former question is a test on a specific uncertainty set resulting in a positive or negative answer while the latter question is a test to determine whether some uncertainty set with the given LFT structure exists that can satisfy model validation conditions. The latter question is of course a necessary condition to the former and it turns out to be much simpler to test. Furthermore, if a finite size model validating set $\mathcal{D}_W$ exist, then it turns out that *all* model validating sets having the same LFT uncertainty structure can be readily parameterized [6].

2.3 3-Step Approach to model validation and parameterization

A new approach breaks up the model validation question into 3 parts:[3]

1. Does a pair of signals (ξ, β) where $\|\beta\| \leq 1$ exists such that $e_y = 0$?
2. Parameterize the set of signals

$$\mathcal{S}_{\phi,\psi} := \{[\xi(\phi, \psi), \beta(\phi, \psi), \eta(\phi, \psi)] : e_y = 0,\ \phi \in \Phi, \psi \in \Psi\}$$

[3] For more details see [6]

3. Does a $\Delta \in \mathcal{D}$ exists such that $\xi = \Delta\eta$ for some signal $(\xi, \eta(\xi,\beta)) \in \mathcal{S}_{\phi,\psi}$?

Figure 8 illustrates the question posed in Step 1. Such a pair of signals exists if and only if

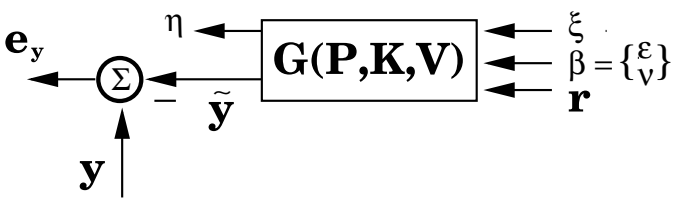

Figure 8: Does (ξ, β) exists, where $\|\beta\| \leq 1$, such that $e_y = 0$?

$$\left.\begin{array}{l} e_y^o \in \mathrm{Im}(M) \\ \|T_2^H (M^+)_\beta e_y^o\| \leq 1 \end{array}\right\} \quad \forall \omega_k \tag{8}$$

where the constant matrices are given by

$$\begin{aligned} e_y^o &:= y_{meas} - G_{23} r \\ M &:= [G_{21}, G_{22}] \\ Im(N_M) &= Ker(M) \\ T_2 &:= Im((N_M)_\nu)^\perp \end{aligned}$$

Notice that M is a crucial matrix which captures the uncertainty freedoms to be used for model validation. This test involves only a constant matrix check at discrete frequency points of interest in contrast to a (non)convex feasibility problem. If the above necessary condition cannot be satisfied, this means that no matter how large the uncertainty radii W (imbedded in G) is, the model is invalidated because either the a priori uncertainty structure is too restrictive or the noise allowance is too small. Hence to proceed in trying to construct a model validating set, one has to improve the nominal plant model, P, and/or modify the uncertainty structure $\mathcal{D}$ to increase its richness, and/or increase the noise allowance by modifying the noise filter model V.

If the above constant matrix test passes, then one can proceed to Step 2 and parameterize the set of signals

$$\mathcal{S}_{\phi,\psi} := \{[\xi(\phi,\psi), \eta(\phi,\psi), \beta(\phi,\psi)] : e_y = 0, \ \phi \in \Phi, \psi \in \Psi\}$$

where all feasible triples (ξ, ϵ, ν) are given by

$$\begin{pmatrix} \xi \\ \beta \end{pmatrix} = \begin{pmatrix} \xi_o \\ \beta_o \end{pmatrix} + \Omega \begin{pmatrix} \phi \\ \psi \end{pmatrix}$$

where ψ is arbitrary and ϕ satisfies

$$\|\phi\| \leq b_o := \sqrt{1 - \|T_2^H (M^+)_\beta e_y^o\|^2} \tag{9}$$

and

$$\Omega := N_M U \begin{bmatrix} \Sigma_1^{-1} & 0 \\ 0 & I_{n_\psi} \end{bmatrix} \tag{10}$$

$$\begin{pmatrix} \xi_o \\ \beta_o \end{pmatrix} := \left[M^+ - N_M ((N_M)_\beta)^+ (M^+)_\beta\right] e_y^o \tag{11}$$

$$(N_M)_\beta := \begin{bmatrix} T_1 & T_2 \end{bmatrix} \begin{bmatrix} \Sigma_1 & 0 \\ 0 & 0 \end{bmatrix} U^H \tag{12}$$

Figure 9 illustrates the final step of the existence test, which is to check whether a $\Delta \in \mathcal{D}$ exists such that $\xi = \Delta\eta$ for some signal pair $(\xi, \eta(\xi,\beta)) \in \mathcal{S}_{\phi,\psi}$ where $\eta = G_{11}\xi + G_{12}\beta + G_{13}r$. It turns out that this part of the existence test is satisfied if and only if there exists

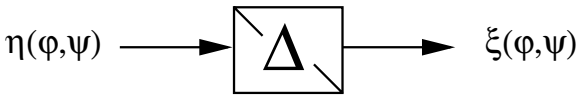

Figure 9: Final step of existence test

$(\xi,\beta) \in \mathcal{S}_{\phi,\psi}$ such that $\xi_i = 0$ or $\eta_i(\xi,\beta) \neq 0$, $\forall i$, i.e. $\mathcal{D}$-realizable, and for each repeated uncertainty block, $(\xi_i, \eta_i(\xi,\beta))$ are collinear. For the special class of uncertainty structure with no repeated uncertainties, i.e. $r = 0$ but not requiring $G(P,K,V)_{11} = 0$, with a satisfaction of the necessary conditions for existence in equation 8, it is almost certain that there exists $(\xi,\beta) \in \mathcal{S}_{\phi,\psi}$ such that $\eta_i(\xi,\beta) \neq 0, \forall i$. This means that for this important special class of uncertainty structure, the necessary conditions in equation 8 are actually necessary and almost sufficient for a model validating set $\mathcal{D}_W$ to exist.

If a model validating set $\mathcal{D}_W$ exists, then *all* model validating sets of plants are given by

$$\mathcal{P}_{W\phi\psi} := \{\mathcal{F}_u(P,\Delta), \Delta \in \mathcal{D}_W\}$$

where $\psi \in \mathcal{C}^{n_\psi}$, $\phi \in \mathcal{C}^{n_\phi}$, $\|\phi\| \leq b_o$, and $W := \mathrm{diag}(w_1 I_{n_1}, \ldots, w_\tau I_{n_\tau})$ is any matrix satisfying

$$\frac{\|\xi_i(\phi,\psi)\|}{\|\eta_i(\phi,\psi)\|} \leq |w_i|, \quad i = 1,\ldots,\tau$$

(ξ,η) is $\mathcal{D}$-realizable and are parameterized by

$$\xi_i = \xi_{o,i} + \Omega_i \left\{ \begin{array}{c} \phi \\ \psi \end{array} \right\} \tag{13}$$

$$\eta_i = \eta_{o,i} + [G_{11} \;\; G_{12}]_i \Omega \left\{ \begin{array}{c} \phi \\ \psi \end{array} \right\} \tag{14}$$

$\mathrm{dist}^{(\mathcal{F}_i)}(\xi_i,\eta_i) = 0, i = 1,\ldots,r$, and

$$\eta_o := [G_{11} \; G_{12}] \left\{ \begin{array}{c} \xi_o \\ \beta_o \end{array} \right\} + G_{13} r. \tag{15}$$

It is intuitively pleasing to note that if model validating sets exists, they are highly non-unique.

2.4 Validation as a feasibility problem

Using the previous parameterization, we re-examine the earlier question, "Is $\mathcal{D}_W$ model (in)validating?" Suppose a model validating set $\mathcal{D}_W$ exists. Since all model validating sets for the chosen uncertainty structure are given by the above parameterization, the original question can be posed as follows:

Given W, at each frequency does a (ϕ,ψ), $\|\phi\| \leq b_o$ exists such that

$$\frac{\|\xi_i(\phi,\psi)\|}{\|\eta_i(\phi,\psi)\|} \leq |w_i|, \quad i = 1,\ldots,\tau \tag{16}$$

where (ξ,η) is $\mathcal{D}$-realizable and $\mathrm{dist}^{(\mathcal{F}_i)}(\xi_i,\eta_i) = 0$, $i = 1,\ldots,r$?

The $\mathcal{D}$-realizable and collinearity conditions can be implicitly satisfied by the following form:

Given W, at each frequency does a (ϕ, ψ), $\|\phi\| \leq b_o$ exists such that

$$\left.\begin{array}{c} \xi_i(\phi,\psi) - \delta_i \eta_i(\phi,\psi) = 0, \quad \delta_i \in \mathcal{F}_i \\ |\delta_i| - |w_i| \leq 0 \end{array}\right\} \quad i = 1, \ldots, r \tag{17}$$

$$\|\xi_i(\phi,\psi)\|^2 - |w_i|^2 \|\eta_i(\phi,\psi)\|^2 \leq 0, \quad i = r+1, \ldots, \tau \quad ? \tag{18}$$

Although ξ_i and η_i are affine in ϕ and ψ as given in equations 13 and 14, the feasibility conditions are in general nonconvex. Specifically, the collinearity requirement due to repeated (and/or real) uncertainty involves a quadratic equality since δ_i is unknown equation 17 and the norm inequalities for the nonrepeated uncertainties although quadratic involves a difference in norms (equation 18). Nevertheless, one is hopeful towards a workable methodology if one observes from equations 17 and 18 that a feasible solution can be generated by first focusing on finding a pair (ϕ, ψ) which satisfies the collinearity condition in equation 17 and then easily selecting sufficiently large weights w_i, $i = 1, \ldots, \tau$, to satisfy equations 17 and 18.

2.5 Optimizing for smallest scaled set

A useful set of model validating plants must be "small but not smaller", i.e., it should not be an unnecessarily large set of plants which will limit performance but it must contain the "true" plant. Given a candidate set $\mathcal{D}_W$ of uncertainty norm radii, W, we seek a corresponding smallest scaled set $\mathcal{D}_{xW}$ which is model validating. This question can be posed by imbedding the previous feasibility problem in the following optimization:

$$\min_{\phi,\psi,\delta_1,\ldots,\delta_r,x^2} \quad x^2$$

subject to

$$\left.\begin{array}{c} \xi_i(\phi,\psi) - \delta_i \eta_i(\phi,\psi) = 0, \quad \delta_i \in \mathcal{F}_i \\ |\delta_i|^2 - x^2 |w_i|^2 \leq 0 \end{array}\right\} \quad i = 1, \ldots, r \tag{19}$$

$$\|\xi_i(\phi,\psi)\|^2 - x^2 |w_i|^2 \|\eta_i(\phi,\psi)\|^2 \leq 0, \quad i = r+1, \ldots, \tau \tag{20}$$

$$\|\phi\|^2 \leq b_o^2 \tag{21}$$

Although the above problem is not convex in general, the conditions involve polynominals in $\phi, \psi, \delta_1, \ldots, \delta_r, x^2$ with are at most cubic order. The existence of a feasible point $(\phi, \psi, \delta_1, \ldots, \delta_r, x^2)$ in the above optimization problem is equivalent to the existence of a model validating set $\mathcal{D}_{xW}$. Of course when $x < 1$, the original candidate uncertainty set, $\mathcal{D}_W$ satisfies model validation conditions. Notice that if there are no repeated uncertainty ($r = 0$), any choice of ψ and ϕ where $\|\phi\| \leq b_o$ will likely admit a model validating set $\mathcal{D}_{xW}$, since a larger uncertainty radii, W will admit a feasible point. However, even without repeated uncertainties, the constraints are in general not convex in ϕ and ψ and therefore the numerical optimization task is likely nontrivial.

The important issue of how one would simultaneously choose apriori weights for parametric $(w_i, i = 1, \ldots, r)$ and nonparametric $(w_i, i = r+1, \ldots, \tau)$ uncertainties to form candidate uncertainty weight is beyond the scope of this work. Whatever is chosen in an application, these candidate uncertainty weights should reflect the relative importance of the uncertainty components by design, based on additional a priori information on the particular application.

2.6 Convex model validation problems

For the special case when $[G_{11}, G_{12}] = 0$, η_i becomes independent of ξ and β (or equivalently ϕ and ψ) so that the term $\eta_i(\phi, \psi)$ simplifies to a constant $\eta_i = G_{13_i} r$ for given data and a convex feasibility/optimization problem results. This means that in general, both the choice of the LFT uncertainty structure and the way unknown exogenous signals affect the model determines whether a convex problem arises. For this special case, the problem of finding a smallest model validating unmodeled dynamics reduces to:

$$\min_{\phi,\psi,\delta_1,\ldots,\delta_r,x^2} \; x^2$$

subject to

$$\begin{aligned} \|\xi_i(\phi,\psi)\|^2 - x^2|w_i|^2\|G_{13_i} r\|^2 &\leq 0, \quad i = 1,\ldots,\tau \\ \|\phi\|^2 &\leq b_o^2 \end{aligned}$$

and since $\xi_i(\phi, \psi)$ is affine and the inequalities represent ordinary norm bounds, a feasible set if it exists will be convex. For computation, we rewrite these as an optimization problem involving a linear cost function subject to a set of linear matrix inequality constraints [11]:

$$\min_z \; c^T z$$

subject to

$$\begin{aligned} \begin{bmatrix} Q_i z - \|\xi_{o,i}\|^2 & \text{sym} \\ S_i z & I \end{bmatrix} &> 0, \quad i = 1,\ldots,\tau \\ \begin{bmatrix} b_o^2 & \text{sym} \\ Lz & I \end{bmatrix} &> 0 \end{aligned}$$

where $z := [\mathrm{Re}(\psi); \mathrm{Im}(\psi); \mathrm{Re}(\phi); \mathrm{Im}(\phi); x^2] \in \mathcal{R}^{2n_\psi + 2n_\phi + 1}$ and

$$\left.\begin{aligned} c &:= [0_{(2n_\psi+2n_\phi)};\ 1] \\ Q_i &:= [-2\mathrm{Re}(\xi_{o,i}^H \Omega_i A),\ |w_i|^2\|G_{13_i} r\|^2] \\ S_i &:= \left[\begin{bmatrix} \mathrm{Re}(\Omega_i) & -\mathrm{Im}(\Omega_i) \\ \mathrm{Im}(\Omega_i) & \mathrm{Re}(\Omega_i) \end{bmatrix} \begin{bmatrix} \mathrm{Re}(A) \\ \mathrm{Im}(A) \end{bmatrix}, 0\right] \\ L &:= \begin{bmatrix} 0_{2n_\phi \times 2n_\psi} & I_{2n_\phi} & 0_{2n_\phi \times 1} \end{bmatrix} \\ A &:= \begin{bmatrix} 0 & 0 & I_{n_\phi} & jI_{n_\phi} \\ I_{n_\psi} & jI_{n_\psi} & 0 & 0 \end{bmatrix} \end{aligned}\right\} \tag{22}$$

In a recent study, [10] notes that even if a selected uncertainty structure in open loop is made to satisfy $[P_{11}, P_{12}] = 0$ (see Figure 7), the presence of feedback can lead to $[G_{11}, G_{12}] \neq 0$ resulting in a nonconvex feasibility test. In general, it can be observed that since $\eta = [G_{11}, G_{12}]\binom{\xi}{\beta} + G_{13} r$, $[G_{11}, G_{12}] = 0$, if and only if all of the following conditions hold:

1. each uncertainty block is not connected to the plant in a feedback,
2. uncertainty blocks are not connected in such a way that an output signal from one block could influence another block,
3. all exogenous input signals do not influence any uncertainty block

These conditions are for open loop plants so that for systems with embedded feedback controllers forming an augmented plant, some of the above conditions may not hold. Clearly these conditions, which are sufficient conditions for convexity, can be very limiting in the choice of the uncertainty structure and exogenous input connectivity. A convenient to use interior-point algorithm for convex problems from LMI Control Toolbox [20] can be used to solve for the global minimum when a feasible set exists.

2.7 Smallest unmodeled dynamics subject to parametric uncertainties

In the previous section, we dealt with repeated scalar and/or real uncertainties that may depend on frequecies. In this section, we consider "parametric uncertainties" which by physical reasons are considered to be constants but unknown. One approach to handling this unknown constants is to consider it as an independent parameter identification problem in the context of system identification, a la [12, 13, 14, 5, 15]. This of course means avoiding model validation and LFT uncertainties entirely. The alternative viewpoint we take uses these unknown constants as additional variables in minimizing the norms of model validating LFT uncertainties.

If parameters imbedded in the plant changes (as in parameter identification problem) such that the crucial model validation design freedom matrix, $M = [G_{21}, G_{22}]$ changes, this can cause cascading changes which are difficult to evaluate in a numerical optimization context. Hence, we try to avoid changing the augmented plant directly by viewing the imbedded plant changes or parametric uncertainties as LFT uncertianties which are allowed to vary without changing the augmented plant.

In the case where we have competing unmodeled dynamics and parametric uncertainties, we suggest fixing an allowance for parametric uncertainties while minimizing non-parametric uncertainties (of course in addition to a fixed noise allowance). This may be more reasonable physically than the approach whereby a priori candidate uncertainty weights are fixed for both parametric and non-parametric uncertianties and then determining a smallest scaled set. The former approach amounts to a slight modification of the optimization problem for a smallest scaled set in the previous section and choosing the x scale in equation (19) to unity.

2.8 Unknown but bounded exogenous signals

To deal with unknown exogenous signals such as process and measurement noise, we consider them as unknown but bounded. No assumptions on the statistics and the independence of the unknown signals are required. In trying to satisfy the model validation conditions, these signals are treated as allowances to be used in finding the minimal norm LFT model uncertainty necessary. As such, erronously assuming an overly conservative level of noise will likely lead to optimistic levels (smaller than actual) of model validating LFT uncertainty. On the other hand, assuming a lower level of noise allowance (than actual) will likely lead to pessimistic levels of (larger than true value) model validating LFT uncertainty. Consequently, it is important to specify a reasonably accurate model of the noise and disturbances in the system for model validation and uncertainty bound determination purposes.

For convenience, the combined noise/disturbance allowance in the canonical form is given by

$$\|\beta(\omega)\|_2 \leq 1 \ \forall\omega \quad \Leftrightarrow \quad \|\beta\|_{l_\infty} := \|V_\beta^{-1}\hat{\beta}\|_{l_\infty} \leq 1 \tag{23}$$

where $V_\beta := \begin{bmatrix} V_\epsilon & 0 \\ 0 & V_\nu \end{bmatrix}$ denotes the filter matrix for disturbance and noise allowances and $\hat{\beta}$ denotes the exogenous signal as it enters the loop. Specifically, V_β is designed to reflect anticipated spectra of $\hat{\beta}$ and to normalize the unknown norm bound of β to unity as in equation (23). The assumed block diagonality in V_β implies the independence of ϵ and ν.

In some systems, reasonably accurate models for V_ϵ and V_ν may be available. In other systems where typical spectrums of $\hat{\epsilon}(\omega)$ and $\hat{\nu}(\omega)$ are available and if their individual channels are known to be independent, a stable discrete time filter can usually be fitted for each channel and realized as a diagonal filter. In some open loop unstable systems (such as the Caltech's Ducted fan in a certain flight configuration), a stabilizing feedback controller is

necessary to collect data. Under such conditions, developing suitable models to represent unknown noise and disturbance effects from data can be tricky because of the amplifying and correlation inducing effects of feedback which is partly determined by loop dynamics, which itself is not precisely known.

2.9 Performance validation using uncertainty model

A successful performance validation of a control law on a physical system is typically an important end goal of any control law design. It is also a definitive test on the validity of the mathematical model used in the analysis of the control system, using a single plant model or a set of plant models. A key premise in robust control is that any uncertainties in the mathematical model is to be contained by an appropriate uncertainty ball around a best (nominal) model. With this premise, a robust controller is designed, which is effectively an optimal control with respect to a particular uncertainty model. Specifically, a robust control law is usually designed by optimizing the predicted worst case performance over the uncertainty model. So in practice, it is crucial that the optimized predicted worst case performance will actually bound the performance based on measurements.

The predicted worst case performance over a set of plants defined by an uncertainty model over a given nominal is illustrated in Figure 10 where skewed-μ is defined at each frequency as [1]

$$\begin{aligned}\mu^s(\omega) &:= \left\{\min \rho : \det\left(I - \begin{bmatrix} I_{unc} & 0 \\ 0 & \rho I_{perf} \end{bmatrix} F_l(P,K)\Delta W\right) = 0, \bar{\sigma}(\Delta) \le 1\right\}^{-1} \\ &= \max_{\bar{\sigma}(\Delta_{unc})\le 1} \bar{\sigma}\left[W_{perf} F_u(F_l(P,K), \Delta_{unc} W_{unc})\right] \end{aligned} \tag{24}$$

where $\Delta := \begin{bmatrix} \Delta_{unc} & 0 \\ 0 & \Delta_{perf} \end{bmatrix}$, and $W := \begin{bmatrix} W_{unc} & 0 \\ 0 & W_{perf} \end{bmatrix}$. In this study, performance

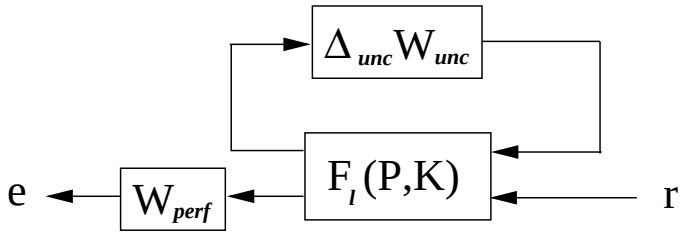

Figure 10: Predicted worst case performance based on identified uncertainty model

validation will mean comparing the predicted performance based on an uncertainty model to the measured performance. More specifically, the measured performance will be defined as the measured maximum amplification over bounded multivariable signals, whereas the predicted performance is taken to mean the predicted maximum amplification over a set of plants. Since it is a bit difficult to test and measure the response of all possible inputs in the hope of directly measuring the worst case signal amplifications, we identify an empirical model of the closed loop system from r to e, T_{er}, with the goal of computing the maximum singular value of its frequency response matrix, $W_{perf}T_{er}$.

In general, any stabilizing control law's performance could be validated using the same uncertainty model, since a useful uncertainty model of a plant should be independent of the control law. Indeed, a consistently successful performance validation of several stable control

law is a reasonable indication of the validity of an uncertainty model in question. Finally, notice that it is a bit difficult to experimentally determine the worst case responses with respect to unknown exogenous inputs. Hence, in the above suggested validation, we compare the measured and identified worst case responses from command input, r, to measured output, e, to the predicted performance μ^s from r to e only.

3 Uncertainty Bound Identification (UBID) Toolbox

3.1 Prerequisites for UBID Toolbox Version 0.1

- MATLAB 6.0 data structure required
- Optimization, LMI, and μ Toolboxes required

3.2 Summary of Commands

Main routines:

Command	Description
`congrad`	Defines constraint function and its gradient for smallest set optimization
`fungrad`	Defines objective function and its gradient for smallest set optimization
`mnmvcl`	A smallest model validating set algorithm
`noise_allow`	Defines noise and disturbance allowances in model validation
`ovbndunc`	Interactively fits overbound of computed model validating uncertainty norm
`sseigunc`	Forms augmented state space plant with eigenvalue uncertainties
`ubid`	Sample main program for computing a smallest model validating set
`ubid_lmi`	Sets up convex program of a smallest set optimization problem
`ubid_uncstr`	Forms uncertainty structure
`weightunc`	Define normalizing uncertainty weights for optimization

Utility routines:

Command	Description
`blkd2x2`	Transforms state matrix into 2x2 block diagonal form
`form_sample`	Divide a time record into windowed-overlapped-zero appended samples
`pinv_frd`	Computes pseudoinverse of a FRD model
`svd_frd`	Computes SVD of a FRD model

Routines from other toolboxes:

Command	Description
`fmincon`	Solve NLP using an SQP algorithm from Optimization Toolbox
`feasp`	Solve convex feasibility problem from LMI Toolbox
`mincx`	Solve convex program from LMI Toolbox
`drawmag`	Interactively fit a specified order stable filter from μ-Toolbox

Computational flow of UBID Toolbox

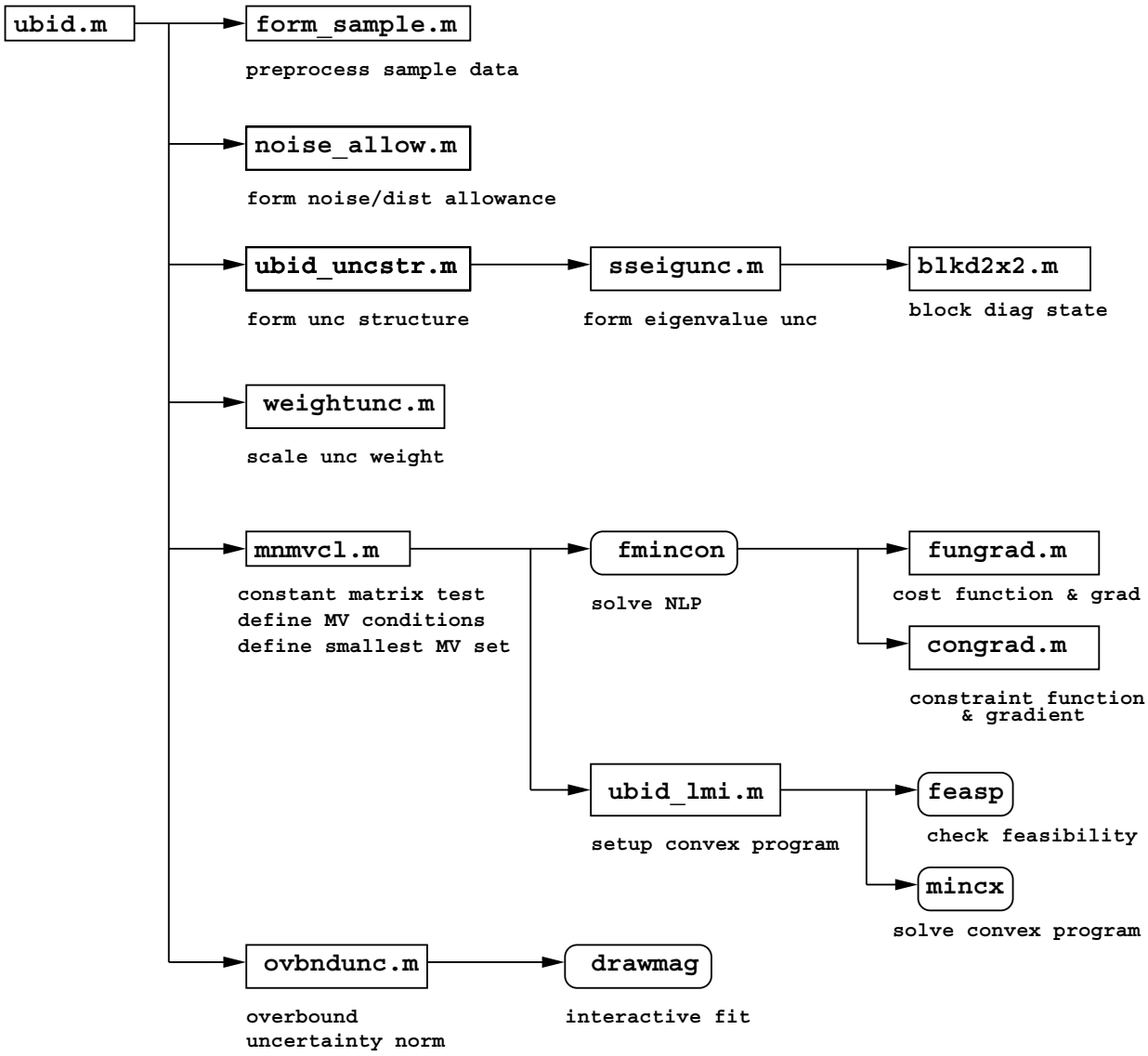

3.3 Command Reference

3.3.1 blkd2x2

blkd2x2

Purpose

Transforms a state space system into 2x2 block diagonal form.

Synopsis

```
[A,B,C,D,P,nreal] = blkd2x2(a,b,c,d,Ts)
```

Description

The inputs (a, b, c, d) are state space matrices and the outputs (A, B, C, D) are block-diagonalized state matrices computed from

$$A = P^{-1} * a * P;\ B = P^{-1} * b;\ C = c * P;\ D = d$$

where P denotes a similarity transformation matrix. The output `nreal` denotes the number of pure real eigenvalue/eigenvectors which are grouped in the first `nreal` blocks followed by 2 by 2 blocks in the `A` matrix corresponding to complex conjugate pairs of eigenvalues. These blocks are arranged in an ascending order of thier absolute frequencies. For a discrete time system with sampling interval `Ts` as an (optional) fifth input argument, an equivalent s-domain frequency is computed from $\frac{1}{T_s} \log z$.

3.3.2 congrad

congrad

Purpose

Define constraint functions and their gradients for a smallest set optimization problem.

Synopsis

```
[Cin,Ceq,Gin,Geq] = congrad(x,xio,etao,EF,PEFGH,Wunc,bo,blkf,cdimM,rankN,...
                    rankM,nrrs,nrcs)
```

Description

This subroutine computes the constraint functions and their gradients for a smallest set optimization problem which is used by the optimizer **fmincon** in MATLAB Optimization Toolbox. This optimizer uses a sequential quadratic programming algorithm to minimize a constrained nonlinear multivariable function. The constraint functions are assumed to be in the following forms: `Cin(x)` $\leq$ `0` and `Ceq(x)` $=$ `0`. Their corresponding constraint function gradients are assumed to be: `Gin(x)` $:=$ `d(Cin(x))/dx` and `Geq(x)` $:=$ `d(Ceq(x))/dx`. The output variables `Cin, Ceq, Gin` and `Geq` are evaluated at the value x where

$x(1 : n_\psi)$	$:= Re(\psi)$	$(n_\psi \times 1)$ real
$x(n_\psi + 1 : 2n_\psi)$	$:= Im(\psi)$	$(n_\psi \times 1)$ real
$x(2n_\psi + 1 : 2n_\psi + n_\phi)$	$:= Re(\phi)$	$(n_\phi \times 1)$ real
$x(2n_\psi + n_\phi + 1 : m)$	$:= Im(\phi)$	$(n_\phi \times 1)$ real
$x(m + 1 : m + n_{rrs})$	$:= d_1, ..., d_{n_{rrs}}$	$(n_{rrs} \times 1)$ real
$x(m + n_{rrs} + 1 : m + n_{rrs} + 2n_{rcs})$	$:= Re(d_{n_{rrs}+1}), Im(d_{n_{rrs}+1}), \ldots$ $Re(d_{n_{rrs}+n_{rcs}}), Im(d_{n_{rrs}+n_{rcs}})$	$(2n_{rcs} \times 1)$ real
$x(m + n_{rrs} + 2n_{rcs} + 1)$	$:= x^2$	real

where $m := 2n_\psi + 2n_\phi$. The remaining parameters which are defined at a given frequency are as follows:

`xio`	$= \xi_o$	$(m \times 1)$ complex
`etao`	$= \eta_o$	$(n \times 1)$ complex
`EF`	$= \Omega$	$n_\eta \times (n_\phi + n_\psi)$ complex, eq(32) [6]
`PEFGH`	$= [G_{11}, G_{12}]\Omega$	$n_\eta \times (n_\phi + n_\psi)$ complex, eq(33) [6]
`Wunc`	= normalizing unc wts	$(rx1)$ complex/real
`bo`	= noise uncertainty radius	real scalar
`blkf`	= uncertainty structure	$(\tau \times 2)$ real matrix
`cdiM`	= number of columns of $M := [G_{21}, G_{22}]$	$(n_\xi + n_\beta)$
`rankN`	= minimum rank (over freq) of varying matrix $(N_M)_\beta$	
`rankM`	= minimum rank (over freq) of varying matrix M	
`nrrs`	= number of Repeated Real Scalar uncertainty blocks	
`nrcs`	= number of Repeated Complex Scalar uncertainty blocks	

3.3.3 form_sample

form_sample

Purpose

Divide time record into windowed-overlapped-zero appended samples.

Synopsis

```
[ymeas_samp,yDFT_samp,omeg,Ts,t_samp,nout,nsamp] = form_sample(ymeas,t,...
                  winpara,wintype)
```

Description

Given a discrete time record, `ymeas` as a 2-D matrix (time varying row-wise, different channel column-wise) and a column vector of discrete time, `t`, this routine construct samples with `winpara(1)` non-zero point lengths. The output variable, `ymeas_samp`, is a 3-D matrix (varying time, output #, sample #). The corresponding output variable, `yDFT_samp` denotes the DFT of `ymeas_samp` and stored as a (1 x nsamp) array of FRD models. The variable `omeg` denotes a column vector of frequencies corresponding to the DFT of the sample time vector, `t_samp` having a sampling interval `Ts` for `nout` channels. The integer `nsamp` denotes the number of samples generated.

The input parameter `winpara(2)` specifies the total number of data points in each sample (which the FFT is applied). Zeros are appended if $winpara(2) > winpara(1)$. The number of samples can be increased by specifying the number of overlap points, `winpara(3)`.

Each sample can be windowed by specifying the parameter, `wintype` as `'rec'` for rectangular, `'han'` for Hanning, and `'ham'` for Hamming windows. The windowing is applied only to the nonzero data component of length `winpara(1)`.

3.3.4 fungrad

fungrad

Purpose

Defines the cost function and its gradient with respect to variables in a smallest model validating set optimization problem.

Synopsis

```
[f,g] = fungrad(x,xio,etao,EF,PEFGH,Wunc,bo,blkf,cdimM,rankN,rankM,nrrs,nrcs)
```

Description

This subroutine computes the cost function, `f` and its gradient, `g`, for a smallest set optimization problem which is used by the optimizer **fmincon** in MATLAB Optimization Toolbox. The above cost function and its gradient are evaluated at the given input optimization variable:

$x(1:n_\psi)$	$:= Re(\psi)$	$(n_\psi \times 1)$	real
$x(n_\psi+1:2n_\psi)$	$:= Im(\psi)$	$(n_\psi \times 1)$	real
$x(2n_\psi+1:2n_\psi+n_\phi)$	$:= Re(\phi)$	$(n_\phi \times 1)$	real
$x(2n_\psi+n_\phi+1:m)$	$:= Im(\phi)$	$(n_\phi \times 1)$	real
$x(m+1:m+n_{rrs})$	$:= d_1, ..., d_{n_{rrs}}$	$(n_{rrs} \times 1)$	real
$x(m+n_{rrs}+1:m+n_{rrs}+2n_{rcs})$	$:= Re(d_{n_{rrs}+1}), Im(d_{n_{rrs}+1}), \ldots$		
	$Re(d_{n_{rrs}+n_{rcs}}), Im(d_{n_{rrs}+n_{rcs}})$	$(2n_{rcs} \times 1)$	real
$x(m+n_{rrs}+2n_{rcs}+1)$	$:= x^2$		real

where $m := 2n_\psi + 2n_\phi$. The remaining input arguments are subroutine parameters defined in the command description **congrad**.

3.3.5 mnmvcl

mnmvcl

Purpose

This program sets up and solves for a smallest scaled model validating set based on [6].

Synopsis

```
[unc,Jmin,options,vFLAG] = mnmvcl(rspec,yspec,Gaug,blkf,Vnoise,Vdist,Ts,...
                    Wunc,iv_low,iv_hig,nskip,ndist)
```

Description

Given DFTs of the command or plant (for open loop system) input, `rspec` and plant output, `yspec`, and allowances for the unknown exogenous output noise and disturbances defined by filters `Vnoise` and `Vdist` respectively, this program attempts to solve for a smallest scaled uncertainty norm bound `unc` amongst all feasible LFT plant sets satisfying model validation conditions in the frequency domain. The minimization is over all feasible LFT augmented plant sets defined by a nominal 2 by 3 block canonical augmented plant, `Gaug`, having the block uncertainty structure `blkf`. The augmented plants are assumed to be discrete linear time-invariant systems with a sampling interval `Ts`, identical to the original discrete time signal which produced `rspec` and `yspec`.

Figure 7 shows the LFT augmented plant with all relevant signals required in the optimization problem. The block diagonal uncertainties are assumed to be in the forms:

$$\begin{aligned} W &:= \text{diag}(w_1 I_{n_1}, \cdots, w_r I_{n_r}, w_{r+1} I_{n_{r+1}}, \cdots, w_{r+c} I_{n_{r+c}}, x \cdot w_{r+c+1} I_{n_{r+c+1}}, \cdots, x \cdot w_\tau I_{n_\tau}) \\ \Delta_B &:= \text{diag}(\delta_1 I_{n_1}, \cdots, \delta_r I_{n_r}, \delta_{r+1} I_{n_{r+1}}, \cdots, \delta_{r+c} I_{n_{r+c}}, \Delta_{r+c+1}, \cdots, \Delta_\tau) \end{aligned}$$

where $\delta_i \in \mathcal{R}$, for $i = 1, \ldots, r$; $\delta_i \in \mathcal{C}$, for $i = r+1, \ldots, r+c$; $\Delta_i \in \mathcal{C}^{n_i \times m_i}$, for $i = r+c+1, \ldots, \tau$. The symbol, Δ_B, denotes a block diagonal uncertainty structure bounded by a unit ball. The symbols r, c, and τ denote the number of repeated real scalar blocks, repeated complex scalar blocks, and total number of uncertainty blocks, respectively. In general, the scalar δ_i will be a function of frequency, in contrast to "parametric" uncertainties which are sometimes explicitly assumed to be constants.

The frequencies, `iv_low` and `iv_hig` define the bandwidth over which model validation conditions are to be satisfied. `nskip` denotes the number of frequency points to be skipped when the frequency points based on fixed time sample period are overly dense. `ndist` denotes the number of unknown exogenous disturbance input.

`mnmvcl` solves for a smallest scale model validating set based on the following nonlinearly constrained optimization formulation:

$$\min_{\phi \in \mathcal{C}^{n_\phi}, \psi \in \mathcal{C}^{n_\psi}, \delta_1, \ldots, \delta_{r+c}, x^2 \in \mathcal{R}_+} x^2$$

subject to

$$\left.\begin{array}{c} \xi_i(\phi, \psi) - \delta_i \eta_i(\phi, \psi) = 0, \quad \delta_i \in \mathcal{R}_i \\ |\delta_i|^2 - |w_i|^2 \leq 0 \end{array}\right\} \quad i = 1, \ldots, r$$

$$\left.\begin{array}{c} \xi_i(\phi,\psi) - \delta_i\eta_i(\phi,\psi) = 0, \quad \delta_i \in \mathcal{C}_i \\ |\delta_i|^2 - |w_i|^2 \leq 0 \end{array}\right\} \quad i = r+1, \ldots, r+c$$

$$\begin{array}{rcl} \|\xi_i(\phi,\psi)\|^2 - x^2|w_i|^2\|\eta_i(\phi,\psi)\|^2 & \leq & 0, \quad i = r+c+1, \ldots, \tau \\ \|\phi\|^2 & \leq & b_o^2 \end{array}$$

Each element in $w_1, \ldots, w_\tau$ of the user specified frequency varying column vector, `Wunc`, defines a radius for each individual uncertainty block. The scaling factor, x, appears only with the radii of the nonrepeated complex blocks, $x \cdot w_i, i = r+c+1, \ldots, \tau$, implying that the scaling minimization is applied only to the nonrepeated complex blocks. This is an assumption in the problem statement which can be modified if additional a priori assumptions on the uncertainty structure indicates otherwise. We seek a smallest scaling, x, such that a set of unit norm-bounded model errors, $\delta_1, \ldots, \delta_{r+c}$, and $\Delta_{r+c+1}, \ldots, \Delta_\tau$ (parameterized by ξ, η), will exactly reproduce the given input and output signals to within unknown but bounded exogenous signal allowance limits (see routine **noise_allow** for a description of signal allowances). It is important to note that the smallest scaling is with respect to user defined radii for each individual nonrepeated complex uncertainty block.

The output `unc` is a frequency varying column vector denoting a set of smallest model validating uncertainty norms satisfying

$$unc_i := \frac{||\xi_i||}{||\eta_i||} = |\delta_i| \leq |w_i|, \quad i = 1, \ldots, r+c$$

for the repeated real and complex blocks and

$$unc_i := \frac{||\xi_i||}{||\eta_i||} = ||\Delta_i|| \leq x|w_i|, \quad i = r+c+1, \ldots, \tau$$

The second output variable `Jmin` denotes the minimum cost function. Notice that satisfying the model validation conditons imply the existence of a set of δ_i and Δ_i about a nominal model but in no way imply that the "true" model error has been recovered or that a "true" model even exists.

`mnmvcl` performs a sufficiency test for convexity based on a norm test of the augmented plant blocks $[G_{11}, G_{12}]$. If this test is passed the subroutine **ubid_lmi** is called which sets up a convex program and solves it using the subroutine **mincx** in LMI Toolbox. If the sufficient test fails, then `mnmvcl` assumes a general nonlinearly constrained optimization problem and uses a sequential quadratic programming algorithm as implemented in **fmincon**, a routine in OPTool. **fmincon** in turn calls **fungrad** which defines the cost function and its gradient, and **congrad** which defines the constraints and its gradients.

3.3.6 noise_allow

noise_allow

Purpose

This routine help generate noise (and disturbance) weight filters to unknown but bounded exogenous signal allowances used in model validation.

Synopsis

```
[vVnoise,Vnoise] = noise_allow(N,Ts,nout,label,ynoise,t_raw)
```

Description

The input variable `N` denotes an N-point DFT sample used in model validation with sampling interval `Ts` while the variable `nout` denotes the number of channels in the noise/disturbance signals. If a sample discrete time history, `ynoise`, is not available, its mean square value (or variance) of the signal is assumed known. The variance for each of the channels are entered interactively when the routine is called with only 3 or 4 input arguments. `label` is an optional script label. If a sample of discrete time noise sequence `ynoise` (2-D matrix with time varying row-wise) is known, the routine is called with all 6 input arguments including a column vector of discrete time points, `t_raw`.

The output variable `vVnoise` denotes the frequency-varying noise weight in FRD format, computed from the fitted continuous state space filter `Vnoise` in SS format.

Approach

Given only the variance of a broadband (power content up to Nyquist frequency) discrete time random signal, we approximate a constant power spectra, S_o from the relation [16]

$$\mathcal{E}[\nu^2] \approx S_o \frac{2\pi}{T_s}$$

The above approximately constant power spectra can be related to a corresponding constant DFT magnitude using the periodogram formula

$$S_o = S_k = \frac{1}{N}|X_k^N|^2, \quad k = 1, \ldots, N$$

where X_k^N denotes the DFT of an N-point sequence $\nu_0, \ldots, \nu_{N-1}$

$$X_k^N := \sum_{i=0}^{N-1} \nu_i e^{\frac{j2\pi ik}{N}}$$

In summary, for the case when only the variances of an independent vector noise signal is known, its noise allowance in terms of its N-point DFT is defined by the constant matrix

$$Vnoise = \sqrt{\frac{NT_s n_{out}}{2\pi \mathrm{diag}\left(\mathcal{E}[\nu^2]_1, \ldots, \mathcal{E}[\nu^2]_{n_{out}},\right)}}$$

The factor $\sqrt{n_{out}}$ is due to the unity 2-norm bound on the magnitude DFT of the vector signal at each frequency. This means that for multiple channels, a generous level of noise allowance can arise.

For the case when a sample discrete time history `ynoise` which is significantly longer than `N` is known, several N-point subsamples can be partitioned and weighted (if desired) and an allowance is estimated by directly fitting a transfer function over the magnitudes of N-point DFT subsamples. The magnitude of DFTs are fitted interactively using stable real rational transfer function using the μ-Tool command **drawmag**. The input-output relationship is

$$X_k^N = V(\omega_k) W_k^N, \quad k = 1, ..., N/2$$

where W_k^N denotes the N-point DFT of a signal $w_0, ..., w_{N-1}$ whose DFT is unity 2-norm bounded and $V(\omega_k)$ denotes the frequency response of a noise allowance filter at frequency ω_k which maps a unity 2-norm bounded DFT signal to the given time sequence. Therefore, assuming a simulated noise whose DFT satisfies $|W_k^N| = 1$ for all k, fitting $|X_k^N|$ is equivalent to fitting $|V(\omega_k)|$ as required.

3.3.7 ovbndunc

ovbndunc

Purpose

Overbound frequency varying uncertainty norm data using stable rational transfer functions.

Synopsis

```
[Wid_z] = ovbndunc(unc_frd,blkf,omeg,iv_low,iv_hig,Ts)
```

Description

The components of the FRD model `unc_frd` consists of the computed model validating uncertainty norms for each block whose structure is defined by each row of `blkf`. The input `omeg` is the linearly spaced frequency points from the original FFT of the discrete time data whose sampling interval is `Ts` seconds. These frequency points are used only to compare the rational function fit, `Wid_z`, to the data itself whose range is limited to the frequency bandwidth in radians defined by bounds `iv_low` and `iv_high`. The output, `Wid_z`, is a fitted discrete time state space model in SS format. The actual fitting is done interactively using the μ-Tool command, **drawmag**.

For a tighter overbound, a linear programming approach given in [17] is recommended.

3.3.8 pinv_frd

pinv_frd

Purpose

Compute the pseudoinverse of a FRD model.

Synopsis

```
[piM_frd] = pinv_frd(M_frd,tol)
```

Description

This routine computes the pseudoinverse (or inverse), `piM_frd` of the input FRD model, `M_frd`. At each frequency point, the MATLAB function **pinv** is used with zero threshold defined by `tol`.

3.3.9 sseigunc

sseigunc

Purpose

Form augmented state-space model with eigenvalue uncertainties.

Synopsis

```
[Prr,blk_eig,nxi_eig,eigz,nreal] = sseigunc(Gnomd,Ts)
```

Description

Input `Gnomd` denote state space matrices for a discrete time nominal system with sampling interval `Ts`. The given nominal state matrix is block diagonalized to 2 by 2 blocks for complex conjugate pairs and 1 by 1 diagonal element for a real eigenvalue using **blkd2x2** routine which also determines the number of purely real eigenvalues, `nreal`, placed first on the diagonal.

When the subroutine is called the user is prompted for the set of nominal eigenvalues to be included as parametric uncertainties. The uncertainty for a purely real nominal eigenvalue is assumed to be purely real also while the uncertainties for each complex conjugate pair is also assumed to be complex conjugate, for consistency. All uncertainties in the eigenvalues are assumed to be independent and real and consists of the real perturbations in the purely real eigenvalue and the real and imaginary component perturbations in the complex conjugate eigenvalues.

`Prr` denotes the resulting augmented plant in discrete time state space, SS format, as shown in figure below. Same notations are used as in μ-Tools User's Guide [3] on pages 4-20 which describes a general affine perturbation for a linear state space model. The uncertainty structure definition matrix `blk_eig` reflects a set of real uncertainty variables which also includes repeated scalars if complex conjugate eigenvalues are present. The remaining output arguments include the number of channels due to eigenvalue uncertainties (i.e. dimension of η or ξ), `nxi_eig`, nominal eigenvalues in z-plane, `eigz`, and the number of purely real eigenvalues, `nreal`.

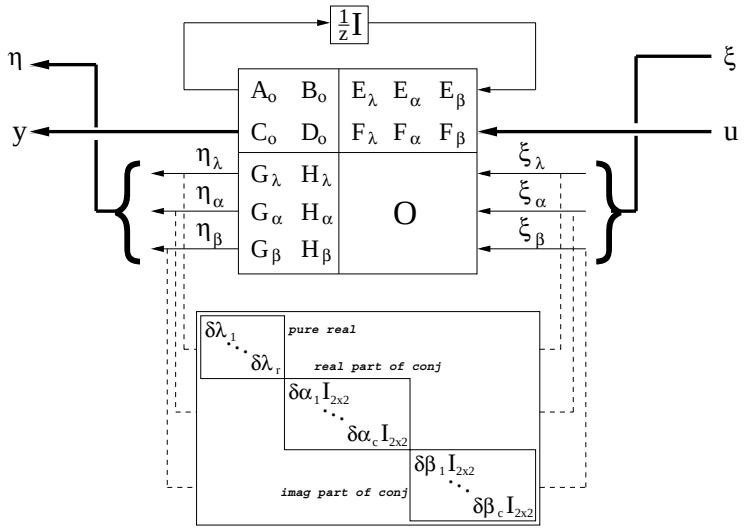

3.3.10 svd_frd

svd_frd

Purpose

Compute the SVD of a FRD model and its rank at each frequency.

Synopsis

```
[uu,ss,vv,rankss] = svd_frd(M_frd,tol)
```

Description

This routine computes the SVD of the input FRD model, `M_frd` where `uu*ss*vv = M_frd`. At each frequency point, the MATLAB function **svd** is used with the rank threshold defined by `tol`. The output variable, `rankss` is a column vector of rank at each frequency.

3.3.11 ubid

ubid

Purpose

Main program for computing a smallest model validating set.

Synopsis

This is a sample main program which calls the following subroutines to compute a smallest model validating set:

form_sample	preprocess sample data
noise_allow	define noise and disturbance allowances
ubid_uncstr	help construct uncertainty structure
weightunc	define relative uncertainty weight for optimization
mnmvcl	check feasibility and optimizes for a smallest set
ovbndunc	overbound uncertainty norms using stable rational filters

Description

To compute a smallest model validating set, various assumptions are made on the time signals to be used in defining the set of all model validating plants, the nominal model, the uncertainty structure, and exogenous noises and disturbances. These assumptions include:

- N-periodic input/output discrete time signal samples
- discrete linear time-invariant systems
- unknown but bounded exogenous noise and disturbances
- Linear Fractional Transformation (LFT) uncertainty structure
- known relative importance of the initial uncertainty weights

3.3.12 ubid_lmi

ubid_lmi

Purpose

Sets up convex program of a smallest set optimization problem.

Synopsis

```
[xopt,copt,EXITFLAG] = ubid_lmi(n_phi,n_psi,xio,etao,coXI,Wunc,bo,blkf)
```

Description

Sets up and solves a class of convex optimization problems defined by $[G_{11}, G_{12}] = 0$. For more general convex problems, this routine can be modified as necessary. The convex optimizer **mincx** found in LMI Toolbox [20] is used which assumes a linear cost function

$$\min_z \quad c^T z$$

subject to LMI constraints

$$\begin{bmatrix} Q_i z - \|\xi_{o,i}\|^2 & \text{sym} \\ S_i z & I \end{bmatrix} > 0, \quad i = 1, \ldots, \tau$$

$$\begin{bmatrix} b_o^2 & \text{sym} \\ Lz & I \end{bmatrix} > 0$$

where $z := [\mathrm{Re}(\psi); \mathrm{Im}(\psi); \mathrm{Re}(\phi); \mathrm{Im}(\phi); x^2] \in \mathcal{R}^{2n_\psi + 2n_\phi + 1}$. The constants, c, Q_i, S_i, L, and A, are defined in equation 22.

The input parameters, `n_phi` and `n_psi` denote the dimensions of the complex vectors, ϕ, and ψ, which are the free parameters defining all model validating sets. `xio` and `etao` denote the constant values of `xi` and `eta` which are the fictitious complex vector signals going out and into the uncertainty block, respectively. The complex matrix, `coXI` denotes the coefficient of the vector $(\phi; \psi)$ in ξ-equation, i.e., $[\Omega_1; \ldots; \Omega_\tau]$ where Ω_i is defined in equation 13. The column vector `Wunc` denotes the uncertainty weights used in the search for a smallest model validating set. It is used to define the relative significance of the various uncertainties which together define a particular model validating set. `bo` denotes the exogenous signal uncertainty allowance radius. `blkf` defines the uncertainty structure.

The output variable `x = xopt` are defined by:

`x(1:n_psi)`	:=	$\mathrm{Re}(\psi)$
`x(n_psi+1:2n_psi)`	:=	$\mathrm{Im}(\psi)$
`x(2n_psi+1:2n_psi+n_phi)`	:=	$\mathrm{Re}(\phi)$
`x(2n_psi+n_phi+1:2n_psi+2n_phi)`	:=	$\mathrm{Im}(\phi)$
`x(2n_psi+2n_phi+1)`	:=	x^2
`copt`	:=	global minimum
`EXITFLAG`	:=	1, global minimum
		0, convex program infeasible

3.3.13 ubid_uncstr

ubid_uncstr

Purpose

Form augmented plant with uncertainty structure.

Synopsis

```
[Paug,blkf,dimp,uncstr_choice] = ubid_uncstr(Po,Ts)
```

Description

Given a nominal model, `Po` this routine help to construct an augmented plant, `Paug` with the uncertainty structure, `blkf` in the following canonical form:

$$\begin{pmatrix} \eta \\ y \end{pmatrix} = \begin{bmatrix} G_{11} & G_{12} & G_{13} \\ G_{21} & G_{22} & G_{23} \end{bmatrix} \begin{Bmatrix} \xi \\ \begin{pmatrix} \varepsilon \\ \nu \end{pmatrix} \\ r \end{Bmatrix}$$

where $\xi = \Delta\eta$. The specific forms for G and Δ depends on the particular type of uncertainty structure selected, `uncstr_choice`, from the following short list of commonly used structures:

`uncstr_choice`	**Type of uncertainty**
0	provided by user (filename, all output variables defined in Synopsis)
1	additive
2	additive + eigenvalue
3	full output multiplicative
4	full output multiplicative + eigenvalue
5	diagonal output multiplicative
6	diagonal output multiplicative + eigenvalue
7	full input multiplicative
8	full input multiplicative + eigenvalue
9	diagonal input multiplicative
10	diagonal input multiplicative + eigenvalue

The six integers, $dimp(1) \ldots, dimp(6)$, define the dimensions of the corresponding vectors, η, ξ, y, ε, ν, and r.

Alternately, the user can load the augmented plant and uncertainty structure from a file by choosing $uncstr\_choice = 0$ option. In this case all variables, `Paug`, `blkf`, and `dimp` must be provided.

The input variable `Ts` denotes the sampling interval in seconds and is necessary only if eigenvalue uncertainties are included.

3.3.14 weightunc

weightunc

Purpose

Define initial uncertainty weight/radii for smallest set optimization.

Synopsis

```
[Wunc,par_bnd] = weightunc(blkf,omeg,Ts)
```

Description

This routine helps the user to select uncertainty weights for use during optimization for finding a smallest scaled model validating set. The selection of these weights should be based on the relative importance of different uncertainty blocks and over frequency for a given uncertainty block. This weighting reflects a priori knowledge by the user on the uncertainty structure of the system, however, the weighting over frequency has not been implemented yet. The optimization problem involves finding a minimum scaling of these user defined weights and still satisfy model validation conditions.

The input consists of the uncertainty block structure, `blkf` using μ-Tool convention [3], the discrete frequency points where weighting needs to be defined, `omeg`, and the sampling time of data, `Ts`. The output `Wunc`, is a frequency varying column vector uncertainty weight in FRD format, to be used in a numerical optimization for a smallest set while `par_bnd` defines a column vector of parameter uncertainty allowance.

A basic question of whether a particular set of plant model defined by `Wunc` cannot be invalidated by a given set of data is a special case of this smallest scaled set optimization problem. Namely, if `Jmin` < 1 (from subroutine **mnmvcl**) then the given set of plant model defined by `Wunc` cannot be invalidated by the given data. If the uncertainty structure leads to a convex program (including a special class where $[G_{11}, G_{12}] = 0$) then, `Jmin` < 1 is a necessary and sufficient test. For a more general uncertainty structure where `Jmin` is the result of a nonliearly constrained optimization problem, the above unit inequality becomes effectively a sufficient test since it is usually difficult to guarantee that a global optimum has been attained. Hence if `Jmin` exceeds 1, the test result is indeterminate.

4 Application Example 1: Uncertainty bounds of a large flexible structure

In this application example, we consider the problem of estimating model uncertainty bounds from data for active vibration control of a large flexible structure. We also show in detail how UBID Toolbox can be used in this problem.

4.1 Control-Structure-Interaction Evolutionary Model

Figure 11 is a schematic of the NASA Langley's flexible structure testbed. We consider a

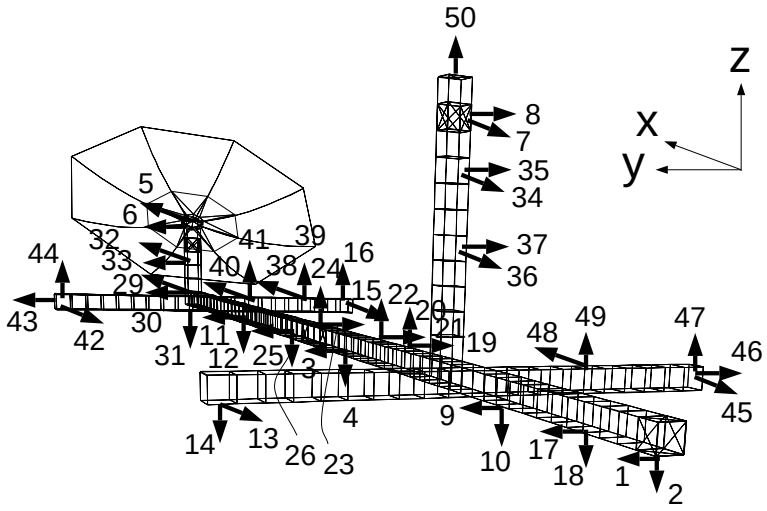

Figure 11: Control-Structure-Interaction Evolutionary Model (CEM).

NASTRAN model of the CEM consisting of 638 finite element grid points and include only the first 30 structural modes which are below 8 Hertz. The expected controller bandwidth is about 2 Hertz and the structural responses are sampled at 20 Hertz. Although many possible actuator and sensors are available for control as shown in the figure, we consider only 3 air thrusters and 3 displacement sensors which are approximately collocated and colinear in the x, y, and z axis corresponding to directions 5, 1, and 2 in the Figure 11. For more details please refer to [18].

For the purposes of illustration and evaluation of the uncertainty bound estimation approach, we assume that a physical system and associated exogenous noises can be represented by a truth model consisting of a 30 structural mode NASTRAN model. We denote the 60-th order true state space model discretized at sampling interval T_s as

$$\begin{pmatrix} x_{k+1} \\ y_k \end{pmatrix} = \begin{bmatrix} A_{true} & B \\ C & D \end{bmatrix} \begin{pmatrix} x_k \\ u_k \end{pmatrix}$$

Response measurements are simulated using this truth model and are used in estimating the uncertainty bounds.

4.2 Nominal model and uncertainty structure

Consider a perturbed system is defined by (A_{pert}, B, C, D) where

$$A_{pert} := A_{true} + \Delta A$$

such that A_{true} and ΔA matrices have the following block diagonal forms

$$A_{true} := \begin{bmatrix} \Lambda_1 & & 0 \\ & \ddots & \\ 0 & & \Lambda_{30} \end{bmatrix} \in \mathcal{R}^{60\times 60}, \qquad \Lambda_i := \begin{bmatrix} \alpha_i & \beta_i \\ -\beta_i & \alpha_i \end{bmatrix} \in \mathcal{R}^{2\times 2}, \quad i = 1, \ldots, 30$$

$$\Delta A := \begin{bmatrix} \delta\Lambda_1 & & 0 \\ & \ddots & \\ 0 & & \delta\Lambda_{30} \end{bmatrix} \in \mathcal{R}^{60\times 60}, \qquad \delta\Lambda_i := \begin{bmatrix} \delta\alpha_i & \delta\beta_i \\ -\delta\beta_i & \delta\alpha_i \end{bmatrix} \in \mathcal{R}^{2\times 2}, \quad i = 1, \ldots, 30$$

Denoting the true eigenvalue conjugate pairs as $\lambda_{i_\pm} := \alpha_i \pm \beta_i$, its perturbations denoted as $\delta\lambda_{i_\pm}$ are assumed constants such that A_{pert} is stable, i.e., $|\lambda_{i_\pm}| < 1$, $|\lambda_{i_\pm} + \delta\lambda_{i_\pm}| < 1$, $i = 1, \ldots, 30$. In this example, all eigenvalues are assumed to occur in complex conjugate pairs for simplicity although in general eigenvalues on the real axis in the z-plane can also be included.

To generate a nominal model as typical in a realistic application, we internally balance the perturbed system containing erroneous eigenvalues, (A_{pert}, B, C, D), using a similarity transformation, P, so that

$$\begin{pmatrix} \tilde{x}_{k+1} \\ y_k \end{pmatrix} = \begin{bmatrix} P^{-1}A_{pert}P & P^{-1}B \\ CP & D \end{bmatrix} \begin{pmatrix} \tilde{x}_k \\ u_k \end{pmatrix}$$

where $\tilde{x}_k := Px_k$ denotes the balanced state at time k. The nominal model is then obtained by keeping only the states corresponding to the 12 largest Hankel singular values. The neglected 48 states reflect unmodeled dynamics.

The above procedure to generate a nominal model is intended to reflect a common applications scenario, where various finite element models with a large number of states are available for a structural system, whos eigenvalues are not totally reliable. The nominal plant model is derived from the perturbed 60 state model, whos frequencies and damping values differ from the truth model even before an order reduction. This reflects inevitable parametric uncertainties about nominal eigenvalues. In addition, notice that the true mode shapes are preserved in the reduced nominal model to the extent of the approximation of the principal component vectors to the modal coordinates for lightly damped flexible structures [19]. Interestingly, in addition to the fact that eigenvalues define the frequency and damping of resonances in structural vibrations, eigenvalues as candidates for parametric uncertainties for flexible structures appears huristically attractive because they are also invariant to similarity transformation.

For the above reasons, we select a subset of the eigenvalues from the nominal model as candidates for parametric uncertainties and additive uncertainties to take into account unmodeled dynamics and mode shape errors, as illustrated in Figure 12. To demonstrate that this choice in the uncertainty structure is sufficient, suppose a true system consists of a high order state space system (A, B, C, D) where A has 2 by 2 block diagonal structure,

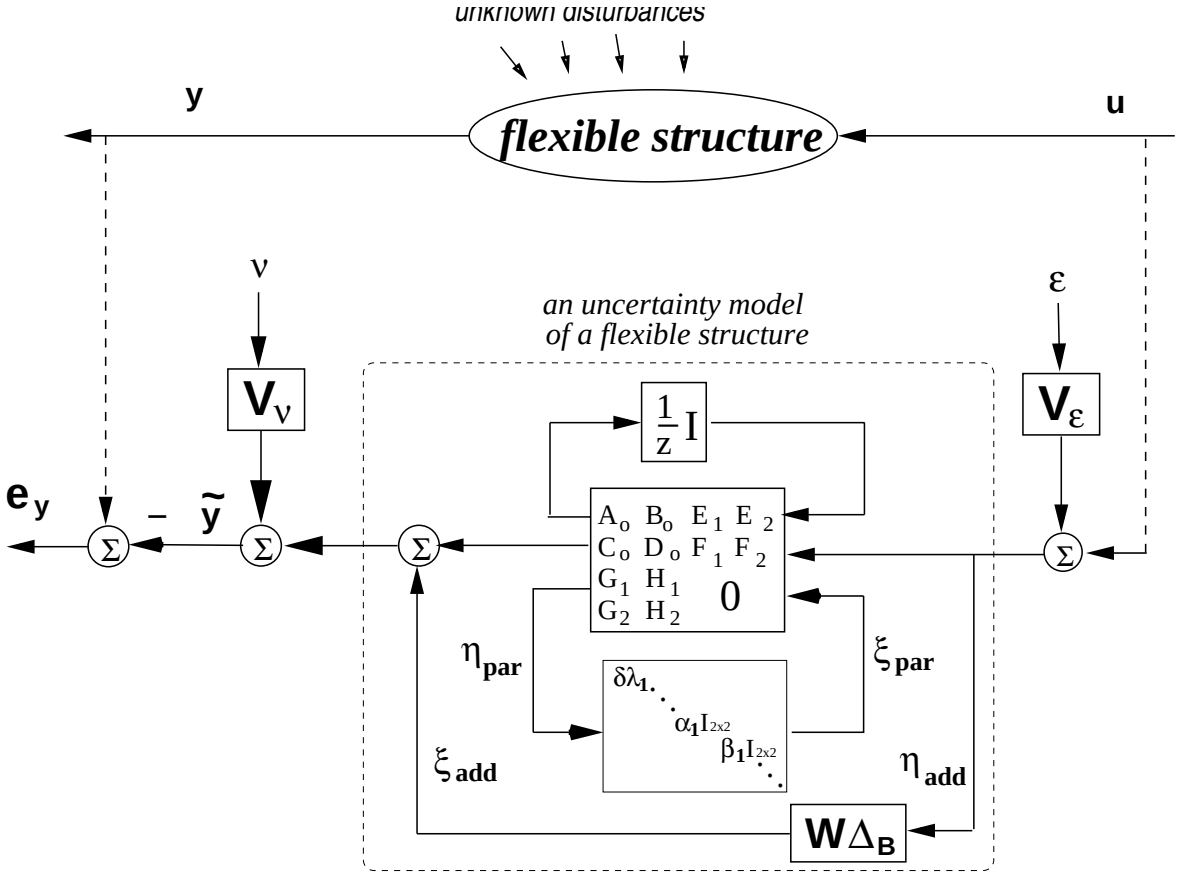

Figure 12: Uncertainty structure connections for a flexible structure

without loss of generality. Furthermore, suppose the matrices are partitioned as follows:

$$\begin{aligned} A &:= \begin{bmatrix} A_1 & \\ & A_2 \end{bmatrix} := \begin{bmatrix} \bar{A}_1 + \delta A_1 & \\ & \bar{A}_2 + \delta A_2 \end{bmatrix} \\ B &:= \begin{bmatrix} B_1 \\ B_2 \end{bmatrix} := \begin{bmatrix} \bar{B}_1 + \delta B_1 \\ \bar{B}_2 + \delta B_2 \end{bmatrix} \\ C &:= \begin{bmatrix} C_1 & C_2 \end{bmatrix} := \begin{bmatrix} \bar{C}_1 + \delta C_1 & \bar{C}_2 + \delta C_2 \end{bmatrix} \\ D &:= \bar{D} + \delta D \end{aligned}$$

where $(\bar{A}_1, \bar{B}_1, \bar{C}_1, \bar{D})$ is intended to represent a lower order nominal model. Then the input/output mapping of the true system can be written as

$$y = \left(\overbrace{\bar{C}_1(zI - \bar{A}_1 - \delta A_1)^{-1}\bar{B}_1 + \bar{D}}^{\substack{nominal\ model \\ with\ eigenvalue\ error}} + \Delta_{add} \right) u$$

where

$$\Delta_{add} := \underbrace{\delta D}_{\substack{feedthrough \\ gain\ error}} + \overbrace{\delta C_1(zI - A_1)^{-1}B_1}^{modal\ output\ error} + \underbrace{\bar{C}_1(zI - A_1)^{-1}\delta B_1}_{modal\ input\ error} + \overbrace{C_2(zI - A_2)^{-1}B_2}^{unmodeled\ dynamics}$$

The point here is that such true model can be captured by additive uncertainty structure, Δ_{add}, about a nominal model with eigenvalue uncertainties. The subsequent issue is how large are the uncertainty balls around the nominal model. Note that the modal output and input error terms arise from the errors δC_1 and δB_1 about their respective nominal values $\bar{C}_1$ and $\bar{B}_1$. Alternatively, δC_1 and δB_1 (along with δD) could be viewed and treated as additional parametric uncertainties in a state space model similar to the treatment of eigenvalue uncertainties captured in δA_1. However, the former untertainty terms are coordinate dependent unlike eigenvalues and hence difficult to treat them as parametric uncertainties.

Figure 13 shows the eigenvalues of the true and nominal models. The bottom figure is a magnified view of the 3 dominating structural resonance modes. The true and nominal eigenvalues appears to match quite closely although the subsequent frequency response comparisons show significant differences. The above tasks to generate the true and nominal models are given in subroutine **ex_cem_data**.

A comparison of the magnitude gains between the true (solid) and nominal (dash) models and the corresponding differences (dot) for all inputs and outputs are shown in Figure 14. The difference plot (dot) show significant discrepencies especially around structural resonance frequences. For example, consider a Bode plot for input 1 to output 1 as given in Figure 15. The figure shows that despite significant errors near their resonance frequencies, the nominal model approximates the three low frequency structural resonances at .9, 4.5 and 15 rad/sec Several higher frequency secondary resonances beyond 20 rad/sec are ignored by the nominal model. The largest discrepency between the true and nominal model frequency responses occurs at the dominating structural resonance at .9 rad/sec.

4.3 Smallest unmodeled dynamics for model validation

The main goal is to determine if the uncertainty bound estimation algorithm can capture both the true unmodeled dynamics and parametric uncertainties from data with reasonable a priori

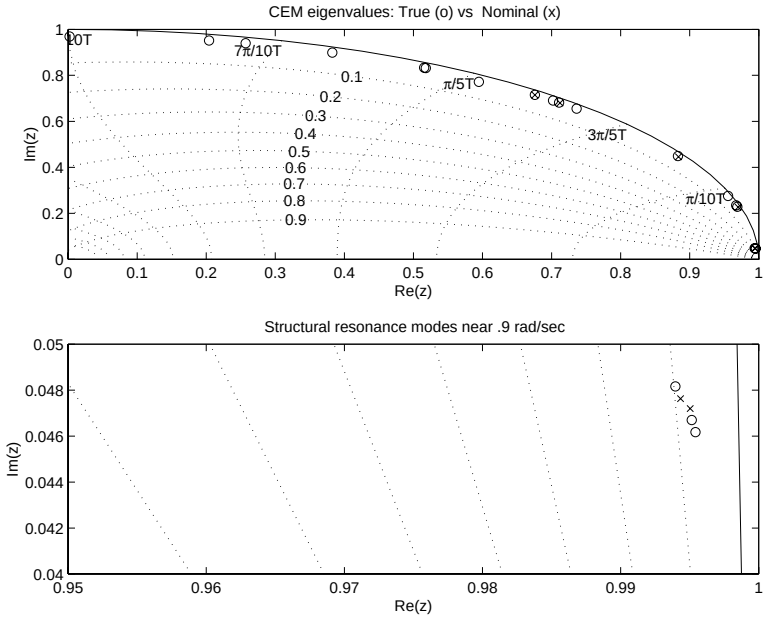

Figure 13: True and nominal eigenvalues of CEM model.

assumptions including noise allowances to account for unknown exogenous disturbances. In the following, we show the results based on the simplest case where only additive uncertainty is used to two other cases where we incorporate a priori parametric eigenvalue uncertainty allowances while seeking smallest additive uncertainties for model validation.

All three input test signals to the true system is generated by independently driving a fourth order Butterworth filter of bandwidth 5 Hertz with a white (bandwidth of Nyquist frequency) Gaussian random signal with unit standard deviation. The additive output noise is similarly chosen to be a white Gaussian random signal with a standard deviation of .01. The test data consists of two periods each about 408 seconds duration. The test signal is only applied during the first 204 seconds followed by free response for another 204 seconds. Notice that the next period begins after most of the transient free response decays to the output noise levels. This is designed to mitigate the erronous effects of nonperiodicity in the computation of DFT's for use in model validation.

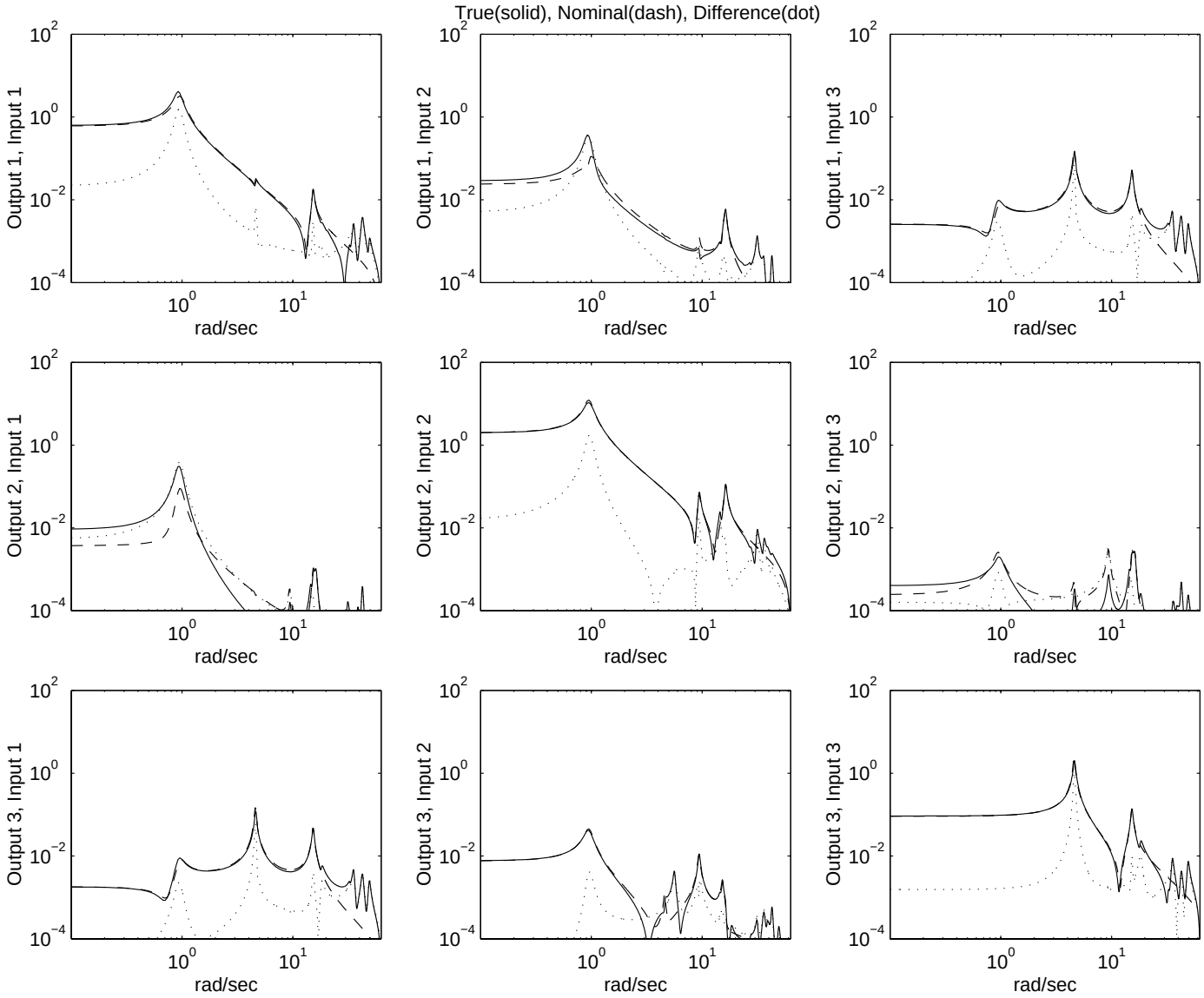

Figure 14: Frequency response magnitude comparison of CEM: outputs 1-3, inputs 1-3.

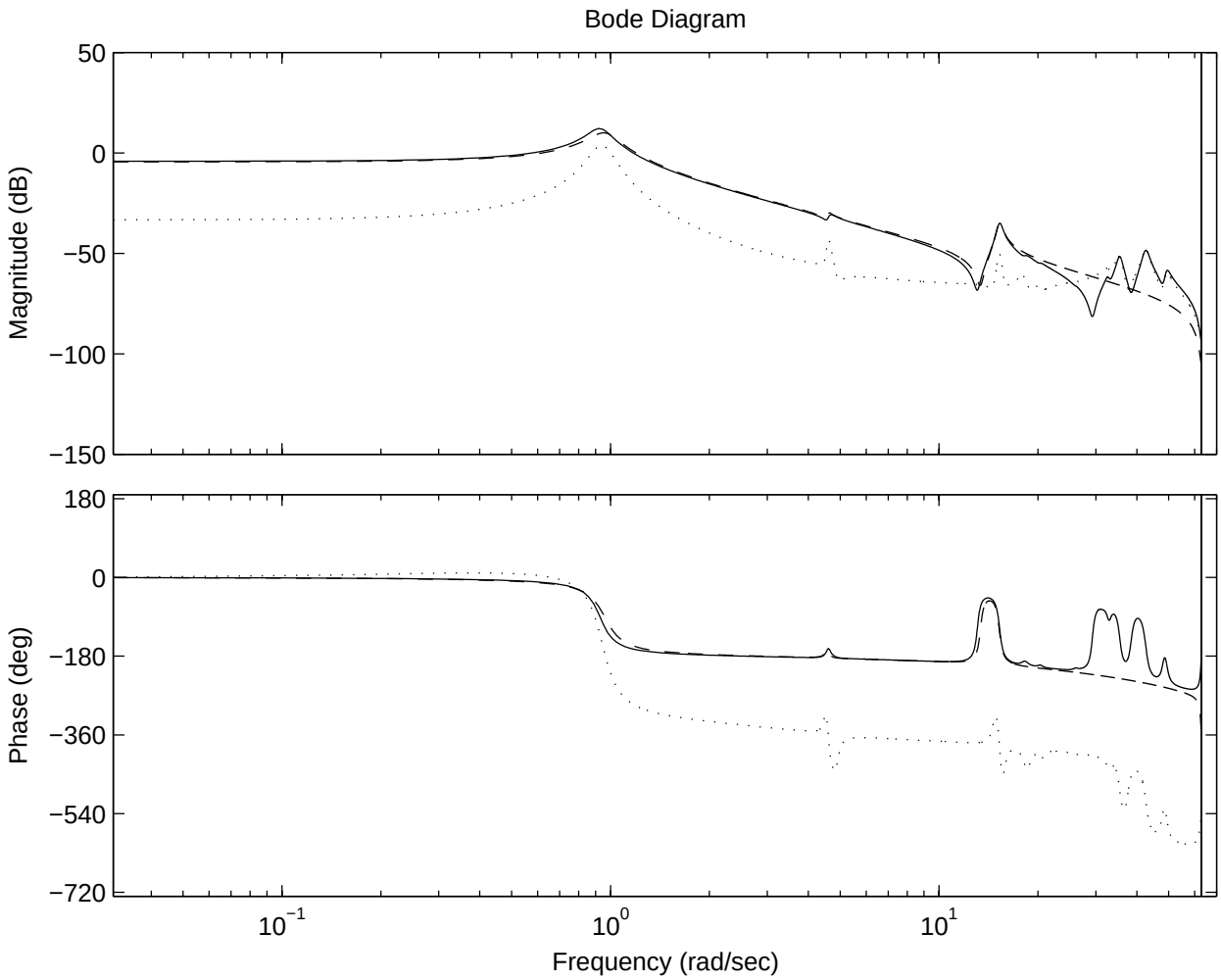

Figure 15: Frequency response comparison of CEM for output 1, input 1: True(solid), Nominal(dash), Difference(dot)

4.3.1 Smallest additive uncertainty

Step 1 Load output and input time histories

- Load raw time histories `ymeas_raw, rmeas_raw`:

```
   LOAD SIMULATED INPUT/OUTPUT DATA, ymeas_raw, rmeas_raw, t_raw
>> load ex_cem_data.mat
```

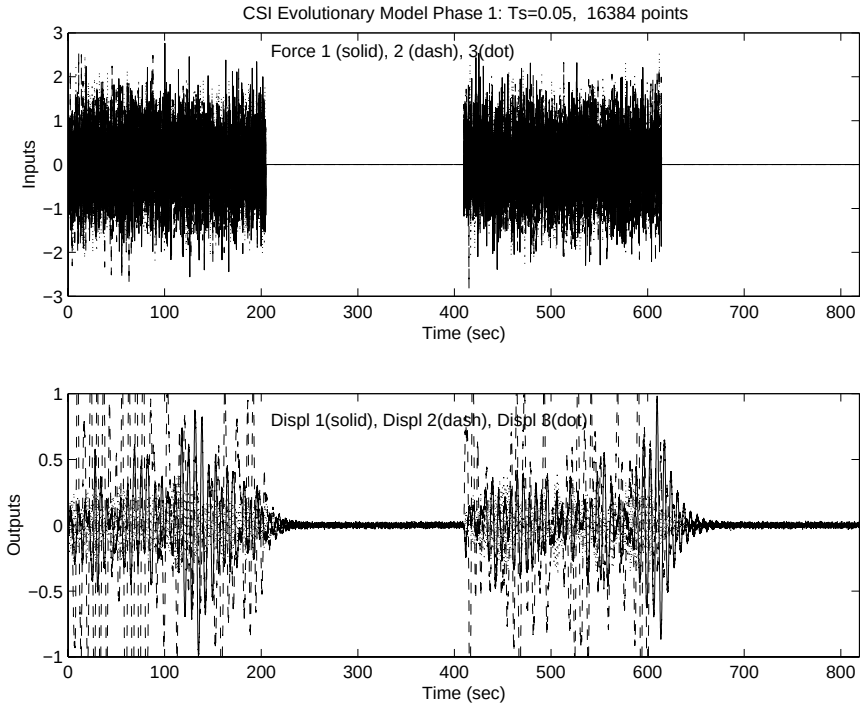

- Window data to form multiple samples by specifying number of nonzero points in sample, `npts`, number of points in sample to apply FFT, `nfft`, number of data points to overlap, `noverlp`. Plots for the sample time histories to be used in uncertainty bound estimation

```
>> [ymeas,yDFT,omeg,Ts,t,nout,nsamp] = form_sample(ymeas_raw,t_raw,winpara, "rec")
   PREPARE TIME RECORDS (WINDOWED-OVERLAPPED-ZERO APPENDED SAMPLES)
     Beginning time of data available = 0
     End time of data available = 819.15
     Number of time points in signal sample (npts) = 8192
     Number of points in sample (nfft), with zeros appended = 8192
     Number of data overlap (noverlp) = 0
>> [rmeas,rDFT,omeg,Ts,t,ninp,nsamp] = form_sample(rmeas_raw,t_raw,winpara,"rec")
   PREPARE TIME RECORDS (WINDOWED-OVERLAPPED-ZERO APPENDED SAMPLES)
     Beginning time of data available = 0
     End time of data available = 819.15
     Number of time points in signal sample (npts) = 8192
     Number of points in sample (nfft), with zeros appended = 8192
     Number of data overlap (noverlp) = 0

 There are 2 data samples - select sample number for MV.. 1
```

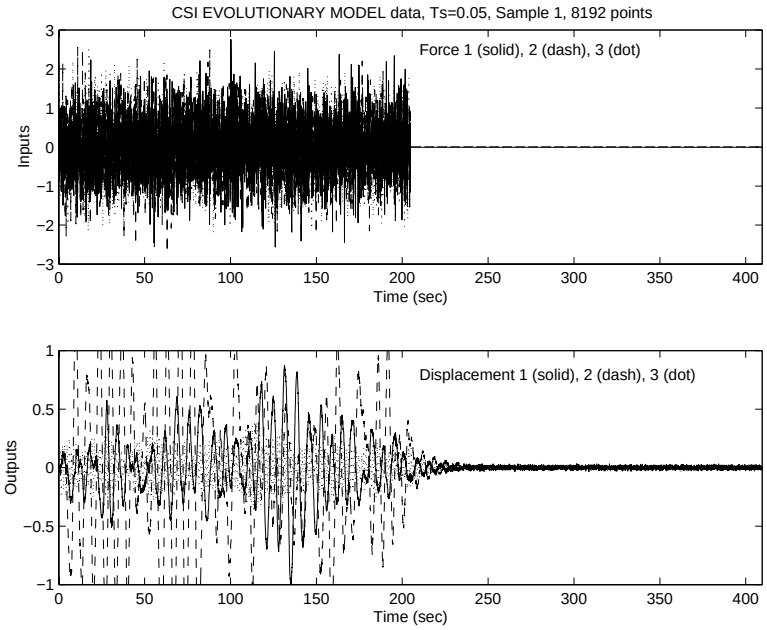

Step 2 Form allowance filters for output noise and exogenous disturbances

- Load output noise time history variable, `ynoise` and fit filter, `Vnoise`

```
   LOAD TRUE OUTPUT NOISE, ynoise
>> load ex_cem_truenoise.mat
>> [vVnoise,Vnoise] = noise_allow(ntime,Ts,nout,["noise_allow_" label ":"],ynoise,t_raw)
   PREPARE TIME RECORDS (WINDOWED-OVERLAPPED-ZERO APPENDED SAMPLES)
     Beginning time of data available = 0
     End time of data available = 819.15
     Number of time points in signal sample (npts) = 8192
     Number of points in sample (nfft), with zeros appended = 8192
     Number of data overlap (noverlp) = 4096
       Interactively fit magnitude DFT, Channel 1..
         Re-fit Channel 1 ? (y/n) n
       Interactively fit magnitude DFT, Channel 2..
         Re-fit Channel 2 ? (y/n) n
       Interactively fit magnitude DFT, Channel 3..
         Re-fit Channel 3 ? (y/n) n
```

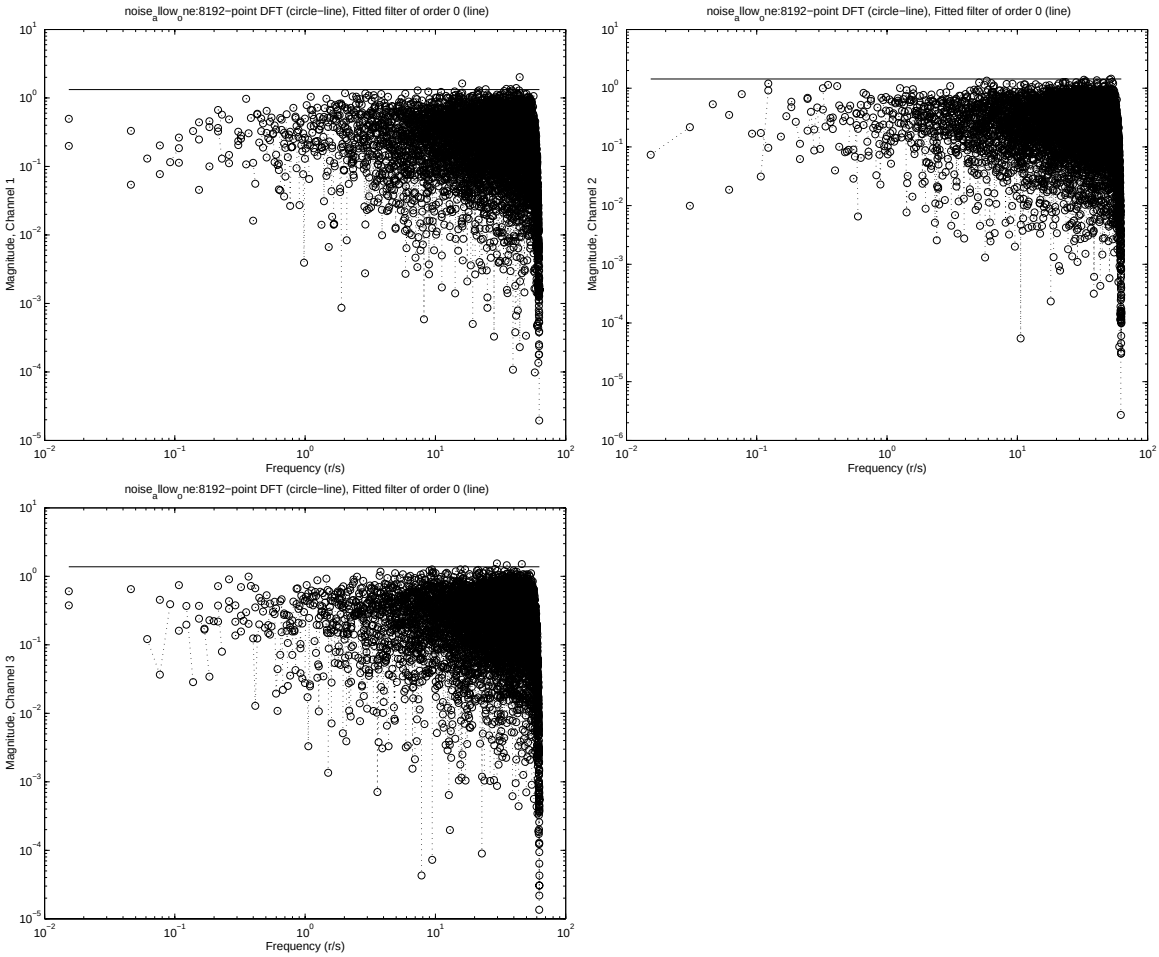

- Define allowance filter for exogenous disturbances, `Vdist` from expected variance

```
>> [vVdist,Vdist] = noise_allow(ntime,Ts,ninp,["dist_allow_" label ":"]
   CONSTRUCT EXOGENOUS SIGNAL ALLOWANCE FILTER FROM VARIANCE ESTIMATE
     Enter variance(MSV) of unknown signal, Channel 1.. 0
     Enter variance(MSV) of unknown signal, Channel 2.. 0
     Enter variance(MSV) of unknown signal, Channel 3.. 0
```

Step 3 Load nominal model, `Po`

```
   LOAD NOMINAL MODEL, Po (SS format)
>> load ex_cem_nominal.mat
   TRUE EIGENVALUE    PERTURBED EIGENVALUE       DIFFERENCE

ans =

   0.9954 + 0.0462i   0.9943 + 0.0476i  -0.0011           -0.0015
   0.9951 + 0.0467i   0.9953 + 0.0470i   0.0001           -0.0003
   0.9940 + 0.0482i   0.9948 + 0.0474i   0.0009            0.0008
   0.9689 + 0.2280i   0.9703 + 0.2264i   0.0014            0.0016
   0.9673 + 0.2342i   0.9673 + 0.2337i  -0.0000            0.0006
   0.9555 + 0.2754i   0.9560 + 0.2751i   0.0005            0.0003
   0.8830 + 0.4490i   0.8827 + 0.4485i  -0.0003            0.0005
   0.7363 + 0.6552i   0.7364 + 0.6549i   0.0001            0.0003
```

```
   0.7109 + 0.6816i   0.7114 + 0.6809i   0.0005            0.0006
   0.7021 + 0.6903i   0.7019 + 0.6882i  -0.0001            0.0021
   0.6758 + 0.7150i   0.6766 + 0.7148i   0.0008            0.0002
   0.5948 + 0.7718i   0.5962 + 0.7733i   0.0014           -0.0014
   0.5179 + 0.8319i   0.5180 + 0.8324i   0.0002           -0.0005
   0.5155 + 0.8333i   0.5148 + 0.8351i  -0.0007           -0.0018
   0.3825 + 0.8989i   0.3822 + 0.9003i  -0.0003           -0.0014
   0.2570 + 0.9397i   0.2590 + 0.9392i   0.0020            0.0005
   0.2040 + 0.9515i   0.2042 + 0.9522i   0.0002           -0.0006
   0.0021 + 0.9691i   0.0013 + 0.9675i  -0.0008            0.0017
  -0.0630 + 0.9658i  -0.0637 + 0.9658i  -0.0007           -0.0000
  -0.0763 + 0.9645i  -0.0758 + 0.9666i   0.0005           -0.0021
  -0.0837 + 0.9638i  -0.0838 + 0.9636i  -0.0001            0.0001
  -0.0971 + 0.9622i  -0.0965 + 0.9602i   0.0006            0.0020
  -0.1948 + 0.9453i  -0.1939 + 0.9450i   0.0009            0.0003
  -0.2219 + 0.9387i  -0.2208 + 0.9394i   0.0011           -0.0007
  -0.3244 + 0.9061i  -0.3240 + 0.9049i   0.0004            0.0013
  -0.3276 + 0.9049i  -0.3292 + 0.9039i  -0.0016            0.0010
  -0.3396 + 0.9002i  -0.3394 + 0.8991i   0.0002            0.0010
  -0.4943 + 0.8214i  -0.4933 + 0.8220i   0.0010           -0.0006
  -0.5133 + 0.8091i  -0.5131 + 0.8083i   0.0002            0.0008
  -0.7389 + 0.6002i  -0.7396 + 0.6018i  -0.0007           -0.0015

   NOMINAL EIGENVALUE (BALANCED REDUCED PERTURBED)

ans =

   0.9950 + 0.0472i
   0.9950 - 0.0472i
   0.9943 + 0.0476i
   0.9943 - 0.0476i
   0.9701 + 0.2264i
   0.9701 - 0.2264i
   0.8838 + 0.4457i
   0.8838 - 0.4457i
   0.7121 + 0.6800i
   0.7121 - 0.6800i
   0.6759 + 0.7144i
   0.6759 - 0.7144i
```

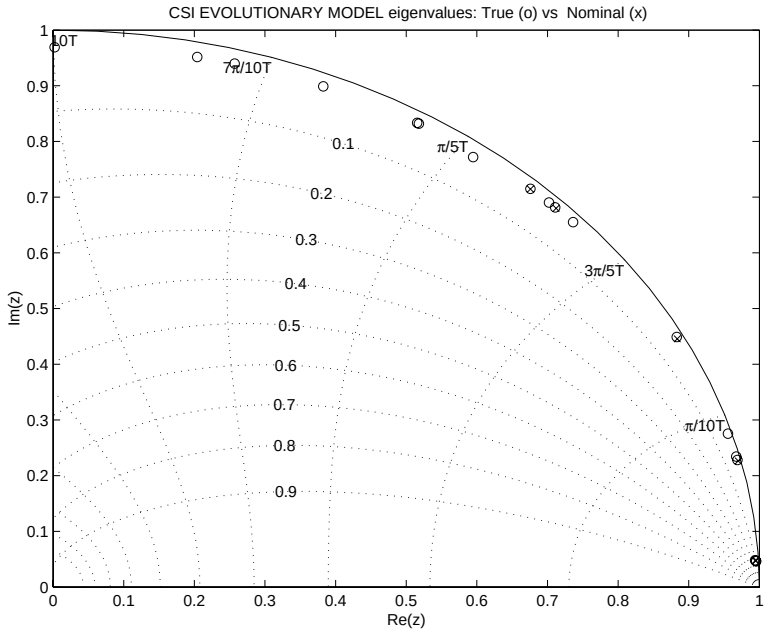

Step 4 Choose additive plus eigenvalue uncertainty structure to form augmented plant `Gaug`. The first three modes are chosen as uncertain parameters.

```
>> [Gaug,blkf,dimp,uncstr_choice] = ubid_uncstr(Po,Ts)
   Form augmented plant with uncertainty structure
   OUTPUTS                                              INPUTS
      eta (dimp(1))   <----- [G11, G12, G13]  <----   xi    (dimp(2))
      y   (dimp(3))   <----- [G21, G22, G23]  <----   epsil (dimp(4))
                                              <----   nu    (dimp(5))
                                              <----   u     (dimp(6))
      ALL WEIGHTS FOR UNKNOWN EXOGENOUS INPUTS, Vdist=Vnoise=I

   Select from the following list of uncertainty structures:
   AUGMENTED PLANT WITH ...
      0.  PROVIDED BY USER
      1.  ADDITIVE UNCERTAINTY
      2.  ADDITIVE + EIGENVALUE UNCERTAINTIES
      3.  FULL OUTPUT MULTIPLICATIVE UNCERTAINTY
      4.  FULL OUTPUT MULTIPLICATIVE + EIGENVALUE UNCERTAINTIES
      5.  DIAGONAL OUTPUT MULTIPLIATIVE UNCERTAINTY
      6.  DIAGONAL OUTPUT MULTIPLICATIVE + EIGENVALUE UNCERTAINTIES
      7.  FULL INPUT MULTIPLICATIVE UNCERTAINTY
      8.  FULL INPUT MULTIPLICATIVE + EIGENVALUE UNCERTAINTIES
      9.  DIAGONAL INPUT MULTIPLIATIVE UNCERTAINTY
     10.  DIAGONAL INPUT MULTIPLIATIVE + EIGENVALUE UNCERTAINTIES
   Enter the uncertainty structure desired (0 - 10)  ----> 1

  ADDITIVE UNCERTAINTY
    eta_add(3)     <----- [G11, G12, G13]  <----    xi_add(3)
    y(3)           <----- [G21, G22, G23]  <----    epsil(3)
                                           <----    nu(3)
                                           <----    u(3)
```

Step 5 Choose reference weights, `Wunc` used in smallest set uncertainty optimization. As defined by `blkf`, the uncertainty blocks consists of six repeated real 2 by 2 blocks with a single full 3 by 3 complex block.

```
>> [Wunc,par_bnd] = weightunc(blkf,om,Ts)

   Define optimizing weights for uncertainty blocks ...

blkf =

     3     3

     Enter CONSTANT weights (over all frequencies) for each uncertainty block as a
     COLUMN vector (corresponds to BLKF variable) --->  1
```

Step 6 Solve for a smallest scaled model validating set.

```
>> [unc_frd,x2,options,vFLAG] = mnmvcl(rDFTi,yDFTi,Gaug,blkf,vVnoise,vVdist,Ts,...
>> Wunc,iv_low,iv_hig,nskip,ndist)
   Check feasible conditions (existence) for model validation:
    -Necessary condition eq(16) satisfied: M full row rank => eyo E Im(M)
    -Necessary condition eq(20) satisfied
     NM_beta is full row rank (T2 does not exist) => LHS of eq(20) is 0

=====================================================================
 [G11 G12] = 0 satisfied, Convex Program solved using LMI Toolbox
=====================================================================
>> [x,copt,EXITFLAG] = ubid_lmi(n_phi,n_psi,xio_ii,etao_ii,EF_ii,Wunc_ii,bo,blkf)
 FREQ 1  0.107 (r/s)  UNC = [  0.002]
>> [x,copt,EXITFLAG] = ubid_lmi(n_phi,n_psi,xio_ii,etao_ii,EF_ii,Wunc_ii,bo,blkf)
 FREQ 2  0.199 (r/s)  UNC = [  0.004]
>> [x,copt,EXITFLAG] = ubid_lmi(n_phi,n_psi,xio_ii,etao_ii,EF_ii,Wunc_ii,bo,blkf)
 FREQ 3  0.291 (r/s)  UNC = [  0.003]
>> [x,copt,EXITFLAG] = ubid_lmi(n_phi,n_psi,xio_ii,etao_ii,EF_ii,Wunc_ii,bo,blkf)
 FREQ 4  0.383 (r/s)  UNC = [  0.031]
>> [x,copt,EXITFLAG] = ubid_lmi(n_phi,n_psi,xio_ii,etao_ii,EF_ii,Wunc_ii,bo,blkf)
 FREQ 5  0.476 (r/s)  UNC = [  0.021]
>> [x,copt,EXITFLAG] = ubid_lmi(n_phi,n_psi,xio_ii,etao_ii,EF_ii,Wunc_ii,bo,blkf)
 FREQ 6  0.568 (r/s)  UNC = [  0.042]
>> [x,copt,EXITFLAG] = ubid_lmi(n_phi,n_psi,xio_ii,etao_ii,EF_ii,Wunc_ii,bo,blkf)
 FREQ 7  0.660 (r/s)  UNC = [  0.025]
>> [x,copt,EXITFLAG] = ubid_lmi(n_phi,n_psi,xio_ii,etao_ii,EF_ii,Wunc_ii,bo,blkf)
 FREQ 8  0.752 (r/s)  UNC = [  0.205]
>> [x,copt,EXITFLAG] = ubid_lmi(n_phi,n_psi,xio_ii,etao_ii,EF_ii,Wunc_ii,bo,blkf)
 FREQ 9  0.844 (r/s)  UNC = [  0.419]
>> [x,copt,EXITFLAG] = ubid_lmi(n_phi,n_psi,xio_ii,etao_ii,EF_ii,Wunc_ii,bo,blkf)
 FREQ 10  0.936 (r/s)  UNC = [  1.357]
     .
     .
     .
>> [x,copt,EXITFLAG] = ubid_lmi(n_phi,n_psi,xio_ii,etao_ii,EF_ii,Wunc_ii,bo,blkf)
 FREQ 200  18.423 (r/s)  UNC = [  0.000]
>> [x,copt,EXITFLAG] = ubid_lmi(n_phi,n_psi,xio_ii,etao_ii,EF_ii,Wunc_ii,bo,blkf)
 FREQ 201  18.515 (r/s)  UNC = [  0.000]
```

```
>> [x,copt,EXITFLAG] = ubid_lmi(n_phi,n_psi,xio_ii,etao_ii,EF_ii,Wunc_ii,bo,blkf)
 FREQ 202  18.607 (r/s)  UNC = [  0.000]
>> [x,copt,EXITFLAG] = ubid_lmi(n_phi,n_psi,xio_ii,etao_ii,EF_ii,Wunc_ii,bo,blkf)
 FREQ 203  18.699 (r/s)  UNC = [  0.000]
>> [x,copt,EXITFLAG] = ubid_lmi(n_phi,n_psi,xio_ii,etao_ii,EF_ii,Wunc_ii,bo,blkf)
 FREQ 204  18.791 (r/s)  UNC = [  0.000]
>> [Wid_z] = ovbndunc(unc_frd,blkf,omeg,iv_low,iv_hig,Ts)
    Curve fit uncertainty bound # 1, blkf = [3,3] ..
    Plot summary of weights? (y/n) n
```

Figure 16 shows the smallest additive uncertainty (circle) that satisfy model validation conditions as compared to the true additive uncertainty (dotted line). A fitted additive uncertainty model is also shown (dashdot line) as a reference. The identified smallest additive uncertainty accurately recovers the true additive uncertainty. However, notice that the true additive uncertainty is due to a combination of both parametric eigenvalue uncertainties and unmodeled dynamics while the identified uncertainty model consists only of additive uncertainty. This demonstrates a limiting property that model validating conditions are only necessary conditions in determining "correct" uncertainty models, i.e., just matching input-output responses are not germane to uncertainty structure. In this example, it is clear that a nominal allowance in the output noise did not have a significant effect on the identified additive uncertainty. Finally, note that due to the simplicity of the uncertainty structure,

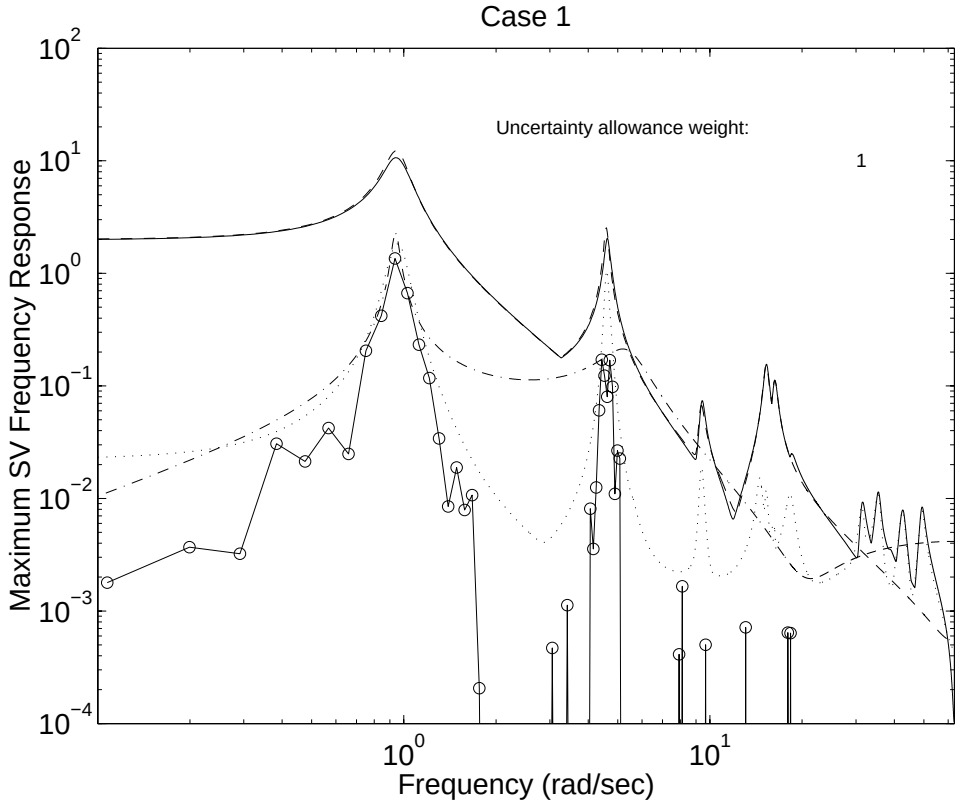

Figure 16: Identified smallest additive uncertainty (circle), true additive uncertainty (dot)

the numerical computations involved convex optimizations and was very efficient.

4.3.2 Smallest additive uncertainty with eigenvalue uncertainty (.001) allowance

Step 4 Choose additive plus eigenvalue uncertainty structure to form augmented plant `Gaug`. The first three modes are chosen as uncertain parameters.

```
   Form augmented plant with uncertainty structure
   OUTPUTS                                              INPUTS
      eta (dimp(1))   <----- [G11, G12, G13]  <----   xi    (dimp(2))
      y   (dimp(3))   <----- [G21, G22, G23]  <----   epsil (dimp(4))
                                              <----   nu    (dimp(5))
                                              <----   u     (dimp(6))
      ALL WEIGHTS FOR UNKNOWN EXOGENOUS INPUTS, Vdist=Vnoise=I

   Select from the following list of uncertainty structures:
   AUGMENTED PLANT WITH ...
      0.  PROVIDED BY USER
      1.  ADDITIVE UNCERTAINTY
      2.  ADDITIVE + EIGENVALUE UNCERTAINTIES
      3.  FULL OUTPUT MULTIPLICATIVE UNCERTAINTY
      4.  FULL OUTPUT MULTIPLICATIVE + EIGENVALUE UNCERTAINTIES
      5.  DIAGONAL OUTPUT MULTIPLIATIVE UNCERTAINTY
      6.  DIAGONAL OUTPUT MULTIPLICATIVE + EIGENVALUE UNCERTAINTIES
      7.  FULL INPUT MULTIPLICATIVE UNCERTAINTY
      8.  FULL INPUT MULTIPLICATIVE + EIGENVALUE UNCERTAINTIES
      9.  DIAGONAL INPUT MULTIPLIATIVE UNCERTAINTY
     10.  DIAGONAL INPUT MULTIPLIATIVE + EIGENVALUE UNCERTAINTIES
   Enter the uncertainty structure desired (0 - 10)  ----> 2

 Mode number    z-eigenvalue          s-eigenvalue
-----------------------------------------------------------
    1         0.99504+0.047202i     -0.077057+0.94803i
    2         0.99433+0.047632i     -0.090722+0.95733i
    3         0.97008+0.22638i     -0.077366+4.5851i
    4         0.88381+0.44571i     -0.2043+9.3416i
    5         0.71212+0.68002i     -0.309306+15.2468i
    6         0.67588+0.71436i     -0.33432+16.2614i
 SELECT EIGENVALUES TO INCLUDE AS PARAMETRIC UNCERTAINTY
     Enter a row of Mode numbers (in increasing order).. [1:3]

AUGMENTED PLANT WITH EIGENVALUE UNCERTAINTIES
State-space model with 15 outputs, 15 inputs, and 12 states.
  OUTPUTS
    due to 0 real eigenvalue uncertainties
    due to 3 complex conjugate eigenvalue pair uncertainties
    due to 3 physical outputs
  INPUTS
    due to 0 real eigenvalue uncertainties
    due to 3 complex conjugate eigenvalue pair uncertainties
    due to 3 physical inputs
>> [Prr,blk_eig,nxi_eig,eigz,nreal] = sseigunc(Po,Ts)

AUGMENTED PLANT WITH ADDITIVE + EIGENVALUE UNCERTAINTIES
    eta_eig(12)     <----- [G11, G12, G13]  <----    xi_eig(12)
    eta_add(3)     <----- [G21, G22, G23]  <----    xi_add(3)
```

```
    y(3)                                    <----    epsil(3)
                                            <----    nu(3)
                                            <----    u(3)
```

Step 5 Choose reference weights, `Wunc` used in smallest set uncertainty optimization. As defined by `blkf`, the uncertainty blocks consists of six repeated real 2 by 2 blocks with a single full 3 by 3 complex block.

```
>> [Wunc,par_bnd] = weightunc(blkf,om,Ts)
   Define optimizing weights for uncertainty blocks ...

blkf =

    -2     0
    -2     0
    -2     0
    -2     0
    -2     0
    -2     0
     3     3

     Enter CONSTANT weights (over all frequencies) for each uncertainty block as a
     COLUMN vector (corresponds to BLKF variable) --->  [.001*ones(6,1);1]
```

Step 6 Solve for a smallest scaled model validating set.

```
>> [unc_frd,x2,options,vFLAG] = mnmvcl(rDFTi,yDFTi,Gaug,blkf,vVnoise,vVdist,Ts,...
>> Wunc,iv_low,iv_hig,nskip,ndist)
   Check feasible conditions (existence) for model validation:
    -Necessary condition eq(16) satisfied: M full row rank => eyo E Im(M)
    -Necessary condition eq(20) satisfied
     NM_beta is full row rank (T2 does not exist) => LHS of eq(20) is 0

============================================================
 [G11 G12] .ne. 0,  use  SQP routine in Optimization Toolbox
============================================================
>> [x,FVAL,EXITFLAG] = fmincon("fungrad",x0,[],[],[],[],vlb,vub,"congrad",options,...
>> xio_ii,etao_ii,EF_ii,GOMEG_ii,Wunc_ii,bo,blkf,ncolM,minrankNMb,minrankM,nrrs,nrcs)
 FREQ 1  0.107 (r/s)  UNC = [  0.003]
>> [x,FVAL,EXITFLAG] = fmincon("fungrad",x0,[],[],[],[],vlb,vub,"congrad",options,...
>> xio_ii,etao_ii,EF_ii,GOMEG_ii,Wunc_ii,bo,blkf,ncolM,minrankNMb,minrankM,nrrs,nrcs)
 FREQ 2  0.199 (r/s)  UNC = [  0.003]
>> [x,FVAL,EXITFLAG] = fmincon("fungrad",x0,[],[],[],[],vlb,vub,"congrad",options,...
>> xio_ii,etao_ii,EF_ii,GOMEG_ii,Wunc_ii,bo,blkf,ncolM,minrankNMb,minrankM,nrrs,nrcs)
 FREQ 3  0.291 (r/s)  UNC = [  0.004]
>> [x,FVAL,EXITFLAG] = fmincon("fungrad",x0,[],[],[],[],vlb,vub,"congrad",options,...
>> xio_ii,etao_ii,EF_ii,GOMEG_ii,Wunc_ii,bo,blkf,ncolM,minrankNMb,minrankM,nrrs,nrcs)
 FREQ 4  0.383 (r/s)  UNC = [  0.008]
>> [x,FVAL,EXITFLAG] = fmincon("fungrad",x0,[],[],[],[],vlb,vub,"congrad",options,...
>> xio_ii,etao_ii,EF_ii,GOMEG_ii,Wunc_ii,bo,blkf,ncolM,minrankNMb,minrankM,nrrs,nrcs)
 FREQ 5  0.476 (r/s)  UNC = [  0.006]
>> [x,FVAL,EXITFLAG] = fmincon("fungrad",x0,[],[],[],[],vlb,vub,"congrad",options,...
>> xio_ii,etao_ii,EF_ii,GOMEG_ii,Wunc_ii,bo,blkf,ncolM,minrankNMb,minrankM,nrrs,nrcs)
```

```
 FREQ 6  0.568 (r/s)  UNC = [  0.002]
>> [x,FVAL,EXITFLAG] = fmincon("fungrad",x0,[],[],[],[],vlb,vub,"congrad",options,...
>> xio_ii,etao_ii,EF_ii,GOMEG_ii,Wunc_ii,bo,blkf,ncolM,minrankNMb,minrankM,nrrs,nrcs)
 FREQ 7  0.660 (r/s)  UNC = [  0.002]
>> [x,FVAL,EXITFLAG] = fmincon("fungrad",x0,[],[],[],[],vlb,vub,"congrad",options,...
>> xio_ii,etao_ii,EF_ii,GOMEG_ii,Wunc_ii,bo,blkf,ncolM,minrankNMb,minrankM,nrrs,nrcs)
 FREQ 8  0.752 (r/s)  UNC = [  0.010]
>> [x,FVAL,EXITFLAG] = fmincon("fungrad",x0,[],[],[],[],vlb,vub,"congrad",options,...
>> xio_ii,etao_ii,EF_ii,GOMEG_ii,Wunc_ii,bo,blkf,ncolM,minrankNMb,minrankM,nrrs,nrcs)
 FREQ 9  0.844 (r/s)  UNC = [  0.059]
>> [x,FVAL,EXITFLAG] = fmincon("fungrad",x0,[],[],[],[],vlb,vub,"congrad",options,...
>> xio_ii,etao_ii,EF_ii,GOMEG_ii,Wunc_ii,bo,blkf,ncolM,minrankNMb,minrankM,nrrs,nrcs)
 FREQ 10  0.936 (r/s)  UNC = [  0.154]   MAX NUMBER ITERATION REACHED
      .
      .
      .
>> [x,FVAL,EXITFLAG] = fmincon("fungrad",x0,[],[],[],[],vlb,vub,"congrad",options,...
>> xio_ii,etao_ii,EF_ii,GOMEG_ii,Wunc_ii,bo,blkf,ncolM,minrankNMb,minrankM,nrrs,nrcs)
 FREQ 200  18.423 (r/s)  UNC = [  0.001]
>> [x,FVAL,EXITFLAG] = fmincon("fungrad",x0,[],[],[],[],vlb,vub,"congrad",options,...
>> xio_ii,etao_ii,EF_ii,GOMEG_ii,Wunc_ii,bo,blkf,ncolM,minrankNMb,minrankM,nrrs,nrcs)
 FREQ 201  18.515 (r/s)  UNC = [  0.001]
>> [x,FVAL,EXITFLAG] = fmincon("fungrad",x0,[],[],[],[],vlb,vub,"congrad",options,...
>> xio_ii,etao_ii,EF_ii,GOMEG_ii,Wunc_ii,bo,blkf,ncolM,minrankNMb,minrankM,nrrs,nrcs)
 FREQ 202  18.607 (r/s)  UNC = [  0.001]
>> [x,FVAL,EXITFLAG] = fmincon("fungrad",x0,[],[],[],[],vlb,vub,"congrad",options,...
>> xio_ii,etao_ii,EF_ii,GOMEG_ii,Wunc_ii,bo,blkf,ncolM,minrankNMb,minrankM,nrrs,nrcs)
 FREQ 203  18.699 (r/s)  UNC = [  0.000]
>> [x,FVAL,EXITFLAG] = fmincon("fungrad",x0,[],[],[],[],vlb,vub,"congrad",options,...
>> xio_ii,etao_ii,EF_ii,GOMEG_ii,Wunc_ii,bo,blkf,ncolM,minrankNMb,minrankM,nrrs,nrcs)
 FREQ 204  18.791 (r/s)  UNC = [  0.001]
>> [Wid_z] = ovbndunc(unc_frd,blkf,omeg,iv_low,iv_hig,Ts)
    Curve fit uncertainty bound # 1, blkf = [-2,0] ..
    Curve fit uncertainty bound # 2, blkf = [-2,0] ..
    Curve fit uncertainty bound # 3, blkf = [-2,0] ..
    Curve fit uncertainty bound # 4, blkf = [-2,0] ..
    Curve fit uncertainty bound # 5, blkf = [-2,0] ..
    Curve fit uncertainty bound # 6, blkf = [-2,0] ..
    Curve fit uncertainty bound # 7, blkf = [3,3] ..
    Plot summary of weights? (y/n) n
```

Figure 17 shows the identified smallest additive uncertainty (circle) subject to eigenvalue uncertainty allowance (of .001 on the first three structural modes) as compared to the true additive error (dot). A fitted additive uncertainty model is also shown (dashdot line) as a reference. The level of the identified smallest additive uncertainty is smaller as expected than the true additive uncertainty because of the eigenvalue uncertainty allowance of .001 on the first three structural modes. Apparently the eigenvalue uncertainty allowance of .001 is not insignificant but less than the true eigenvalue error which is between .0003 to .0021 (please refer to the eigenvalues given in Step 3 of the previous case). Obviously, there are no clear rules in the selection of a priori levels of parametric uncertainty allowances. However, it is clear that incorporating "reasonable" levels of parametric uncertainty allowances may be helpful in determining accurate uncertainty models. In this case involving repeated scalar parametric uncertainties, solving a sequence of nonlinear optimization problems were required and the numerical computations involved were non trivial but is not central to the

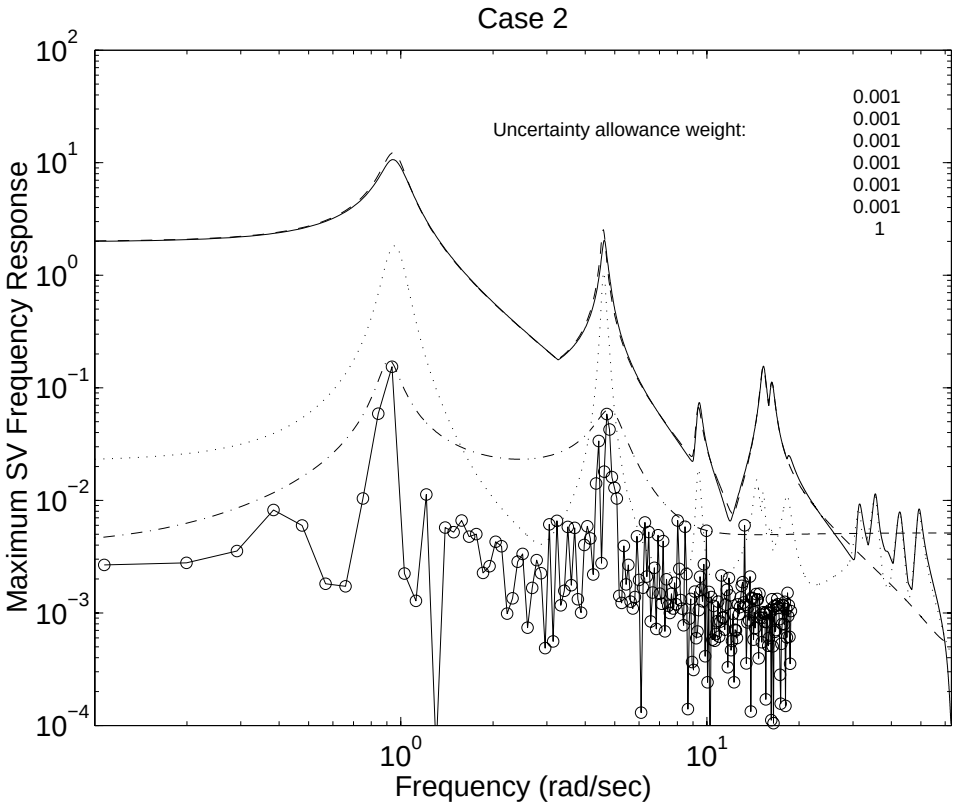

Figure 17: Identified smallest additive uncertainty (circle) with eigenvalue uncertainty allowance (.001), true additive uncertainty (dot)

study reported here.

4.3.3 Smallest additive uncertainty with eigenvalue uncertainty (.002) allowance

Step 5 Choose reference weights, `Wunc` used in smallest set uncertainty optimization. As defined by `blkf`, the uncertainty blocks consists of six repeated real 2 by 2 blocks with a single full 3 by 3 complex block.

```
>> [Wunc,par_bnd] = weightunc(blkf,om,Ts)
   Define optimizing weights for uncertainty blocks ...

blkf =

    -2     0
    -2     0
    -2     0
    -2     0
    -2     0
    -2     0
     3     3

     Enter CONSTANT weights (over all frequencies) for each uncertainty block as a
     COLUMN vector (corresponds to BLKF variable) --->  [.002*ones(6,1);1]
```

Step 6 Solve for a smallest scaled model validating set.

```
>> [unc_frd,x2,options,vFLAG] = mnmvcl(rDFTi,yDFTi,Gaug,blkf,vVnoise,vVdist,Ts,Wunc,iv_low,iv_hig,
   Check feasible conditions (existence) for model validation:
    -Necessary condition eq(16) satisfied: M full row rank => eyo E Im(M)
    -Necessary condition eq(20) satisfied
     NM_beta is full row rank (T2 does not exist) => LHS of eq(20) is 0

============================================================
 [G11 G12] .ne. 0,  use  SQP routine in Optimization Toolbox
============================================================
>> [x,FVAL,EXITFLAG] = fmincon("fungrad",x0,[],[],[],[],vlb,vub,"congrad",options,...
>> xio_ii,etao_ii,EF_ii,GOMEG_ii,Wunc_ii,bo,blkf,ncolM,minrankNMb,minrankM,nrrs,nrcs)
 FREQ 1  0.107 (r/s)  UNC = [  0.002]
>> [x,FVAL,EXITFLAG] = fmincon("fungrad",x0,[],[],[],[],vlb,vub,"congrad",options,...
>> xio_ii,etao_ii,EF_ii,GOMEG_ii,Wunc_ii,bo,blkf,ncolM,minrankNMb,minrankM,nrrs,nrcs)
 FREQ 2  0.199 (r/s)  UNC = [  0.003]
>> [x,FVAL,EXITFLAG] = fmincon("fungrad",x0,[],[],[],[],vlb,vub,"congrad",options,...
>> xio_ii,etao_ii,EF_ii,GOMEG_ii,Wunc_ii,bo,blkf,ncolM,minrankNMb,minrankM,nrrs,nrcs)
 FREQ 3  0.291 (r/s)  UNC = [  0.004]
>> [x,FVAL,EXITFLAG] = fmincon("fungrad",x0,[],[],[],[],vlb,vub,"congrad",options,...
>> xio_ii,etao_ii,EF_ii,GOMEG_ii,Wunc_ii,bo,blkf,ncolM,minrankNMb,minrankM,nrrs,nrcs)
 FREQ 4  0.383 (r/s)  UNC = [  0.008]
>> [x,FVAL,EXITFLAG] = fmincon("fungrad",x0,[],[],[],[],vlb,vub,"congrad",options,...
>> xio_ii,etao_ii,EF_ii,GOMEG_ii,Wunc_ii,bo,blkf,ncolM,minrankNMb,minrankM,nrrs,nrcs)
 FREQ 5  0.476 (r/s)  UNC = [  0.006]
>> [x,FVAL,EXITFLAG] = fmincon("fungrad",x0,[],[],[],[],vlb,vub,"congrad",options,...
>> xio_ii,etao_ii,EF_ii,GOMEG_ii,Wunc_ii,bo,blkf,ncolM,minrankNMb,minrankM,nrrs,nrcs)
 FREQ 6  0.568 (r/s)  UNC = [  0.001]
>> [x,FVAL,EXITFLAG] = fmincon("fungrad",x0,[],[],[],[],vlb,vub,"congrad",options,...
>> xio_ii,etao_ii,EF_ii,GOMEG_ii,Wunc_ii,bo,blkf,ncolM,minrankNMb,minrankM,nrrs,nrcs)
 FREQ 7  0.660 (r/s)  UNC = [  0.006]
>> [x,FVAL,EXITFLAG] = fmincon("fungrad",x0,[],[],[],[],vlb,vub,"congrad",options,...
>> xio_ii,etao_ii,EF_ii,GOMEG_ii,Wunc_ii,bo,blkf,ncolM,minrankNMb,minrankM,nrrs,nrcs)
 FREQ 8  0.752 (r/s)  UNC = [  0.003]
>> [x,FVAL,EXITFLAG] = fmincon("fungrad",x0,[],[],[],[],vlb,vub,"congrad",options,...
>> xio_ii,etao_ii,EF_ii,GOMEG_ii,Wunc_ii,bo,blkf,ncolM,minrankNMb,minrankM,nrrs,nrcs)
 FREQ 9  0.844 (r/s)  UNC = [  0.003]
>> [x,FVAL,EXITFLAG] = fmincon("fungrad",x0,[],[],[],[],vlb,vub,"congrad",options,...
>> xio_ii,etao_ii,EF_ii,GOMEG_ii,Wunc_ii,bo,blkf,ncolM,minrankNMb,minrankM,nrrs,nrcs)
 FREQ 10  0.936 (r/s)  UNC = [  0.005]
      .
      .
      .
>> [x,FVAL,EXITFLAG] = fmincon("fungrad",x0,[],[],[],[],vlb,vub,"congrad",options,...
>> xio_ii,etao_ii,EF_ii,GOMEG_ii,Wunc_ii,bo,blkf,ncolM,minrankNMb,minrankM,nrrs,nrcs)
 FREQ 200  18.423 (r/s)  UNC = [  0.001]
>> [x,FVAL,EXITFLAG] = fmincon("fungrad",x0,[],[],[],[],vlb,vub,"congrad",options,...
>> xio_ii,etao_ii,EF_ii,GOMEG_ii,Wunc_ii,bo,blkf,ncolM,minrankNMb,minrankM,nrrs,nrcs)
 FREQ 201  18.515 (r/s)  UNC = [  0.001]
>> [x,FVAL,EXITFLAG] = fmincon("fungrad",x0,[],[],[],[],vlb,vub,"congrad",options,...
>> xio_ii,etao_ii,EF_ii,GOMEG_ii,Wunc_ii,bo,blkf,ncolM,minrankNMb,minrankM,nrrs,nrcs)
 FREQ 202  18.607 (r/s)  UNC = [  0.001]
>> [x,FVAL,EXITFLAG] = fmincon("fungrad",x0,[],[],[],[],vlb,vub,"congrad",options,...
```

```
>> xio_ii,etao_ii,EF_ii,GOMEG_ii,Wunc_ii,bo,blkf,ncolM,minrankNMb,minrankM,nrrs,nrcs)
 FREQ 203  18.699 (r/s)  UNC = [  0.000]
>> [x,FVAL,EXITFLAG] = fmincon("fungrad",x0,[],[],[],[],vlb,vub,"congrad",options,...
>> xio_ii,etao_ii,EF_ii,GOMEG_ii,Wunc_ii,bo,blkf,ncolM,minrankNMb,minrankM,nrrs,nrcs)
 FREQ 204  18.791 (r/s)  UNC = [  0.001]
>> [Wid_z] = ovbndunc(unc_frd,blkf,omeg,iv_low,iv_hig,Ts)
    Curve fit uncertainty bound # 1, blkf = [-2,0] ..
    Curve fit uncertainty bound # 2, blkf = [-2,0] ..
    Curve fit uncertainty bound # 3, blkf = [-2,0] ..
    Curve fit uncertainty bound # 4, blkf = [-2,0] ..
    Curve fit uncertainty bound # 5, blkf = [-2,0] ..
    Curve fit uncertainty bound # 6, blkf = [-2,0] ..
    Curve fit uncertainty bound # 7, blkf = [3,3] ..
    Plot summary of weights? (y/n) n
```

Figure 18 shows the identified smallest additive uncertainty (circle line) subject to eigenvalue uncertainty allowance (of .002 on the first three structural modes) as compared to the true additive error (dot line). A fitted additive uncertainty model is also shown (dashdot line) as a reference. The level of the identified smallest additive uncertainty is very small as expected than the true additive uncertainty because of the eigenvalue uncertainty allowance of .002 on the first three structural modes was comparable to the true eigenvalue error which dominated the additive errors at the lower frequencies.

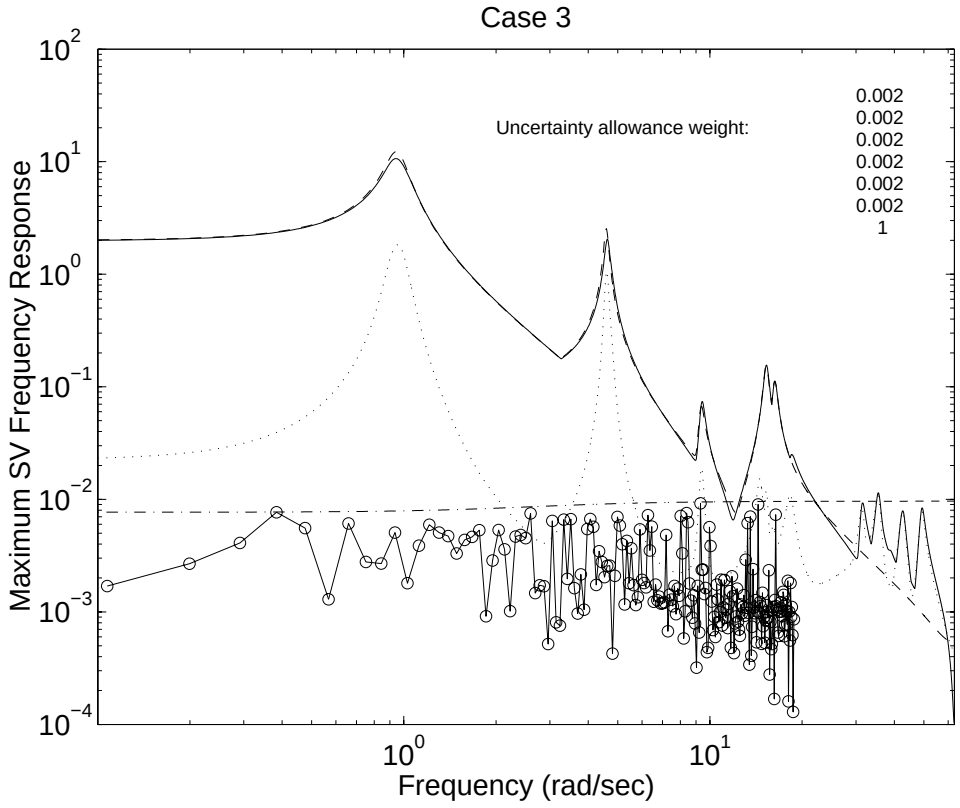

Figure 18: Identified smallest additive uncertainty (circle) with eigenvalue uncertainty allowance (.002), true additive uncertainty (dot)

4.3.4 Smallest additive uncertainty with uncertain mode 3 only

As a comparison, Figure 19 shows what happens to the identified smallest additive uncertainty if the eigenvalue uncertianty allowance is increased two fold to .004 but only mode # 3 (resonant frequency approximately 4.5 rad/sec) as assumed uncertain with the same output noise allowance. Figure 19 shows that the sharp error peak near 4.5 rad/sec due to

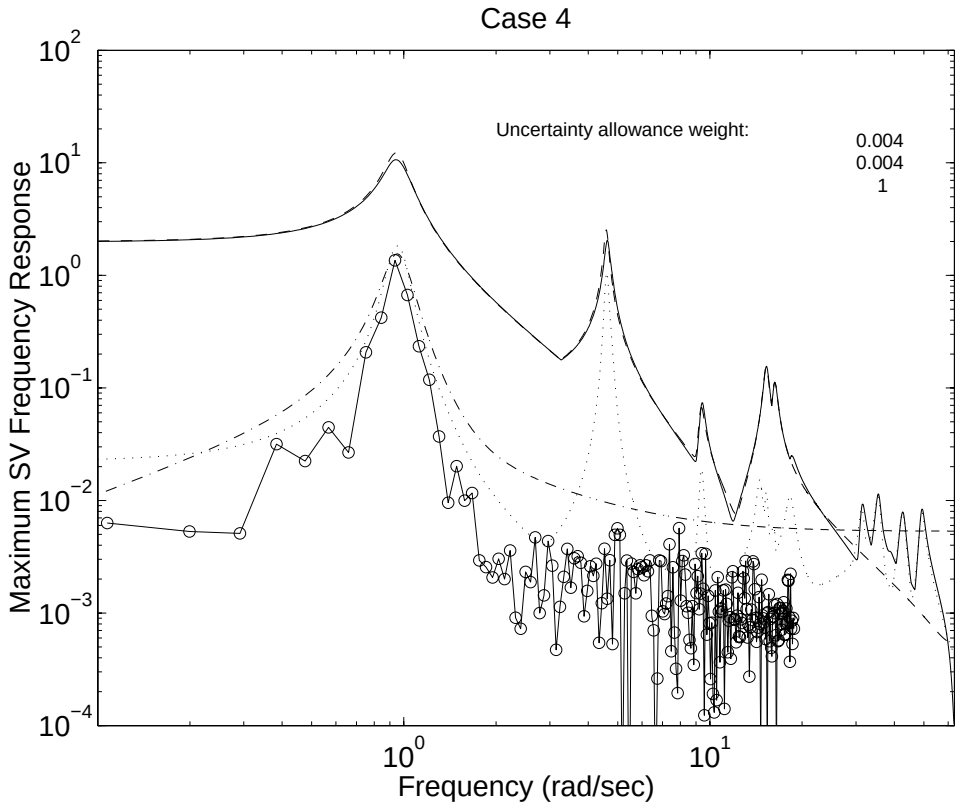

Figure 19: Identified smallest additive uncertainty (circle) with eigenvalue uncertainty allowance (.004) only on mode # 3, true additive Thisuncertainty (dot)

the parametric error has been accounted for by the uncertainty allowance of .004 at mode # 3. The other major error peak caused the parametric error near .95 rad/sec is covered by the additive uncertainty because apparently the large (more than twice of true parameteric error) neighboring eigenvalue allowance did not reduce the additive uncertainty at .95 rad/sec. This behavior is expected since structural resonances due to distinct modes are generally uncoupled. Note that doubling the parametric allowance did not noticably decrease the additive uncertainty. Of course from a robust control design point of view, this apparently unnecessarily large parametric uncertainty level limits the attainable performance robustness unnecessarily. This example again demonstrates the highly non-unique nature of model validating uncertainty sets as highlighted in this study.

5 Application Example 2: Performance validation of a ducted fan

5.1 Caltech Ducted Fan

In this section we outline uncertainty bounds obtained from measured data for the purpose of predicting the dynamic behavior of a realistic physical system, i.e. validate a system's closed loop performance to within a reasonable uncertainty model for an independent controller. Discrepencies between responses predicted by analytical and identified models and actual measurements are highlighted. The predictive capability of various model validating sets of uncertianties are evaluated using simulated and experimental data. Despite the presence of a high level of aerodynamic disturbance with limited data, which significantly limited both identification and model validation results, the model validating uncertainties led to improved predictions of closed loop performance.

A schematic of the Ducted Fan is described in Figure 20. Details on the description of the testbed are given in [22]. Briefly, a set of encoders measure ψ, z and θ, and a filter is used in

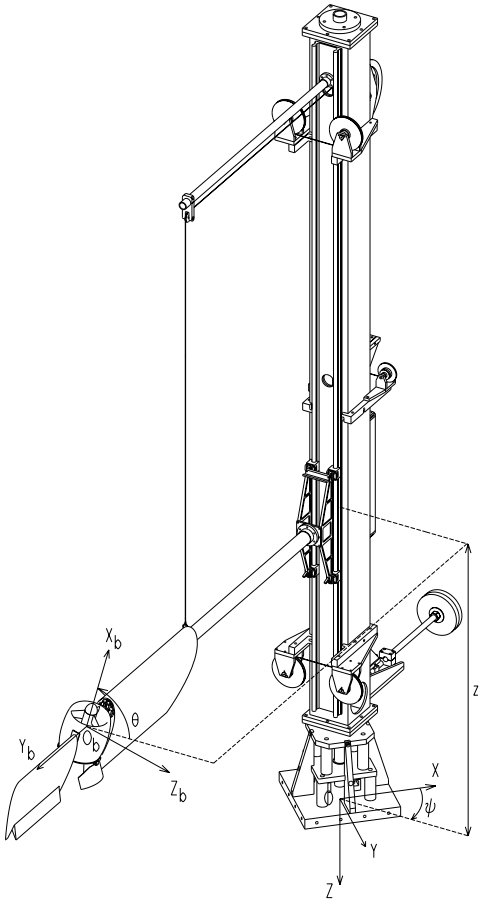

Figure 20: Ducted fan testbed schematic.

the ψ channel to estimate its velocity. The measured outputs are given by $\frac{d\psi}{dt}$ (airspeed), z (altitude), and θ (angle of attack), about trim. A derivative filter used to estimate airspeed inevitably introduces a small phase lag which we can neglect in the nominal model but is implicitly accounted for in the uncertainty model. The inputs in the following experiments consist of the fan motor voltage, V_m, and the paddle angle, δ_p.

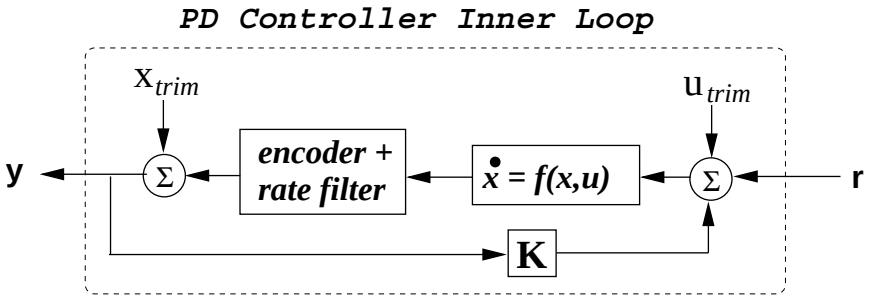

Figure 21: Motion about a trim at level flight stabilized by a PD controller.

The base sampling rate for the experiments are 100 Hz which is sufficient to mitigate aliasing effects with the implementation of a digital anti-aliasing filter having a break frequency of 5 Hz. A corresponding small phase lag was deemed a good tradeoff to mitigate allias-ing effects in the feedback loop during controller implementation at 20 Hz. This lower rate also helps to maximize the time length of recordable data, given memory limitations during testing while satisfying effective bandwidth requirements. Since the open loop dynamics of the Ducted fan is marginally stable for this particular level flight, a Proportional-Derivative (PD) controller is designed and implemented (for details see Appendix) in all subsequent experiments to stabilize and regulate its attitude, altitude, and rotation rate about a trim whose linearized motion is shown in Figure 21.

Three independent sets of experiments each 20 minutes duration were completed. The first set involves zero test inputs and are used for identifying noise spectra in closed loop. The second set is used for system identification and model validation. The third set of experiments involve an additional controller over the PD controller for the purpose of performance prediction and validation.

5.2 Nominal model and uncertainty structure

5.2.1 Analytical model

Among many choices in coordinate systems and state variables, consider an analytical model described by a set of first order ordinary differential equations having states, $[V, z, \dot{z}, \theta, \dot{\theta}]$, with inputs $u^T = [V_m, \delta_p]$ and outputs $y^T = [d\psi/dt, z, \theta]$. A trim condition at level flight is obtained at a forward flight velocity, $V_o = 6$ m/s, zero altitude, z, and elevator deflection, δ_e, and a perturbed linear model about the trim is defined. For more details, please refer to Appendix.

The accuracy of an analytical model of the Ducted fan depends on many factors. A partial list includes the following: proper application of physical principles and selection of associated physical parameters governing aerodynamics on the boom, wing, and shroud, motor velocity; thrust dependence on applied voltage and paddle deflections, airspeeds; structural flexure in boom, cables, and gears; nature of friction or energy dissipation between moving parts including stiction; fan motor dynamics; wall effects on the flow field, etc. Component wind tunnel test data is used to develop aerodynamic models which is also not totally accurate. In addition, a difficult but crucial task is to develop a model of the transient aerodynamic disturbance/noise effects, which appears to account for much of the noisy closed loop system response. By periodically flying through its own wake in level flight, the resulting unsteady aerodynamic forces will depend on past control input histories, current attitude and position. This periodicity is evident from output noise periodograms

Variable	Analytical model	Identified model
V_m	0.4665	0.4178
δ_p	0.6745	0.3971
$d\psi/dt$	0.8341	0.8391
z	0.9595	0.6600
θ	0.8542	0.5156

Table 2: Prediction errors based on l_2 norms over .1 to 10 rad/sec.

which show peaks whose frequency matched the nominal z-axis rotation rate of the Ducted fan (see Figure 24). This means that the exogenous output noise is actually correlated to both input and output variables which will cause unknown bias errors in the identification of an empirical model.

5.2.2 Identified models

In all subsequent identification results, we apply the Subspace Model Identification [25, 15] algorithm. The order indicator obtained directly from time domain data show no significant gap to indicate a natural order of the system based on measured data in Figure 52, in stark contrast to the presence of a clear order for simulated data in Figure 43. Nevertheless, inspired by analytical models having 5 plant states plus 4 PD controller states (see Appendix for details), an 8th order reduced model is chosen for the system consisting of plant and the PD controller. As an indication of the degree of reliability in this particular identification algorithm, it was found that, for example, if a 9th or larger order is selected, unstable closed loop systems with unrealistic poles and zeros at unpredictable locations can appear.

5.2.3 Comparison of analytical and identified models

Figure 22 shows an identified frequency response across plant from δ_p to θ with PD controller. The frequency response of these identified models roughly resemble corresponding analytical models over the bandwidth of interest, namely, .1 to 10 rad/sec. For example, at .2 and 2 rad/sec, where the gains match well, there is about 40 to 50 degrees of phase discrepency. The match appears to be better in the second input, namely, paddle angle δ_p, than for the fan motor voltage input V_m (see Figure 53 for the rest of the comparison). This better match in the second input is consistent with physical intuition, an indication of a better analytical model in the dynamics associated with the paddle angle input, particularly in the prediction of the altitude z and angle of attack θ.

Following the notion [5] that a model is a means to predict the output response due to an arbitrary input, the above discrepencies do not necessarily indicate that either model is more accurate than the other since both predictions, of frequency responses from the command inputs, may differ significantly from the measured spectra. Accordingly, Table 2 shows prediction errors of all input and output signals based on analytical and identified models when compared to measured signals. These prediction errors are actually l_2 norms over the frequency range of interest, .1 to 10 rad/sec (equivalent to a weighted RMS), and are normalized by the l_2 norms of the corresponding measured signals. Although the prediction errors for the identified model is significantly less than that of the analytical model (except the $d\psi/dt$ channel), still there are significant discrepencies for both models when compared to measured signals. Since the predicted signals do not include the effects of unknown exogenous signals, the above discrepencies are due to an unknown mixture of model errors and unaccounted unknown exogenous signals, which is estimated next.

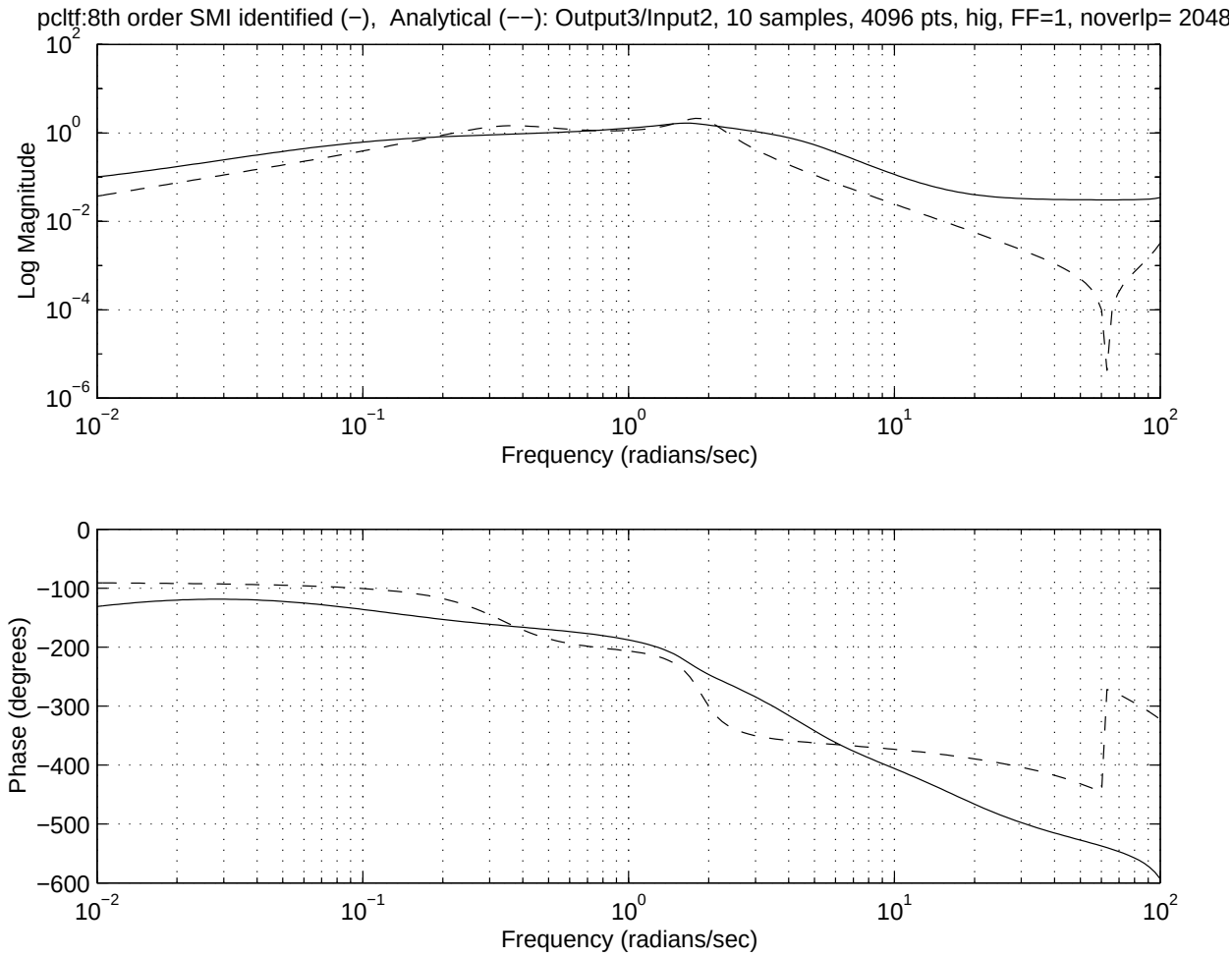

Figure 22: Frequency response from δ_p to θ with PD controller: identified 8th order (solid), analytical (dash).

5.2.4 Equivalent output noise model

Figure 23 illustrates the noise identification problem for a closed loop system. Figure 23a shows the unknown output noise q within the inner loop PD controller, K. The end goal of noise identification in this study, is to obtain a suitable filter, V, such that some unknown but unity bounded discrete-time white noise, ν, sequentially drive the filters V, and plant output sensitivity $(I - PK)^{-1}$, resulting in an "equivalent" output noise model suitable for subsequent model and performance validations and robust control application with an outer loop controller, C. Note that the "equivalent" output noise is intended to describe the particular approach whereby all unknown exogenous signals are modeled as an additive noise at the plant output.

A simple (but perhaps overly simple) approach to generate an output noise model is to directly fit the periodograms of individual output channels under zero command input. This implies that the equivalent output noise model, $(I - PK)^{-1}V$, is assumed to be diagonal which of course is not true because we know that the PD closed loop response due to output tracking command is strongly coupled meaning that the output sensitivity filter is not diagonal. An alternative and more physically compatible approach followed here is to assume that q is an independent set of exogenous inputs. To estimate the output spectrum

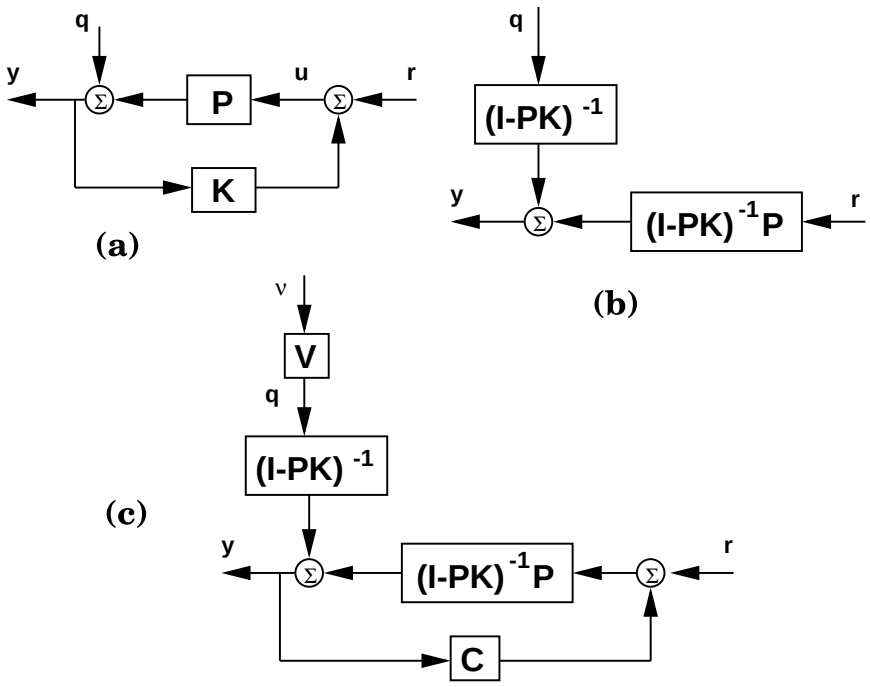

Figure 23: Noise model identification schematic: (a) unknown disturbance q with known inner loop controller K, (b) additive noise at output with inner loop closed, (c) system with an outer loop controller C with normalized noise ν.

of q, we utilize previously identified frequency responses of the input sensitivity and closed loop frequency response across plant. As outlined in the Appendix, an overdetermined set of loop conditions given by equations 32, are used to solve for q directly. Finally, the diagonal filter V is obtained by the unit norm condition of signal ν.

Figure 24 shows the identified equivalent output noise spectrum, q, based on zero inputs, $r = 0_{2\times1}$, closed loop experimental data. The figure also shows the fitted diagonal normalizing filter V for each channel. The identified spectra, q, indicates that there exists a large disturbances at about $2.5n$ rad/sec where $n = 1, \ldots$ and most prominent in airspeed, $d\psi/dt$ followed by angle of attack, θ, but not noticable for altitude, z. The frequency of these peaks match the rotation rate about the z-axis. Interestingly, the above noticable absence of periodicity in altitude is intuitively consistent.

Finally, notice the high levels of noise (corresponding time signals are shown in Figure 41) which is consistent with independently measured signal to noise ratios discussed in more detail in Appendix. The interested reader is referred to the Appendix sections for more discussions concerning the results and algorithms used to determine output noise models, analytical and identified models. The algorithms used were successfully validated on simulated data before application to actual experimental data.

5.2.5 Uncertainty structure

Figure 25 shows the interconnections of the uncertainty model and the equivalent output noise model to the inner loop PD controller, K, and the outer loop controller, C. The uncertainty model chosen consists of a multiplicative uncertainty at the output of the inner loop PD controller. A bounded but unknown equivalent noise, ν, is chosen as additive at the output of the inner loop PD controller and is filtered by output sensitivity and normalizing

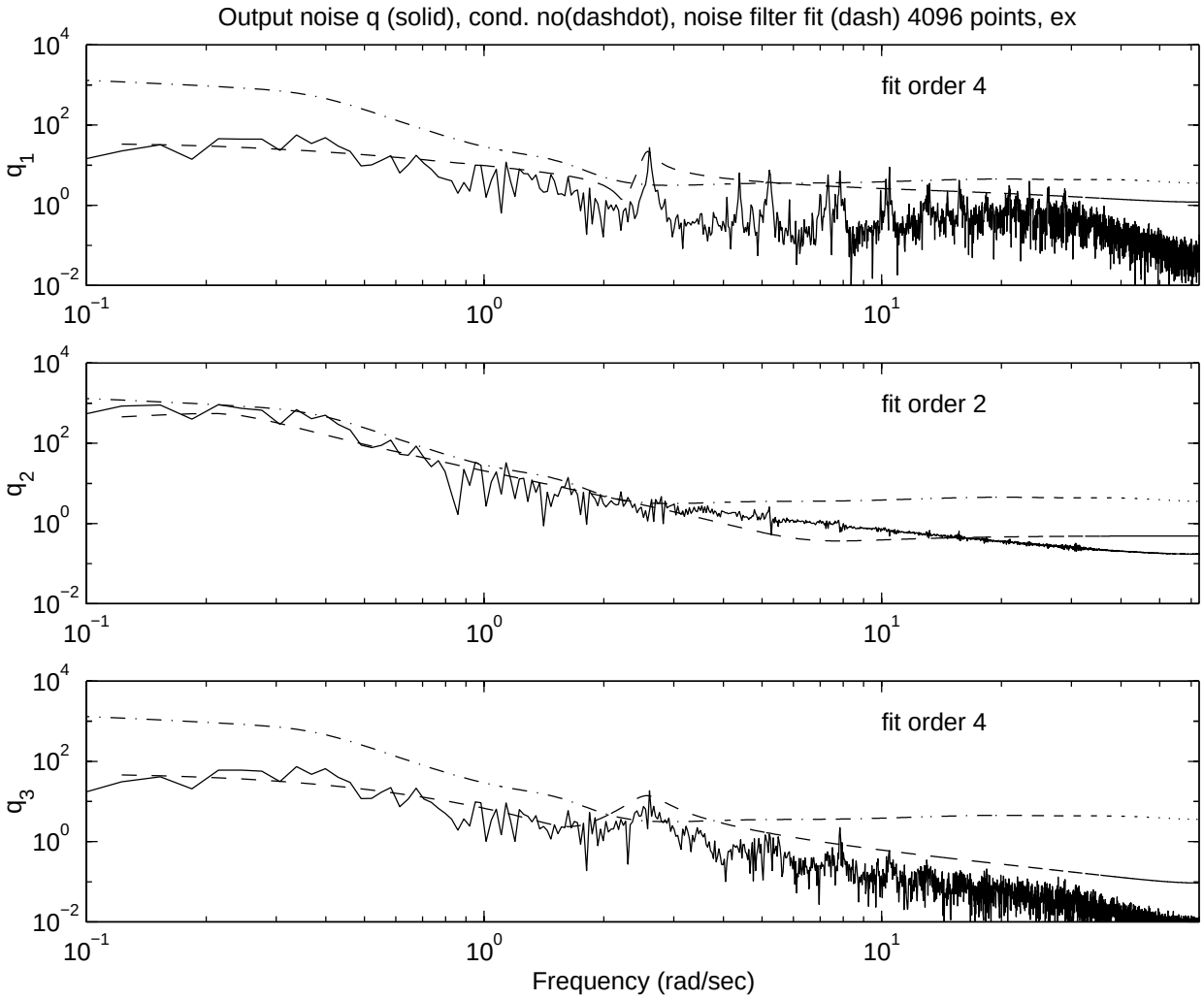

Figure 24: Identified output noise q (solid), fitted noise V (dash), condition number(dashdot), 4096 points DFT, 5 samples.

diagonal filter V. The nominal model consists of the transfer function matrix from command input r to the closed inner loop output of the plant y, i.e., $(I - PK)^{-1}P$. The simplified uncertainty structure chosen along with a zero input disturbance allowance gives the following augmented plant:

$$\left\{ \begin{array}{c} \eta \\ y \end{array} \right\} = \underbrace{\left[\begin{array}{ccc} 0 & [0,0] & (I-PK)^{-1}P \\ I & [0,V_n] & (I-PK)^{-1}P \end{array} \right]}_{G(P,K,V)} \left\{ \begin{array}{c} \xi \\ \binom{\epsilon}{\nu} \\ r \end{array} \right\}$$

where $V_n := (I-PK)^{-1}V$. Notice from the above augmented plant that because $[G_{11},\ G_{12}] = 0$, the feasibility test for model validation of this particular connection of uncertainty structure and noise model is convex which greatly simplifies the subsequent numerical optimization problem. Notice that this sufficient condition is easily violated, if for example an equivalent input noise is defined at the input, to go with the output multiplicative uncertainty, i.e., $G_{12} \neq 0$.

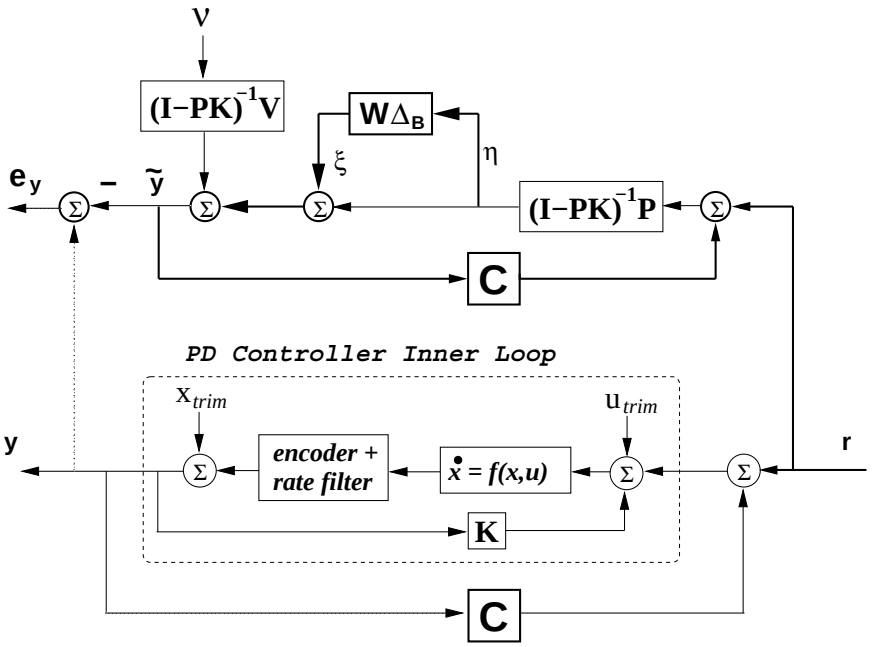

Figure 25: Uncertainty model interconnection about a level flight trim for Ducted fan.

5.3 Smallest unmodeled dynamics for model validation

Consider the problem of finding a smallest model validating output multiplicative uncertainty given an output noise allowance, consisting of the product of the fitted noise filter, V, shown in Figure 24, and an output sensitivity filter. In this study, an output sensitivity filter is constructed by forming the product, $I_{3\times 3} + T_{yr}K$ where T_{yr} is an identified model of the inner loop across plant and K is the given inner loop PD controller (for more details please see Appendix). As discussed earlier, this question can be posed as an optimization problem involving a linear cost function subject to a set of linear matrix inequality constraints at each frequency:

$$\begin{aligned} \min_{z} \; & c^T z \\ \text{subject to } & \begin{bmatrix} Q_i z - \|\xi_{o,i}\|^2 & \text{sym} \\ S_i z & I \end{bmatrix} > 0, \; i = 1, \ldots, \tau \\ & \begin{bmatrix} b_o^2 & \text{sym} \\ Lz & I \end{bmatrix} > 0 \end{aligned}$$

where $z := [\mathrm{Re}(\psi); \mathrm{Im}(\psi); \mathrm{Re}(\phi); \mathrm{Im}(\phi); x^2] \in \mathcal{R}^{2n_\psi + 2n_\phi + 1}$, and the set of constants c, Q_i, S_i, and L are defined in equation 22, b_o is defined in equation 9, and $\xi_{o,i}$ is the ith uncertainty component of ξ_o which is defined in equation 11. For unstructured uncertainty case, $\tau = 1$, while for diagonal uncertainty case, $\tau = 3$.

The interior-point algorithm found in MATLAB's LMI Toolbox [20] is used to solve for the global minimum. With multiplicative uncertainties for all output channels, the existence of a model validating set is obviously not in question and the interest lies in determining the necessary magnitude level and frequency shape of the unmodeled dynamics (which implicitly includes some unknown level of contribution from parametric errors in the nominal model). Table 3 show the various cases considered which arises from a combination of nominal model, assumed uncertainty structure, and a choice on the level of output noise allowance based on a factor of fitted noise spectrum.

Case	Nominal	Uncertainty str	Noise
Exp1-2-D	Analytical	Diagonal	.5× fitted
Exp1-3-D	Analytical	Diagonal	fitted
Exp1-4-D	Analytical	Diagonal	2× fitted
Exp4-2-D	Identified	Diagonal	.5× fitted
Exp4-3-D	Identified	Diagonal	fitted
Exp4-4-D	Identified	Diagonal	2× fitted
Exp1-2-F	Analytical	Unstructured	.5× fitted
Exp1-3-F	Analytical	Unstructured	fitted
Exp1-4-F	Analytical	Unstructured	2× fitted
Exp4-2-F	Identified	Unstructured	.5× fitted
Exp4-3-F	Identified	Unstructured	fitted
Exp4-4-F	Identified	Unstructured	2× fitted

Table 3: Cases considered for computing smallest output multiplicative uncertainty.

Figure 26 shows the smallest model validating *diagonal* output multiplicative uncertainties based on analytical and identified nominal models. Assuming *unstructured* output multiplicative uncertainties instead, Figure 27 shows the smallest model validating maximum singular values of the uncertainties based on analytical and identified nominal models. The effects of using different levels of equivalent output noise allowances are also shown: the diamond solid line denotes uncertainties obtained based on a unit factor of fitted noise allowance, the triangle dotted line is based on twice the fitted noise allowance, and the square dotted line is based on half the fitted noise allowance (refer Table 3). Based on the results in Figures 26 and 27 we make the following observations:

1. Larger noise allowance leads to smaller model validating unmodeled dynamics. However, at twice the fitted noise allowance, the identified nominal model case gives unrealistically small levels of unmodeled dynamics (say 1 % or less at many frequency points). This also means that the validation was likely achieved mostly with noise allowance, which could lead to unrealistic predictions of robust stability.

2. Identified nominal model cases resulted in smaller uncertainty levels than analytical nominal model, for both types of uncertainty structure and three different noise allowance levels. Since the uncertainty ball of the identified nominal model is smaller than that of analytical nominal model, the identified nominal model appears to be more accurate than the analytical nominal model. This result is consistent with the earlier prediction error analysis of nominal models.

3. The maximum singular value of the unstructured uncertainty cases resulted in smaller uncertainty levels than structured uncertainty cases (its maximum over all channels). This is not surprising since unstructured uncertainty has a larger number of uncertainty components than diagonal uncertainty. However, a smaller normed uncertainty set do not necessarily imply a smaller set of plants if the number of uncertainty components are different.

4. At lower frequencies, say < 2 rad/sec, smaller uncertainty levels are required for both types of nominal model and uncertainty structure. This may be due to the following reasons:

   - The frequency responses of both analytical and identified nominal models have larger gains at lower frequencies (see Figures 53), and the multiplicative uncertainty at output represents a factor of these responses.

- The nominal model is actually more accurate at lower frequencies; for example, the analytical and identified transfer functions from δ_p to θ match better at lower frequencies between .1 to 2 rad/sec then over 2 to 30 rad/sec range (see Figure 22).
- The use of a larger noise allowance at lower frequencies which inadvertently can reduce model uncertianty level. A larger identified noise spectra at lower frequencies is indicated in Figure 24.

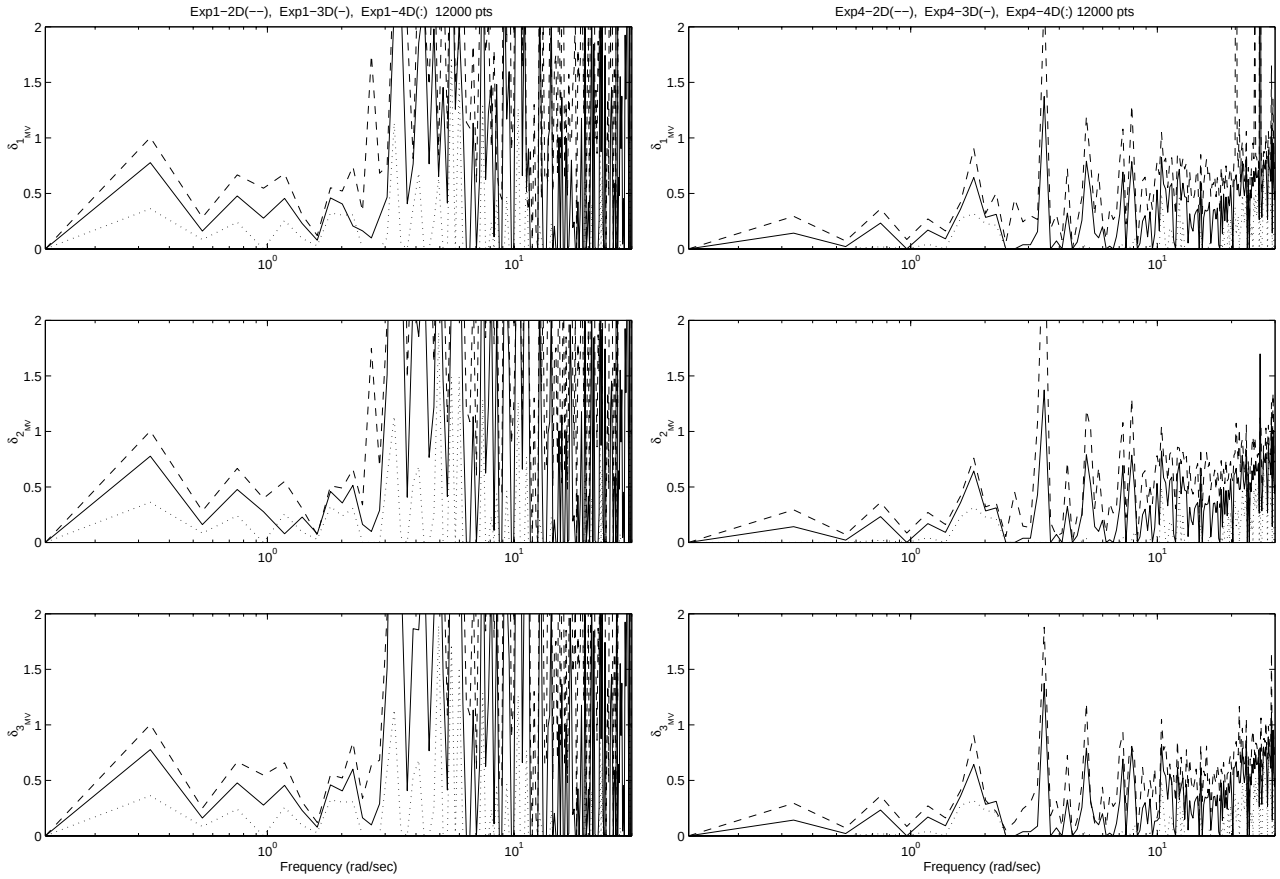

Figure 26: Smallest diagonal output multiplicative uncertainty about analytical (left) and identified (right) nominal models: noise allowances of .5× fitted (dash), fitted (solid), 2× fitted (dot).

In summary, the above model validating uncertainty levels obtained from experimental data for the Ducted fan is not small. Simulation results (see Appendix for details) also indicate that these results can be sensitive and therefore unreliable in the presence of a high level of noise in data, exactly, what was observed in dealing with measurement data. This large uncertainty level appears to be due to two reasons:

1. significantly inaccurate nominal models which is evident from early prediction error analysis of both models, and
2. large exogenous disturbance and noise which is evident from earlier construction of noise models which causes DFT errors from nonperiodicity.

We have also shown that this lack of periodicity cannot be eliminated by innovative tapered time windowing. In fact, simulation studies indicate that with a high level of noise in data,

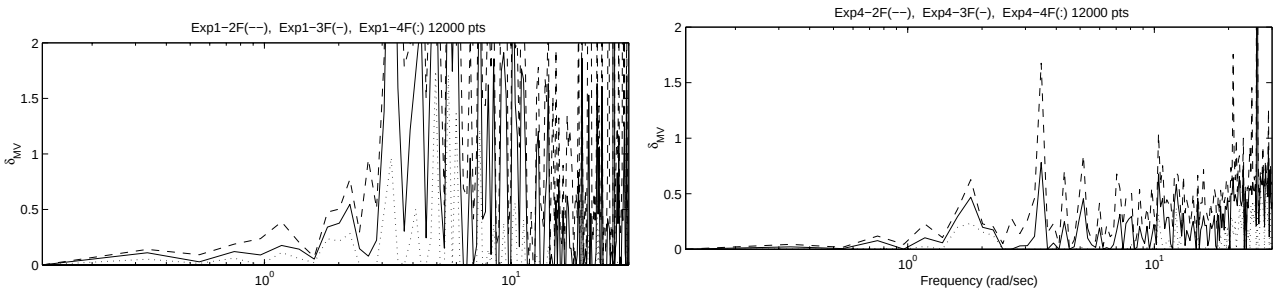

Figure 27: Smallest unstructured maximum singular value of the output multiplicative uncertainty about analytical (left) and identified (right) nominal models: noise allowances of .5× fitted (dash), fitted (solid), 2× fitted (dot).

it is difficult to recover the correct model error, even with an accurate nominal model and correct uncertainty structure. On the other hand, simulation studies also suggests that incorrect or indeterminate uncertainty structure do not preclude satisfying model validation conditions. For example, assuming unstructured uncertainty when the correct model error is diagonal resulted in a smaller normed unstructured uncertainty (when compared to the norm of true diagonal model error), exactly what was observed in dealing with measurement data. Nevertheless, since the important property of an uncertainty model is in its predictive capability of closed loop performance rather than its particular uncertainty structure or size, we next show the results of its predictive capability of closed loop performance for an independent outer loop controller.

5.4 Performance validation analysis

In this section, we show comparisons between measured worst case performance and various predicted performance bounds based on corresponding model validating uncertainty sets. The measured worst case performance is defined here as the maximum possible closed loop amplification over bounded signals. In contrast, the predicted performance bounds are based on the predicted worst case signal amplification over a corresponding model validating set of plants. Closed loop refers to a second controller loop with C around the inner controller loop involving K. In the Ducted fan, the inner loop controller was necessary since the open loop was marginally unstable to collect data for system identification.

Figure 28 illustrates how closed loop performance can be validated. The idea is that the measured worst case disturbance amplification of the closed loop system is bounded by (or comparable to) the predicted worst case disturbance amplification based on an uncertainty model. This predictive capability is an important necessary characteristic of a useful uncertainty model in the context of robust control. The predicted worst case performance for a

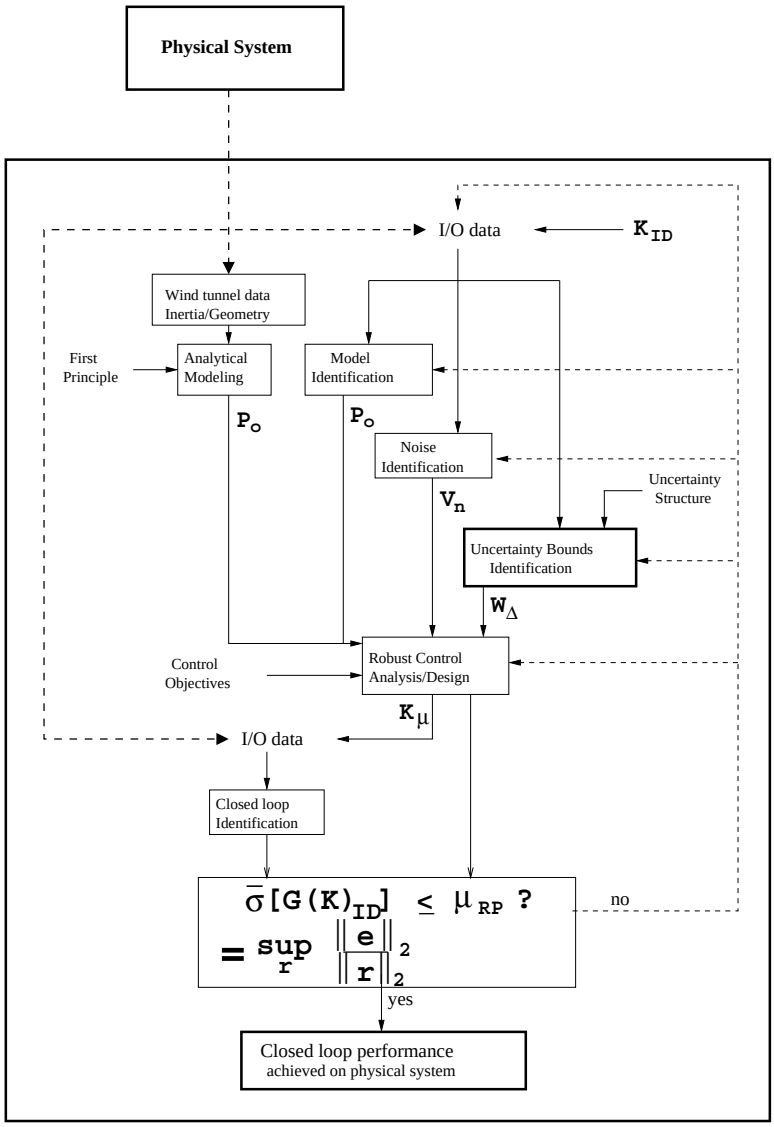

Figure 28: Performance validation schematic for Ducted fan: predicted versus measured

given nominal and uncertainty model is illustrated in Figure 29 where skewed-μ [1] is defined at each frequency and is given by

$$\mu_s := \{\min \rho : \det(I - R(\rho)M(P,K,V,C)\Delta_B W) = 0, \bar{\sigma}(\Delta_B) \leq 1\}^{-1} \quad (25)$$

$$= \max_{\substack{\bar{\sigma}(\Delta_{unc})\leq 1 \\ \Delta_{unc}\in\mathcal{D}}} \bar{\sigma}\left[W_{perf}\mathcal{F}_u(M(P,K,V,C), \Delta_{unc}W_{unc})\right] \quad (26)$$

where

$$R(\rho) := \begin{bmatrix} I_{unc} & 0 \\ 0 & \rho I_{perf} \end{bmatrix}$$

$$M(P,K,V,C) := \mathcal{F}_l\left(\begin{bmatrix} I \\ I \end{bmatrix} G(P,K,V)[I,I],\ C\right)$$

$G(P,K,V)$ denotes the augmented nominal system consisting of the inner loop whereas $M(P,K,V,C)$ denotes the nominal closed loop system with the second controller. Equation (26) indicates that μ_s denotes the worst case maximum singular value frequency response at a given frequency. This worst case is over the uncertainty model set, $\mathcal{D}$, while the maximum singular value reflects the multivariable nature of input and output signals and its spatial dependence. Equation (25) connects μ_s to the more well known μ which is typically used to compute the former by a scaling procedure described in more detail for example in [1].

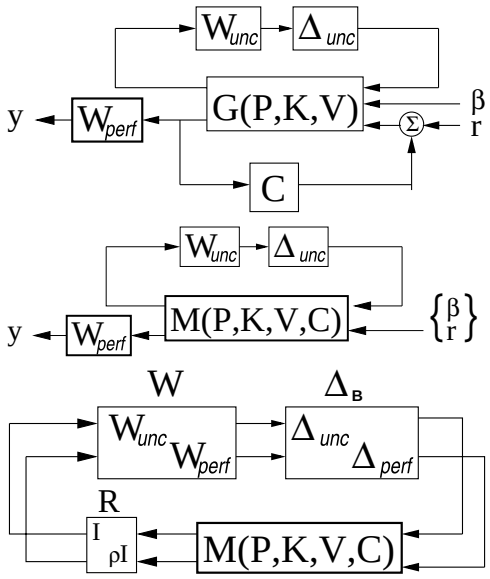

Figure 29: Computation of worst case performance from r to y (top), canonical form (middle), performance channel scaled and closed (bottom).

From equation 26 and middle figure in Figure 29, note that μ_s includes a directional worst case with respect to unknown exogenous inputs, β. For performance validation purposes, this is a bit difficult to experimentally measure the worst case responses with respect to *unknown* exogenous inputs. Hence, although mathematical models for the exogenous noise are available, we consider only the measurable worst case response from command input, r, to measured output, y, corresponding to the μ_s with performance from r to y only. Therefore, the following performance validation results do not include the responses due to unknown exogenous signals, which is known to be significant. Furthermore, since it is a non trivial

matter to test all possible command inputs in the hope of directly measuring the worst case signal amplification, we circumvent this by identifying an empirical model of the closed loop system with the goal of computing the maximum singular value of its empirical frequency response matrix, resulting in an indirect measurement of worst case directional response.

Figure 30 shows a comparison of the measured worst case response (line), to the predicted responses: nominal (dash), μ_s based on structured uncertainty (line-circle) and unstructured uncertainty (line-square). These predicted responses are based on an *analytical* nominal model. Figure 31 shows similar comparisons but its predicted responses are based on an *identified* nominal model. Both predicted responses are based on an assumed noise allowance of fitted noise with factor 1. Based on the results in Figures 30 and 31, we make the following

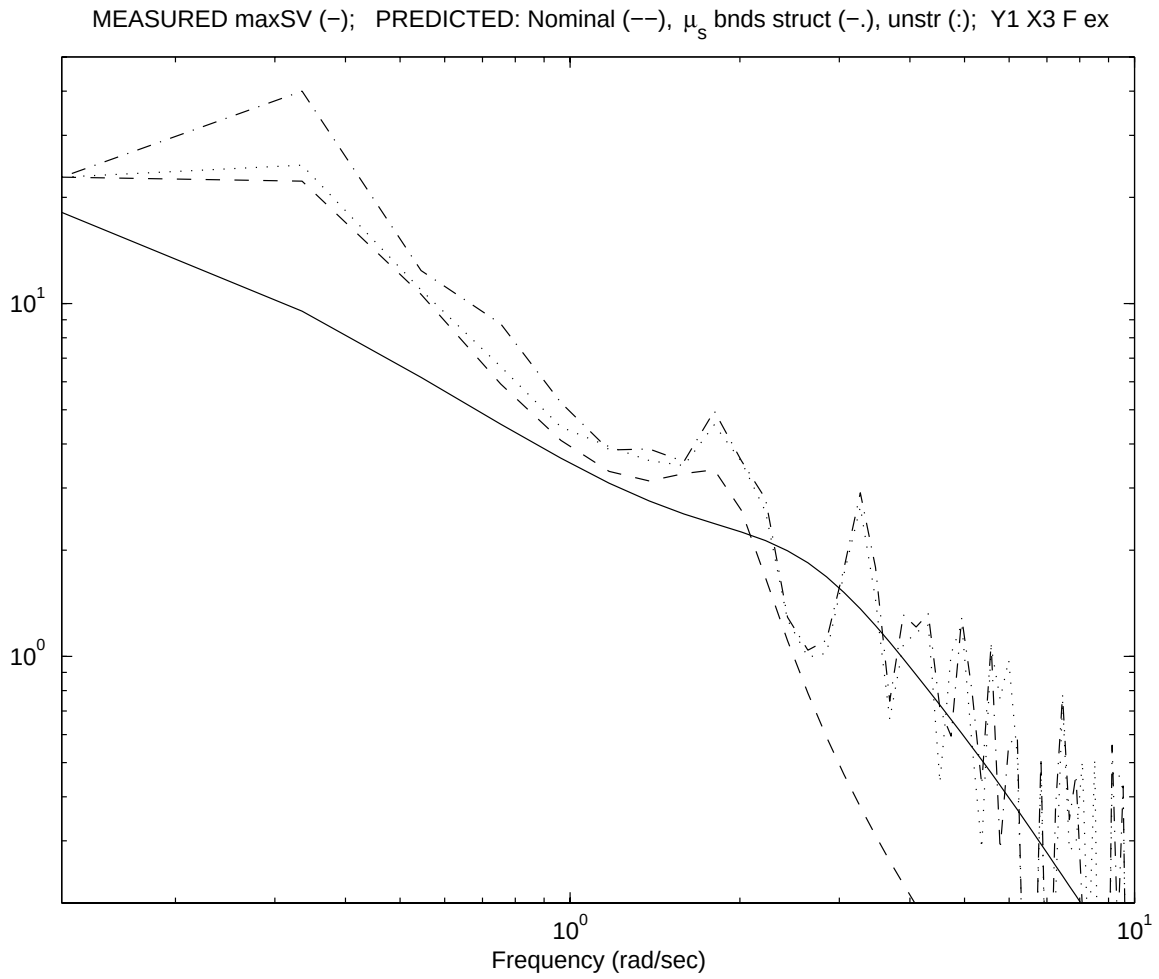

Figure 30: Worst case response from r to y with noise allowance fit factor 1: *analytical* nominal model with diagonal and unstructured uncertainties.

observations:

1. Without using uncertainty models, the predicted performance based on *identified* nominal model (dash line in Figure 31) gives a much better match with measured response (solid line) than performance based on *analytical* nominal model (dash line in Figure 30). This is consistent with both pervious analysis of uncertainty size levels and prediction errors. Most prominently, the *analytical* nominal model predicts an overly pessimistic response at lower frequencies and overly optimistic response at higher fre-

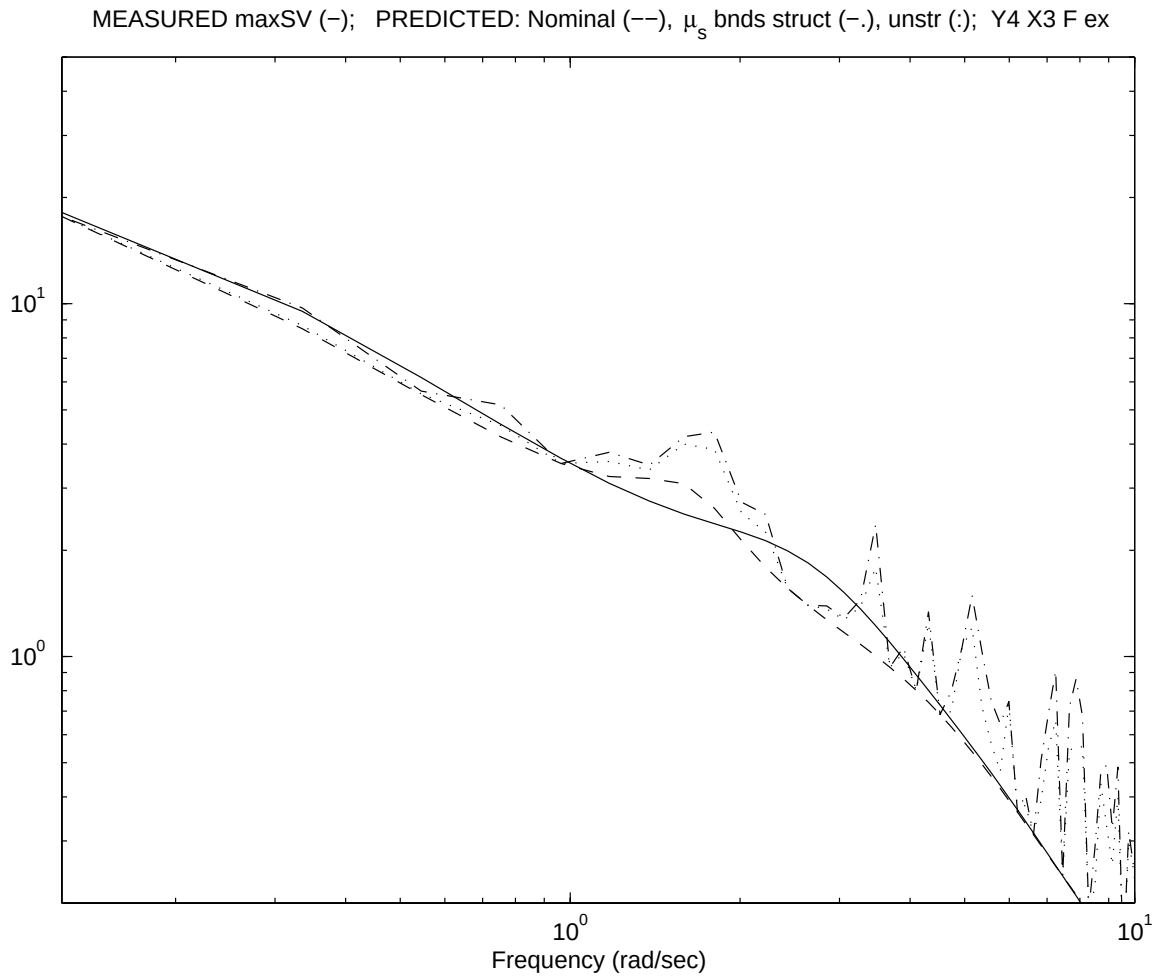

Figure 31: Worst case response from r to y with noise allowance fit factor 1: *identified* nominal model with diagonal and unstructured uncertainties.

quencies beyond 2 rad/sec. On the other hand, the *identified* nominal model predicts a slightly optimistic response at most frequencies except over a narrow bandwidth within 1 and 2 rad/sec (see Figure 31).

2. Using uncertainty models, the predicted worst case response (i) worsens the pessimism at lower frequencies but improves the overly optimistic prediction at higher frequencies for the *analytical* nominal model case (dot and dash-dot lines in Figure 30), and (ii) improves the slightly optimistic prediction at lower frequencies but worsens the slightly optimistic prediction at higher frequencies for the *identified* nominal model case (dot and dash-dot lines in Figure 31). Since errors at lower frequencies (say < 2 rad/sec) dominate and therefore its prediction more significant, we infer that using uncertainty models improved the *identified* nominal mode based prediction while it increased the conservatism of the *analytical* nominal model based prediction.

3. The predicted worst case performance locally peaks and then drops significantly to the predicted nominal levels between 1 to 3 rad/sec. The local drop in worst case performance corresponds to the large resonant noise allowance (Figure 24) leading to smaller model validating unmodeled dynamics. Conversely, the local peaks of the worst case performance (Figures 30 and 31) correspond to a local drop in the noise allowance

(Figure 24) leading to larger model validating unmodeled dynamics. This is a result of treating noise as a given allowance in computing the minimum unmodeled dynamics necessary to satisfy model validation conditions.

4. The deviation of predicted responses based on *identified* nominal model (dot and dash-dot lines in Figure 30) is significantly less from its corresponding nominal predicted response than the deviation of the predicted responses based on *analyical* nominal model (dot and dash-dot lines in Figure 31) to its corresponding nominal predicted response. This smaller deviations of predicted responses is consistent with the smaller sizes of the model validating uncertainties for the *identified nominal model* case.

5. The deviation of the predicted responses based on *unstructured* uncertainty (dotted lines) from the predicted nominal response is significantly smaller than the corresponding deviation based on *diagonal* uncertainty (dash-dot lines) for both types of nominal model. This deviation is particularly large in the *analytical* nominal model based predictions at lower frequencies; perhaps the assumed *diagonal* uncertainty structure could not easily account for a *large* coupled dynamics error that occurs for a *analytical* nominal model. Based on comparisons to measured responses (solid lines), the *unstructured* uncertainty (dotted lines) appears to be more suitable for use with *analyical* nominal model while the *diagonal* uncertainty (dash-dot lines) appears to be more suitable for use with *identified* nominal model.

Figures 32 to 35 show the effects of varying levels of noise allowances $(.5, 1, 2)$ of fitted noise, on the closed loop performance, for both types of nominal models and both types of uncertainty structure. The measured worst case is shown as a reference by a solid line. From the four figures, note the following observations:

1. With increasing *noise allowance* (from dot to dashdot to dash lines), the level of unmodeled dynamics decreases and the predicted worst case response decreases for both types of nominal models and uncertainty structures.

2. Varying the noise allowance levels did not significantly improve the overly pessimistic predictions based on *analytical* nominal model (Figures 32 and 33) mainly because the level of pessimistic predictions dominates. However, note that with the use of smaller noise allowance (.5), the prediction based on *analytical* nominal model at higher frequencies (say > 2.5 rad/sec) matched the measurement more closely, although less significant.

3. Using a noise allowance level of 1.0, the predicted response, based on *identified* nominal model with diagonal uncertainty (Figures 34), closely matched the measured response. In contrast, this "correctly" scaled noise allowance level of 1.0, did not appear to give better results if unstructured uncertainty is used (Figure 35).

4. The predicted worst case responses based on *unstructured* uncertainties (Figures 33 and 35) appears to be less sensitive to noise allowance levels for either type of nominal model than *diagonal* uncertainties (Figures 32 and 34).

As a summary based on the above observations, the predicted worst case closed loop performance based on a model validating diagonal uncertainty about the *identified* nominal model with the more realistically scaled noise allowance (i.e. fit factor of 1.0), gave the closest match to the maximum singular value of the identified closed loop system at lower frequencies where the outputs were largest. The presence of a high level of exogenous disturbances due to unknown unsteady aerodynamics, concentrated near the rotation frequency of about 2.5 rad/sec, is a significant obstacle in the uncertainty level determination methodology and

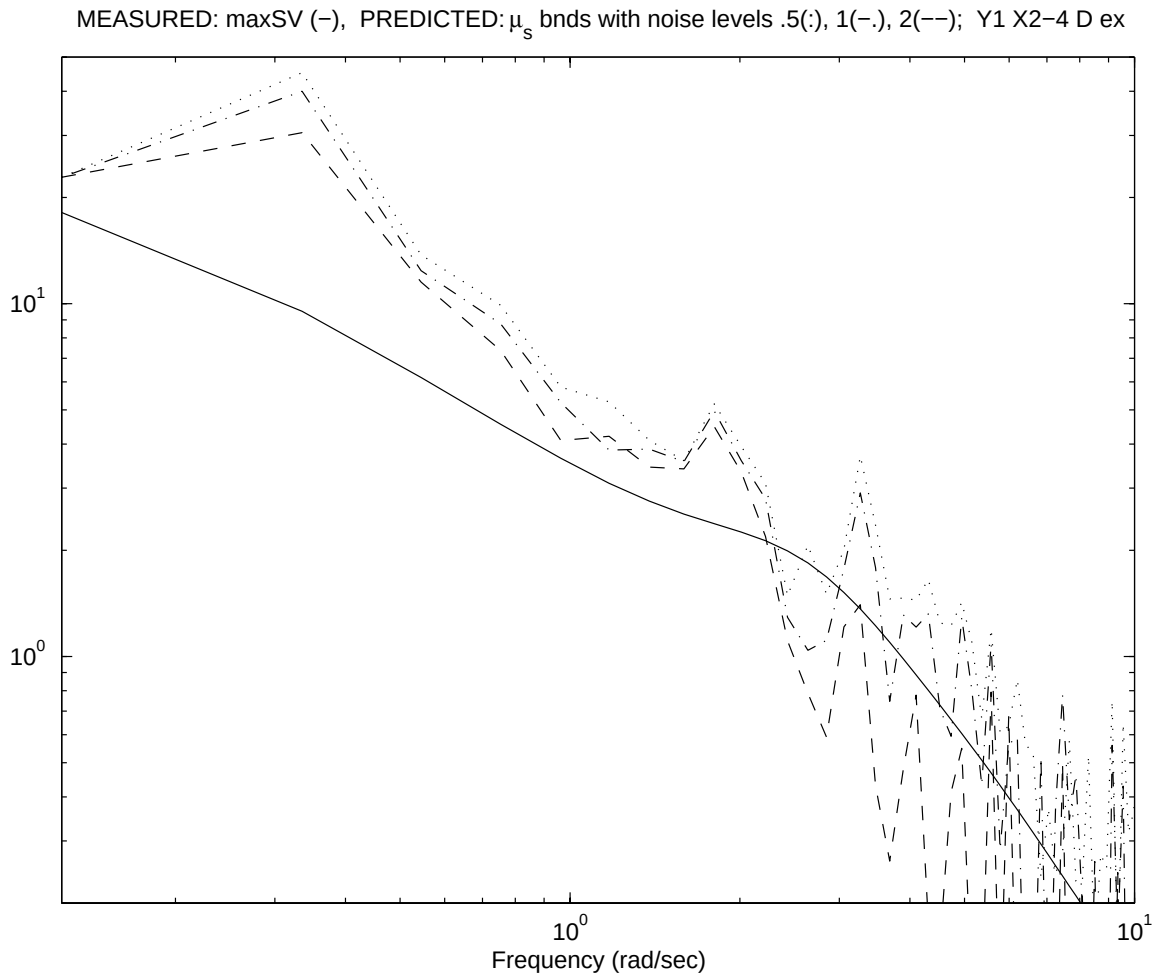

Figure 32: Worst case response from r to y for analytical nominal model with diagonal uncertainty: effects of noise allowances .5 (dot), 1 (dashdot), 2 (dash), and measured (solid).

subsequent performance validation near this frequency. On the other hand, unknown disturbances always present in physical systems is always a limiting factor in model validation.

Despite some success in the above performance predictions, the selection of a set of uncertain parameters and structure of unmodeled dynamics is not completely clear. Furthermore, any particular uncertainty parameter and structure that leads to a model validating set is likely to be redundant and there is no clear "best" selection suggested by the physics of the Ducted fan testbed. Nevertheless, experimental results appended by simulation results suggest that it may not be necessary to know the "correct" uncertainty structure, to obtain uncertainty models that are useful for robust control applications.

Finally, the limitations of the results and scope of this study is noted that further research could address. This includes (i) performance validation is limited to worst case response comparisons based on maximum singular values and could be extended to gain and phase variations of each input-output channel, (ii) a procedure for the performance validation involving the worst case unknown exogenous disturbance and noise is not clear and therefore not considered, (iii) an improved procedure for obtaining an equivalent output noise model from closed loop measurements is desirable, and (iv) techniques for distinguishing exogenous random noise from model error effects from limited closed loop response data is desirable.

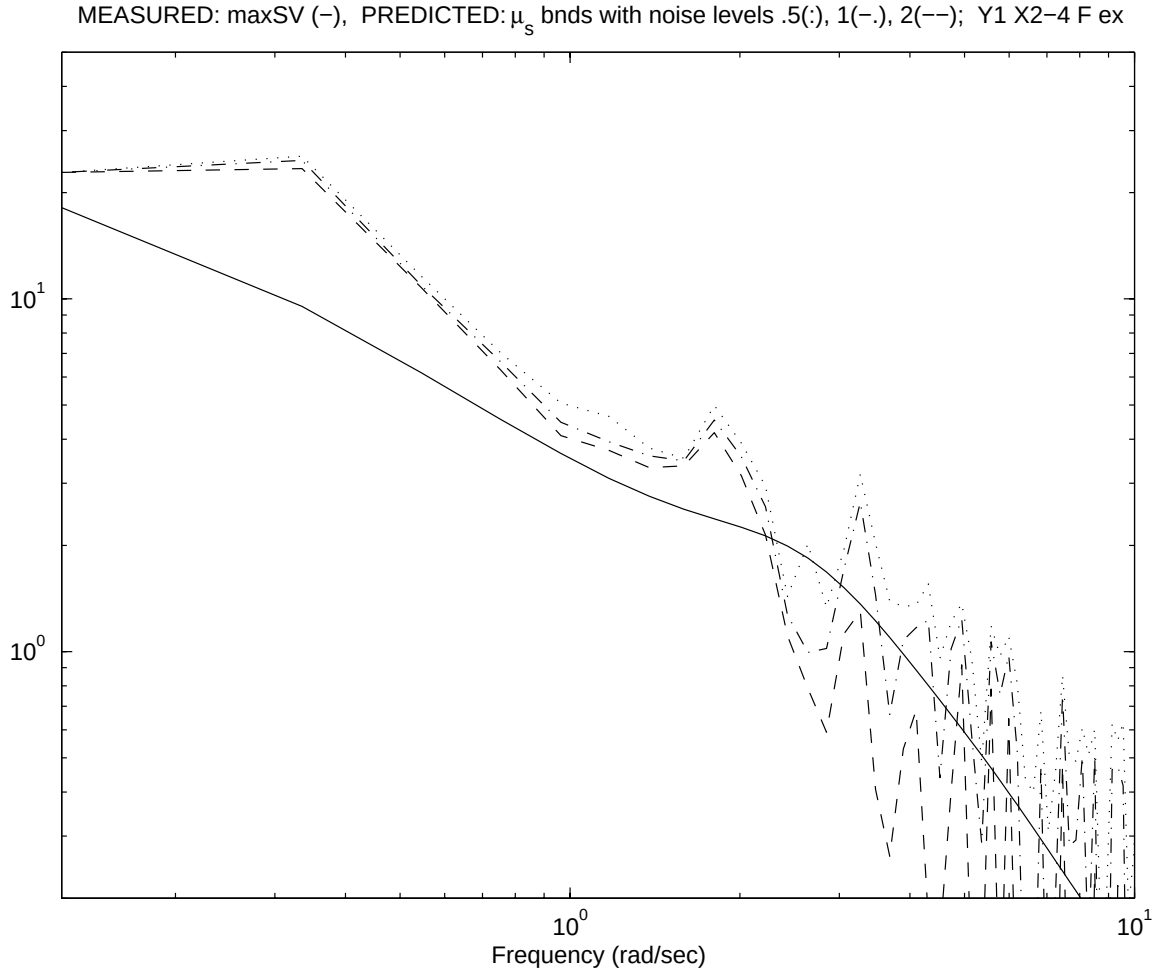

Figure 33: Worst case response from r to y for analytical nominal model with unstructured uncertainty: effects of noise allowances .5 (dot), 1 (dashdot), 2 (dash), and measured (solid).

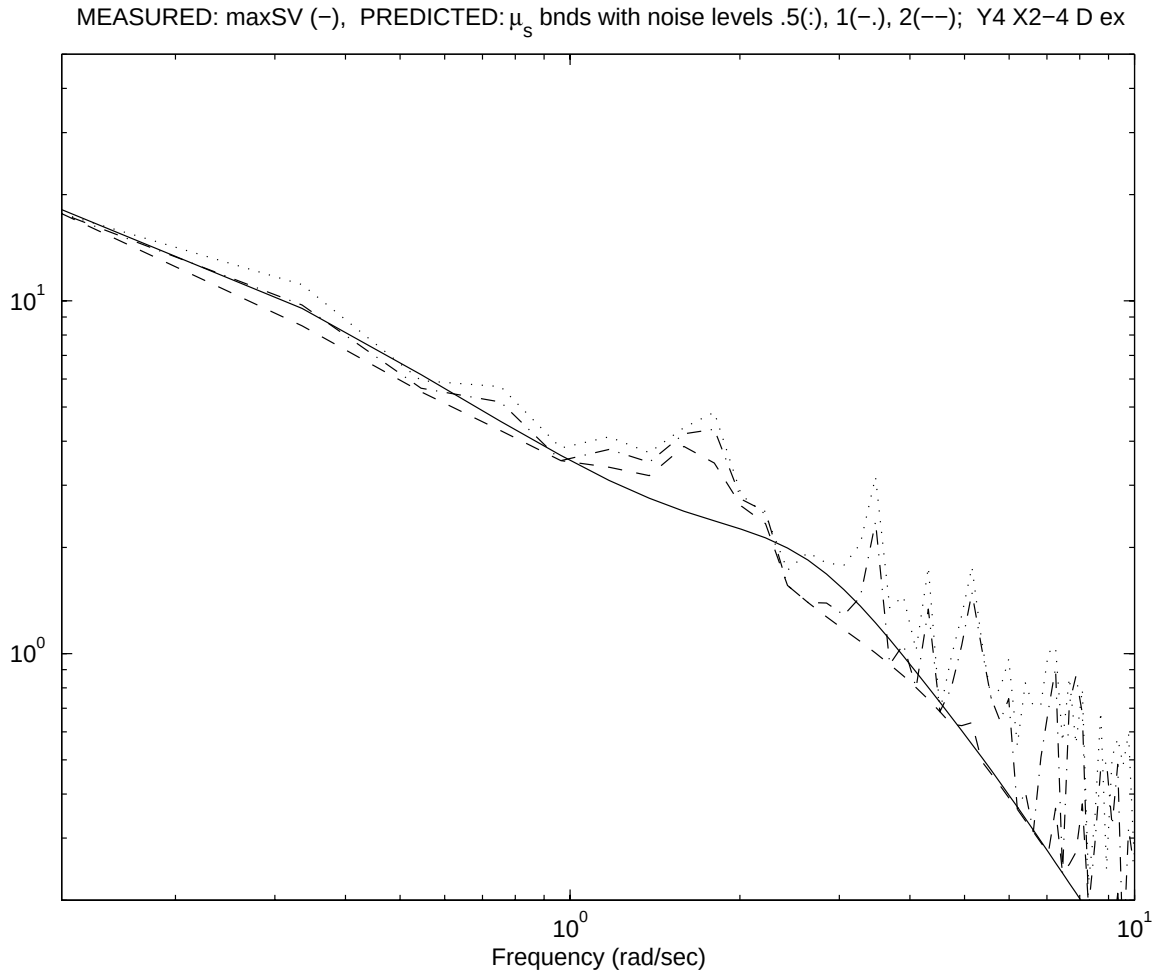

Figure 34: Worst case response from r to y for identified nominal with diagonal uncertainty: effects of noise allowances .5 (dot), 1 (dashdot), 2 (dash), and measured (solid).

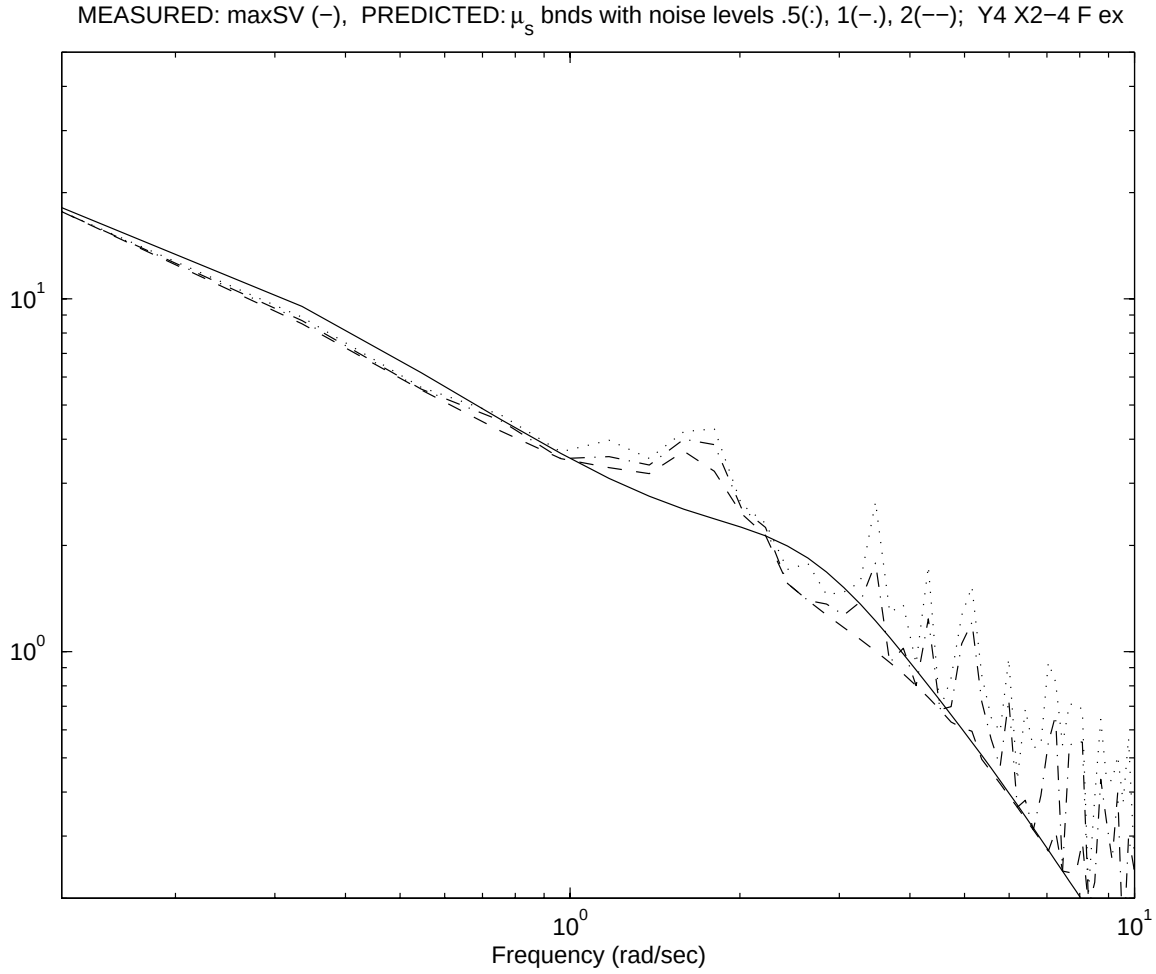

Figure 35: Worst case response from r to y for identified nominal with unstructured uncertainty: effects of noise allowances .5 (dot), 1 (dashdot), 2 (dash), and measured (solid).

A Ducted Fan in level flight

A schematic of the Ducted Fan is described in Figure 36 and Figure 37. $(0, X, Y, Z)$ is an inertial coordinate system, (O_s, X_s, Y_s, Z_s) a stand center of mass, body fixed coordinate system, (O_b, X_b, Y_b, Z_b) a shroud center of mass, body fixed coordinate system, and (O_w, X_w, Y_w, Z_w) the wind coordinate system. ψ is the angle between $[OX)$ and the projection of $[O_sX_s)$ on

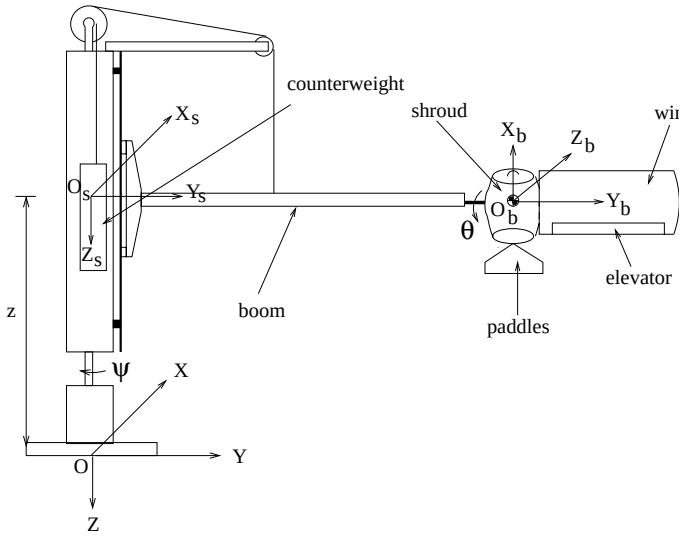

Figure 36: Ducted Fan Body

the plane (XOY), θ, the pitch axis angle i.e. the angle between the local horizontal $[O_sX_s)$ and the $[O_bX_b)$ axis and z the algebraic distance OO_s. The airspeed at the center of mass of the ducted-fan (shroud+wing+boom) is denoted by $V_s = \frac{\dot{\psi}}{r_s}$, the angle of attack by α_s, the flight path angle by γ_s, the paddle angle by δ_p, the elevator angle by δ_e and the motor voltage by V_m. Subscripts s and w denote variables related to shroud and wing respectively. The Lagrange's equations of motion are given by

$$I_Z^s \ddot{\psi} = -r_s F_{X_s}^s - r_w F_{X_s}^w - r_b F_{X_s}^b - \dot{\theta} I_{X_b}^p \Omega \cos\theta \quad (27)$$

$$(m_b + m_f + \frac{m_c}{r^2})\ddot{z} = mg + F_{Z_s}^s + F_{Z_s}^w + F_{Z_s}^b \quad (28)$$

$$I_{Y_b r}^f \ddot{\theta} = M_{Y_s}^s + M_{Y_s}^w + I_{X_b}^p \dot{\psi} \Omega \cos\theta \quad (29)$$

where I_Z^s is the moment of inertia of the fan, boom and counterweight about OZ; $I_{Y_b r}^f$, the moment of inertia of the fan about O_bY_b when wing in rearward position; $I_{X_b}^p$, the moment of inertia of the propeller and the motor about O_bX_b; $F_{X_s}^b$, the X_s component of the boom aerodynamic force; $F_{X_s}^w$ and $F_{Z_s}^w$, the X_s and Z_s components of the wing aerodynamic force; $M_{Y_s}^w$, the Y_s component of the wing aerodynamic moment; $F_{X_s}^s$ and $F_{Z_s}^s$, the X_s and Z_s components of the shroud aerodynamic force; $M_{Y_s}^s$, the Y_s component of the shroud aerodynamic moment; r_b, the effective moment arm for the boom; r_w, the effective moment arm for the wing; r_s, the distance between O_b and the plane XOZ; m_b the mass of the boom; m_c, the mass of the counterweight; m_f, the mass of the fan; r, the pulley gear ratio; g, the gravity and Ω the motor velocity; $m := m_b + m_f - \frac{m_c}{r}$.

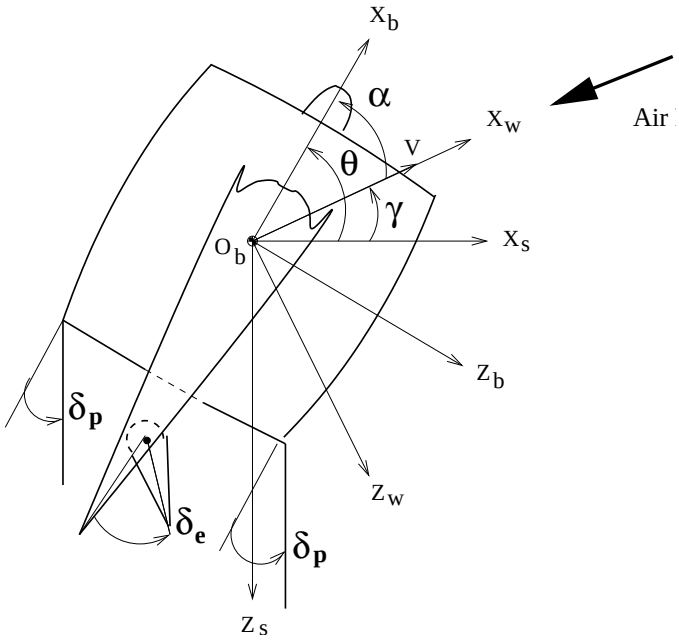

Figure 37: Shroud and Wing Conventions

Boom and wing aerodynamics Due to the rotation of the fan, the wing will experience increasing velocities from its root. A similar situation occurs for the boom. The aerodynamic forces of the wing and boom may be written as:

$$\begin{aligned} F^b_{X_s} &= F^b_{X_s}(\dot{\psi}, \dot{z}, C_{D_b}) \\ F^w_{X_s} &= F^w_{X_s}(\dot{\psi}, \dot{z}, C^w_D, C^w_L) \\ F^w_{Z_s} &= F^w_{Z_s}(\dot{\psi}, \dot{z}, C^w_D, C^w_L) \\ M^w_{Y_s} &= M^w_{Y_s}(\dot{\psi}, \dot{z}, C^w_M, C^w_D, C^w_L) \end{aligned}$$

where C_{D_b} is the drag coefficient of the boom (cylinder) and C^w_D, C^w_L and C^w_M, determined by a series of wind tunnel tests, are functions of α_w and δ_e. For now, the effects of all other derivatives are assumed negligible.

Shroud Forces and Moments There are two contributions to the shroud aerodynamic forces and moments: the thrust from the ducted fan engine and the aerodynamic forces of the shroud. In order to determine the shroud forces $F^s_{X_s}$ and $F^s_{Z_s}$, and moment $M^s_{Y_s}$, four 2-D table lookup ($F^{sT}_{X_b}$, C^s_D, C^s_L and C^s_M) as a function of α_s, V_m or δ_p are necessary.

Motor Speed A 2-D table lookup, function of V_m and δ_p, will be used to determine the motor velocity Ω. The effects of V and α are neglected.

The actuators are assumed to be perfect and the moments of inertias of the fan (shroud and wing) and the propeller about (O_bX_b) and (O_bZ_b) are neglected.

A.1 Linearized, unstable model about trim

A ducted fan analytical model can be described from equations 27 to 29 by a set of first order ODEs $\dot{x} = f(x,u)$ where $x^T = [V, z, \dot{z}, \theta, \dot{\theta}]$ and $u^T = [V_m, \delta_p, \delta_e]$ where $V := \dot{\psi} r_s$ and $r_s = 2.35$ is the radius in meters to convert angular to linear velocity. Although the horizontal linear distance navigation variable, ψr_s which is the integral of V, is not necessary as a state, the navigation variable, z, is necessary to control the altitude during experiments since the vertical movement is constrained by the testbed. Figure 21 is a schematic of the linearization about a trim point. A trim condition at level flight is obtained by solving the above non-linear algebraic equations at a forward flight velocity, $V_o = 6$ m/s, and zero altitude, z, and elevator deflection, δ_e, for the pitch angle θ, the motor voltage V_m, and the paddle angle δ_p. In other words, the trim conditions satisfy the following conditions:

$$x_{trim}^T = [V_o, 0, 0, \theta_{trim}, 0]\,, \quad u_{trim}^T = [V_{m_{trim}}, \delta_{p_{trim}}, \delta_{e_{trim}}]\,, \quad f(x_{trim}, u_{trim}) = 0_{1\times 5}$$

By computing the Jacobian of f about the trim point a perturbed linear model was obtained about, $V = 6$ m/s, $z = 0$ m, $\theta = 9.8104$ deg, $V_m = 1.0927$ Volt, $\delta_p = -9.1725$ deg, $\delta_e = 0$ deg, using (`linmod.m`) with the following results:

$$\frac{d}{dt}\begin{pmatrix} \delta V \\ \delta z \\ \delta \dot{z} \\ \delta\theta \\ \delta\dot{\theta} \end{pmatrix} = \begin{bmatrix} -0.0698 & 0 & -0.0269 & -0.7696 & 0 \\ 0 & 0 & 1.0000 & 0 & 0 \\ -0.1984 & 0 & -0.6141 & -3.6847 & 0 \\ 0 & 0 & 0 & 0 & 1.0000 \\ -0.0881 & 0 & -0.1544 & -0.8899 & 0 \end{bmatrix} \begin{pmatrix} \delta V \\ \delta z \\ \delta \dot{z} \\ \delta\theta \\ \delta\dot{\theta} \end{pmatrix} + \begin{bmatrix} 0.5569 & -0.0088 \\ 0 & 0 \\ -0.0344 & -0.1432 \\ 0 & 0 \\ 0.7034 & -2.3021 \end{bmatrix} \begin{pmatrix} \delta V_m \\ \delta_p \end{pmatrix}$$

$$y := \begin{pmatrix} \delta\dot{\psi} \\ \delta z \\ \delta\theta \end{pmatrix} = \begin{bmatrix} -1/r_s & 0 & 0 & 0 & 0 \\ 0 & 1 & 0 & 0 & 0 \\ 0 & 0 & 0 & 1 & 0 \end{bmatrix} \begin{pmatrix} \delta V \\ \delta z \\ \delta \dot{z} \\ \delta\theta \\ \delta\dot{\theta} \end{pmatrix}$$

Table 4 show the eigenvalues and eigenvectors of the linear continuous time plant model. This model predicts the following:

λ_1: rigid body mode in z-axis

$\lambda_{2,3}$: (stable, unstable) pair of slow ($\omega = .02\ Hz$) z-$\dot{\psi}$ axes coupled mode; Phugoid motion

$\lambda_{4,5}$: damped oscillating ($\omega = .15\ Hz, \zeta = .35$) θ-z-$\dot{\psi}$ axes coupled mode

	λ_1	λ_2	λ_3	$\lambda_{4,5}$
Degree-of-Freedom	0	-0.1195	0.1370	-0.3507 ± 0.9127i
δV	0	0.0989	0.1060	-0.0637 - 0.1177i
δz	1	0.9880	0.9846	-0.6390 + 0.2532i
$\delta \dot{z}$	0	-0.1181	0.1349	-0.0070 - 0.6721i
$\delta\theta$	0	0.010	-0.0332	-0.1625 + 0.0561i
$\delta\dot{\theta}$	0	-0.0013	-0.0045	0.0058 - 0.1680i

Table 4: Eigenvalues and eigenvectors of the unstable, continuous, analytical model.

The encoders directly measure ψ, z and θ, and a filter is used in the ψ channel to estimate its velocity. Hence the measured outputs are assumed to be $\frac{d\psi}{dt}$, z and θ, about trim. This derivative filter inevitably introduces a phase lag which we ignore for simplicity. In addition, the encoder outputs and actuator inputs are sampled and held at 100 Hz. This sampling rate

appears sufficiently fast to mitigate aliasing effects with the implementation of a digital anti-aliasing filter having a break frequency of 5 Hz. The filter was designed after preliminary testing and analysis of an analytical model of the Ducted fan which indicated that the system's significant dynamics was limited to about 2 Hz and it was decided that a discrete time controller will be designed and implemented at 20 Hz. A small phase lag introduced by this filter was deemed a good tradeoff to mitigate alliasing effects in the feedback loop during controller implementation.

Finally, it turns out that the above trim point is marginally unstable (or stable ?) and a stabilizing controller is required to collect any reasonable length of measurement.

A.2 Truth plant model and controller for simulation

The previous unstable analytical plant model is taken as the unknown true plant for generating simulated data. A truth plant model is defined for the purpose of simulation study only and is intended to define a particular idealized physical system and is assumed to be uniquely defined by a given mathematical model. [4] The main goal in this section is to determine how well (and validate) system identification algorithms recover a given true plant from simulated measurement data, before we consider actual measurement data. Although the physical states in general cannot be recovered through system identification, we identify and compare coordinate invariant physical properties such as plant eigenvalues and input-output maps such as frequency response. In addition, since the measured outputs are physical variables, a physical interpretation of the mode shape is possible.

The truth plant model is discretized at 20 Hz, which corresponds to the sampling rate of an actual laboratory experiment. The following Proportional-Derivative (PD) controller discretized at 20 Hz is used in the generation of the subsequent closed loop simulation data.

$$\begin{pmatrix} x_1 \\ x_2 \\ x_3 \\ x_4 \end{pmatrix}_{k+1} = \begin{bmatrix} 0.441 & 0.013 & 0 & 0 \\ -13.110 & -0.148 & 0 & 0 \\ 0 & 0 & 0.441 & 0.013 \\ 0 & 0 & -13.110 & -0.148 \end{bmatrix} \begin{pmatrix} x_1 \\ x_2 \\ x_3 \\ x_4 \end{pmatrix}_k + \begin{bmatrix} 0 & 0.558 & 0 \\ 0 & 13.110 & 0 \\ 0 & 0 & 0.558 \\ 0 & 0 & 13.110 \end{bmatrix} \begin{pmatrix} \delta\dot{\psi} \\ \delta z \\ \delta\theta \end{pmatrix}_k$$

$$\begin{pmatrix} \delta V_m \\ \delta_p \end{pmatrix}_k = \begin{bmatrix} 0 & 0 & 0 & 0 \\ 0 & -0.014 & 0 & 0.226 \end{bmatrix} \begin{pmatrix} x_1 \\ x_2 \\ x_3 \\ x_4 \end{pmatrix}_k + \begin{bmatrix} 1.703 & 0 & 0 \\ 0 & -0.047 & 1.131 \end{bmatrix} \begin{pmatrix} \delta\dot{\psi} \\ \delta z \\ \delta\theta \end{pmatrix}_k$$

This controller consists of two separate feedback loops, namely, the first input δV_m feeds back only $\delta\dot{\psi}$ while the second input δ_p feeds back a linear combination of δz and $\delta\theta$. The first input is designed to regulate the constant rate rotation by providing a negative proportional feedback on the deviation of the flight velocity about trim while the second input is designed to stabilize and regulate both its attitude and altitude. It is physically significant to note that this particular controller actually stabilizes the Ducted fan in a laboratory experiment. The closed loop performance of this PD controller is used as a baseline to validate the performance of an independent controller in an outer loop.

[4] However, in many physical systems which are of engineering interest, a "true" plant defined by a unique mathematical model may not exist. Hence, much debate revolves around the mismatch between measured data and that predicted by various "true" mathematical models, which motivates voulmnous previous work in areas such as system identification, model validation, robust control and countless related experiments.

A.3 Comparison of analytical model response to measurement

To get an idea of the accuracy of the analytical model, we compare the spectra of the measured closed loop output (input) to the predicted closed loop output (input) from the analytical model driven by the same test signal used in the experiment. The unstable analytical plant model with the PD controller used in the experiment is stable in closed loop. No unknown noise or disturbance is assumed in the simulated response.

Figures 38 and 39 show measured (solid) and predicted (dash) magnitude spectra of the closed loop outputs and inputs, respectively. Specifically, note that

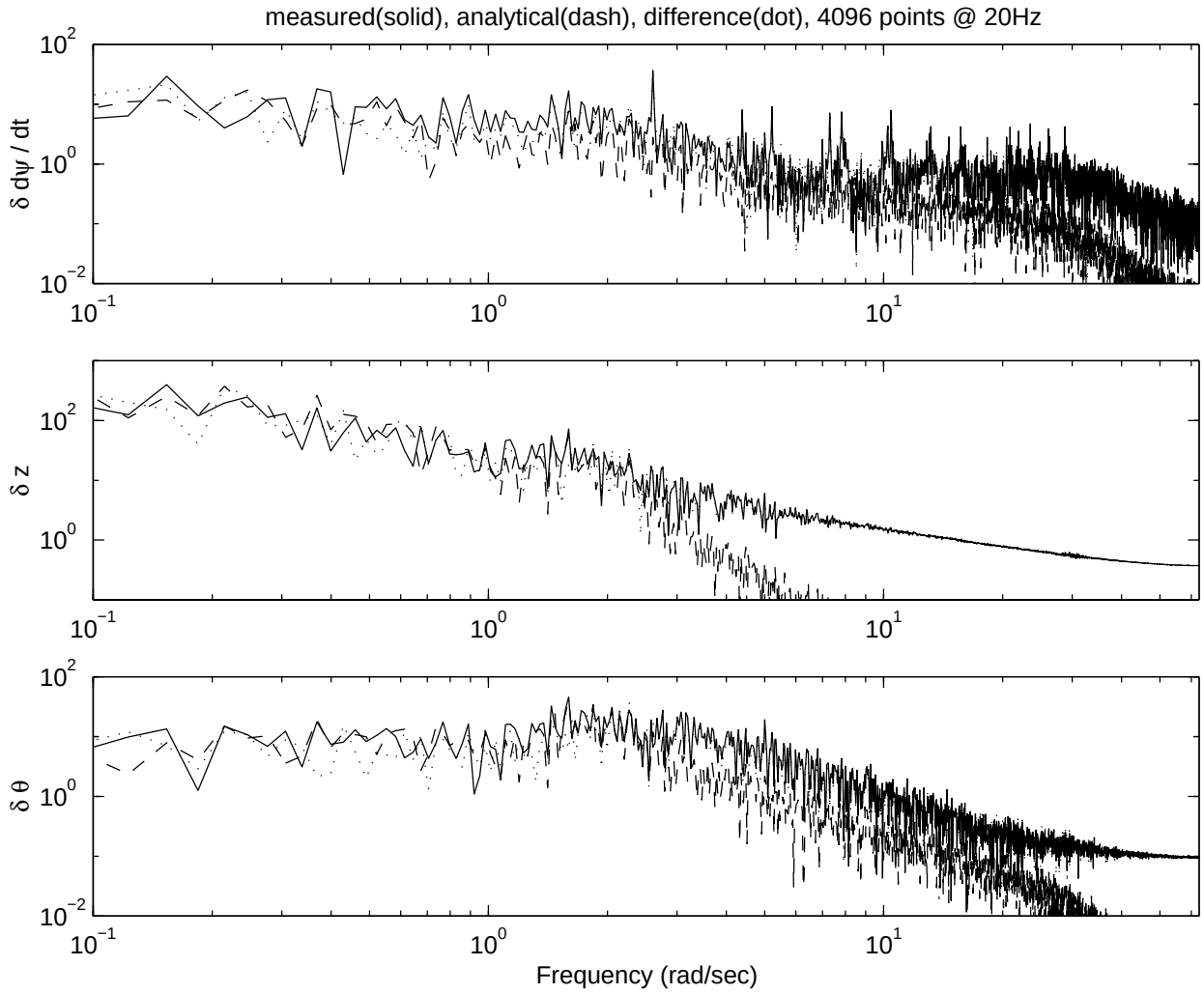

Figure 38: Measured magnitude spectra of PD closed loop output vs analytical model prediction

- The first channel in the measured output, $\delta d\psi/dt$, and the fan voltage input, V_m, show resonant peaks at about 2.5 rad/sec which corresponds to the nominal rotation rate of the Ducted fan about the z-axis, i.e., $d\psi/dt = V/r_s = (6m/s)/(2.35m) = 2.55$ rad/sec. There also appears to be higher harmonic resonant peaks at about 5 and 10 rad/sec.
- The discrepencies, as a percentage of its nominal response in the output spectra, is generally larger with increasing frequencies. This is likely due to the combination of (i)

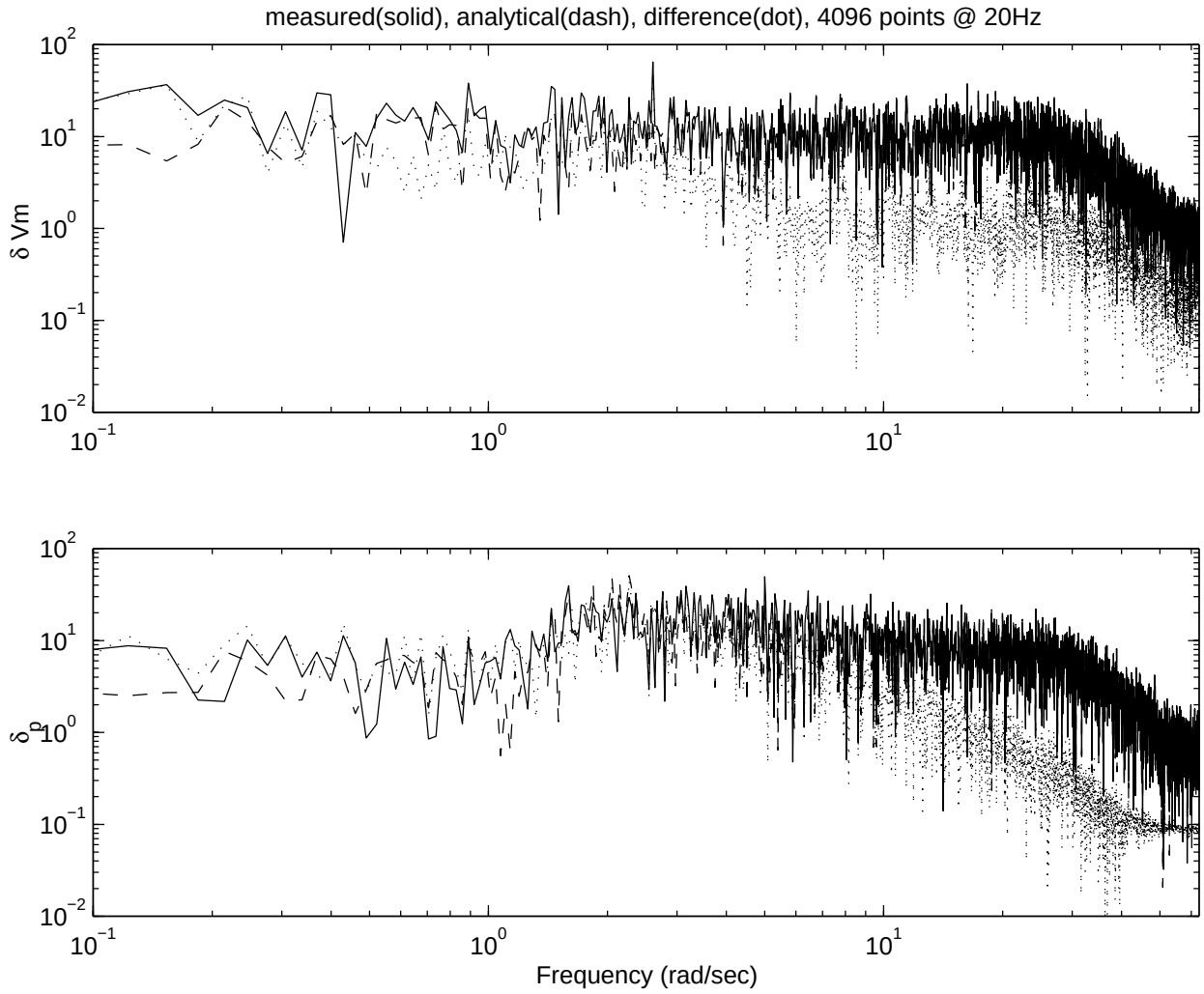

Figure 39: Measured magnitude spectra of PD closed loop inputs vs analytical model predicticition

a less reliable analytical model at higher frequencies and (ii) the presence of wideband noise which plays a more prominent role at higher frequencies where the plant rolls off.

In summary, there are significant discrepencies between the spectra of the measured closed loop output and the output simulated from an analytical model in all five channels. Note that similarities in the spectra magnitudes may appear more optimistic than it actually is since their phases could be totally off. Hence, the figures also show the magnitude of the differences in their complex spectra (dot). To get some feel for model errors from these signals, we compute the following signal ratios

$$\begin{aligned} \frac{\|y_{meas} - y_{sim}\|}{\|y_{sim}\|} &\lesssim \bar{\sigma}(\Delta_{out\ mult}) \\ \frac{\|y_{meas} - y_{sim}\|}{\|r\|} &\lesssim \bar{\sigma}(\Delta_{add}) \end{aligned}$$

which are given in Figures 40. The above ratios roughly approximates a lower bound on the 2-norm of a complex 3 by 3 full-block output multiplicative uncertainty and the 2-norm of a 3

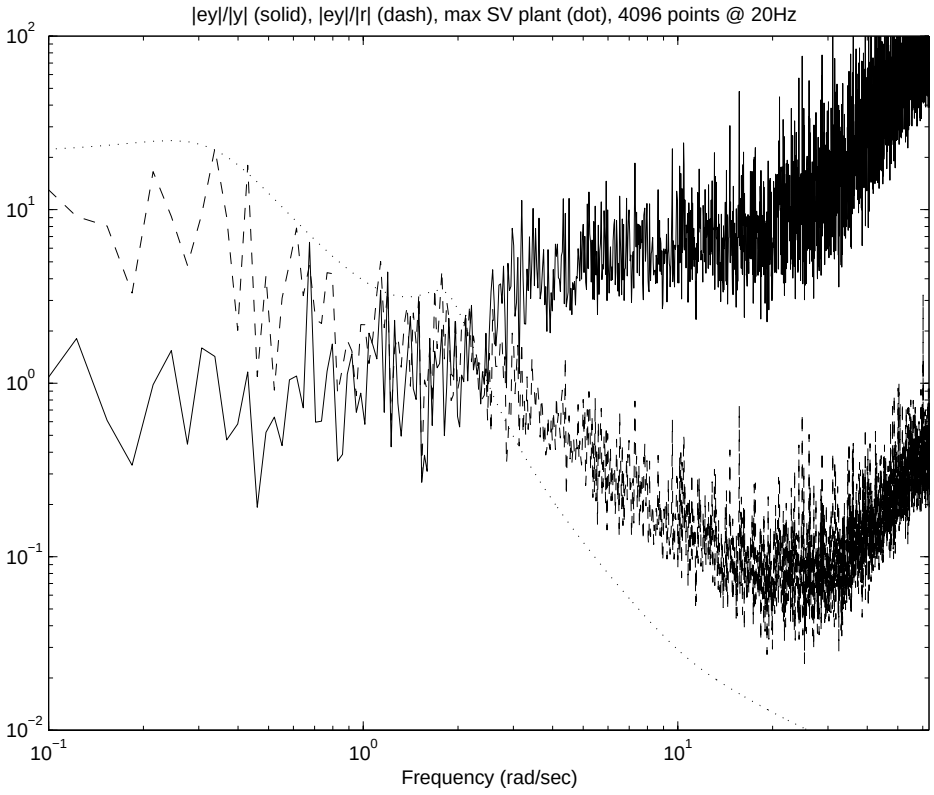

Figure 40: Ouput difference signal ratios.

by 2 additive uncertainty, respectively. The figure shows that the multiplicative uncertainty increases with frequency while in the additive uncertainty it decreases. This makes sense because the multiplicative uncertainty is a factor of the noiminal plant which rolls off as indicated by the maximum singular value frequency response of the closed loop system using analytical plant model (dotted line).

To get a feel for the noise and disturbance levels in the system, Figure 41 shows the measured closed loop time histories when the system is forced (left column) and free (right column). Clearly, the system is very noisy particularly in the forward motion (first channel). The perturbed forward motion ($\delta d\psi/dt$), in both the forced and free closed loops matche the rotation rate about the z-axis. This is more evident from an estimated equivalent output noise spectrum which show peaks whose frequency matches the z-axis rotation rate of the Ducted fan. By flying through its own wake periodically, the resulting turbulent aerodynamic forces will depend on past control input histories (fan speed and vector thrust angle) and current attitude and position. This causes the exogenous output noise to be correlated to both input and output variables which will cause unknown bias errors in the identification of an empirical model. In addition, a vertical drift or a very slow oscillation is also present in the z plot of free response.

In summary, a large discrepency exists between the predicted spectra from the analytical model and measured data which suggests a significant level of inaccuracy in the analytical model. Furthermore, the unknown noise and disturbances in the system appears significant indicating that an empirical nominal model development through system identification may not be trivial, and properly accounting for unknown exogenous disturbances in any validation process is clearly important. Of course, the accuracy of any analytical model of the Ducted fan depends on the assumptions made about the physical system during model development.

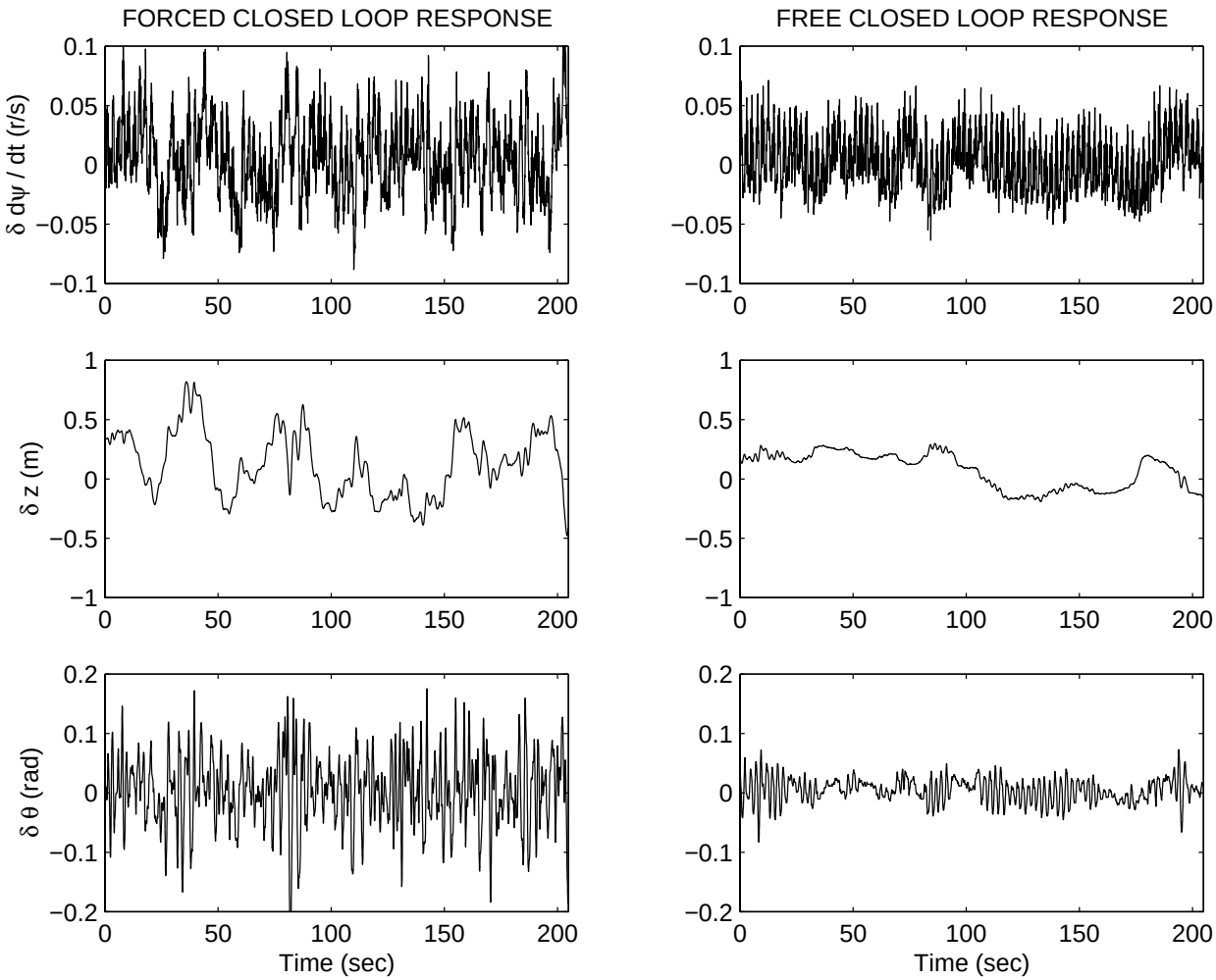

Figure 41: Forced (left column) and free (right column) closed loop output measurements.

A partial list of these assumptions involve:

- inertial properties, dimensions, and center of gravity location, ...
- nature of friction, energy dissipation mechanism, stiction, between rotating parts, ...
- structural flexure in the composite boom, suporting cables, gears, ...
- aerodynamic models
  - boom aerodynamics, $F^b_{X_s}(\dot{\psi}, \dot{z}, C_{D_b})$
  - wing aerodynamics, $F^w_{X_s}(\dot{\psi}, \dot{z}, C^w_D, C^w_L)$, $F^w_{Z_s}(\dot{\psi}, \dot{z}, C^w_D, C^w_L)$, $M^w_{Y_s}(\dot{\psi}, \dot{z}, C^w_M, C^w_D, C^w_L)$
  - shroud aerodynamics, $F^s_{X_s}$, $F^s_{Z_s}$, $M^s_{Y_s}$
- motor velocity dependence, $\Omega(V_m, \delta_p)$
- wall and turbulent wake effects on aerodynamics
- uncertainties in tabulated component wind tunnel test data

Therefore, the Ducted fan is difficult to model accurately with confidence because it is difficult or near impossible to verify all the assumptions related to the above list.

A.4 Identified models from simulated data

In this section, we investigate whether an empirical model obtained directly from experimental data can reduce the significant discrepency that exists for the analytical model. We show system identification results based on simulated data to validate the identification method which is subsequently applied to experimental data. Based on both simulation and experimental results, we discuss inherent limitations in the system identification approach. All closed loop simulated data in this chapter is generated from an assumed unstable analytical truth model with a known PD control law.

A.4.1 System identification algorithm

We briefly outline a popular a time domain identification method called the Subspace Model Identification (SMI) [25, 26] which we use to obtain all subsequent system identification results in this report. The identification software *SMI Toolbox Version 1.0* was obtained from [27]. The SMI method is based on approximating structured subspaces of observability matrix from input-output data and then directly realizing state space matrices from the data equation with the aid of a shift-invariant property of the observability matrix. An output-error state space structure is assumed as shown in Figure 42 which also covers black-box models such as ARMAX and OE [5]. The following is a description of the ordinary MOESP

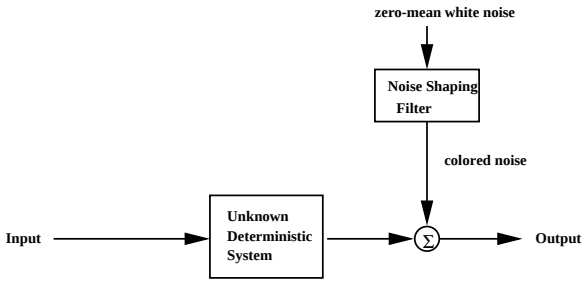

Figure 42: Output Error State Space model identification (MOESP) setup.

algorithm in a nutshell:

1. Suppose we have measured input and output data sequence from time index j to $(j+N+i-2)$

$$[u_j, \ldots, u_{j+N+i-2}], \quad [y_j, \ldots, y_{j+N+i-2}] \qquad u_k \in R^m \quad y_k \in R^l$$

2. Assume that this finite segment of the data sequence satisfy the noise-free LTI relation

$$\text{Assumption 1:} \qquad x_{k+1} = Ax_k + Bu_k, \quad y_k = Cx_k + Du_k$$

meaning that the following data equation holds:

$$\underbrace{\begin{bmatrix} y_j & y_{j+1} & \cdots & y_{j+N-1} \\ y_{j+1} & y_{j+2} & \cdots & y_{j+N} \\ \vdots & & \ddots & \\ y_{j+i-1} & y_{j+i} & \cdots & y_{j+N+i-2} \end{bmatrix}}_{Y_{j,i,N}} = \underbrace{\begin{bmatrix} C \\ CA \\ \vdots \\ CA^{i-1} \end{bmatrix}}_{\Gamma_i} \underbrace{\begin{bmatrix} x_j & x_{j+1} & \cdots & x_{j+N-1} \end{bmatrix}}_{X_{j,N}}$$
$$+ \underbrace{\begin{bmatrix} D & 0 & & \cdots & 0 \\ CB & D & 0 & \cdots & 0 \\ CAB & CB & D & \cdots & 0 \\ \vdots & & & \ddots & \vdots \\ CA^{i-2}B & & & \cdots & D \end{bmatrix}}_{H_i} \underbrace{\begin{bmatrix} u_j & u_{j+1} & \cdots & u_{j+N-1} \\ u_{j+1} & u_{j+2} & \cdots & u_{j+N} \\ \vdots & & \ddots & \\ u_{j+i-1} & u_{j+i} & \cdots & u_{j+N+i-2} \end{bmatrix}}_{U_{j,i,N}} \tag{30}$$

3. To obtain an approximation to column space of Γ_i, assume the following:

   Assumption 2: (A, B, C, D) is minimal of order n
   Assumption 3: $i > n$
   Assumption 4: $rank \begin{bmatrix} U_{1,i,N} \\ X_{1,N} \end{bmatrix} = mi + n$

   and a RQ factorization of the fat (by assuming a sufficiently long measured time segment, i.e., a large N) data matrix pair is computed

$$\begin{bmatrix} U_{1,i,N} \\ Y_{1,i,N} \end{bmatrix} = \begin{bmatrix} R_{11} & 0 \\ R_{21} & R_{22} \end{bmatrix} \begin{bmatrix} Q_1 \\ Q_2 \end{bmatrix}$$

   where R_{11} and R_{22} are lower triangular matrices and the rows of Q_1 and Q_2 are orthonormal. With Assumptions 1 to 4, it can be shown that $Image(R_{22}) = Image(\Gamma_i)$ and an orthonormal bases for $Image(\Gamma_i)$ can be computed from the SVD

$$R_{22} = \begin{bmatrix} U_n & U_n^{\perp} \end{bmatrix} \begin{bmatrix} S_n & \\ & S_2 \end{bmatrix} \begin{bmatrix} V_n^T \\ (V_n^{\perp})^T \end{bmatrix}$$

4. The orthonormal base matrix, U_n, which is related to the unknown observability matrix, Γ_i by $U_n = \Gamma_i T$ where T is an unknown square nonsingular matrix, can be used to compute state and output matrices A_T and C_T using a structural property of observability matrix

$$\underbrace{\begin{bmatrix} C \\ CA \\ \vdots \\ CA^{i-2} \end{bmatrix}}_{\Gamma_i^{(1)}} A = \underbrace{\begin{bmatrix} CA \\ CA^2 \\ \vdots \\ CA^{i-1} \end{bmatrix}}_{\Gamma_i^{(2)}} \tag{31}$$

   Since T is square and nonsingular, the above "shift-invariant" property can be rewritten as

$$\underbrace{\Gamma_i^{(1)} T}_{U_n^{(1)}} \underbrace{(T^{-1} A T)}_{A_T} = \underbrace{\Gamma_i^{(2)} T}_{U_n^{(2)}}$$

so that A_T can be computed uniquely since $U_n^{(1)}$ has full column rank per assumptions 2 and 3. The corresponding output matrix, C_T, can be determined by noting that U_n is the observability matrix in transformed coordinates and therefore the partitioned matrix consisting of the first l-rows of U_n is C_T.

5. Notice from the noise-free data equation (30) that if A and C are known, the only unknowns are B and D which appears linearly. Hence, after some algebraic gymnastics [25], one can obtain the following overdetermined equation ($(li-n)i \times m$ equations with $(m+n) \times m$ unknowns)

$$\begin{bmatrix} \Xi(:,1:m) \\ \vdots \\ \Xi(:,m(i-1)+1:mi) \end{bmatrix} = \begin{bmatrix} U_n^{\perp}(1:l,:)^T & \dots & U_n^{\perp}(l(i-1)+1:li)^T \\ \vdots & & \vdots \\ U_n^{\perp}(l(i-1)+1,:)^T & \dots & \end{bmatrix} \begin{bmatrix} I_l & 0 \\ 0 & U_n^{(1)} \end{bmatrix} \begin{bmatrix} D \\ B_T \end{bmatrix}$$

where $\Xi := (U_n^{\perp})^T R_{21} R_{11}^{-1}$, and a least squares solution of B_T and D can be obtained. It is important to note that a least squares solution will result in satisfying only approximately both the shift invariant property, equation (31), and the noise-free data equation (30) and this limitations on model accuracy is unclear.

Overall, SMI approach is computationally easy but the performance of the method is unproven under noise and disturbance (SMI is a deterministic approach), nonperiodic test signal, uncertainty in the assumed minimal order of the state. Various recent work reported in IFAC's Symposium on System Identification SYSID 2000 [15] is a testament to the high level of interest in this particular identification method. Hence, before we consider experimental data, we evaluate this algorithm using simulated data.

A.4.2 Identified models of $(I-KP)^{-1}$ from simulated data

Simulated data containing low (variance $\sigma = 10^{-8}$) and high (variance $\sigma = .03$) measurement noise levels are considered. The simulated high noise level roughly approximates the actual measurement noise levels in terms of signal to noise ratio. In the system identification simulations for the high noise level cases, 100 minutes of data (or 29 signal samples each approximately 3.4 minutes duration sampled at 20 Hertz) are assumed while for the low noise level cases only 20 minutes of data (or 5 signal samples) are assumed. In actual experiments, the measurement data is 20 minutes duration.

Figure 43 shows the singular values which help determine suitable orders for the input sensitivity state space model corresponding to low (left figure) and high (right) noise cases. In both cases, a (carefully selected at) random upper bound order of 18 is chosen to compute the singular values of the Hankel matrix. Notice from the low noise case (left figure) that nine singular values corresponding to the true closed loop system states stands out because of the very low noise floor. This is in sharp contrast to the high noise case (right figure) where the high noise floor conceal states beyond the first five.

In the low noise case, it was found that although the largest singular value gap occurs after the first nine states, thus suggesting a natural reduced order, both 9 and 8th order realizations were unstable and the largest stable realization order was 7. In the high noise case however, the largest singular value gap occurs after the first five states but this gap is relatively small. Therefore in both cases, all 9 states of the truth model was not recovered. In retrospect, this limitation is expected in most nontrivial applications in system identification where the lesser observable and/or controllable states are difficult to recover due to their relative lack of participation in the output signal.

Figures 44 and 45 show the frequency responses for the true and identified 7th order input sensitivity model corresponding to low and high noise cases respectively. The dash

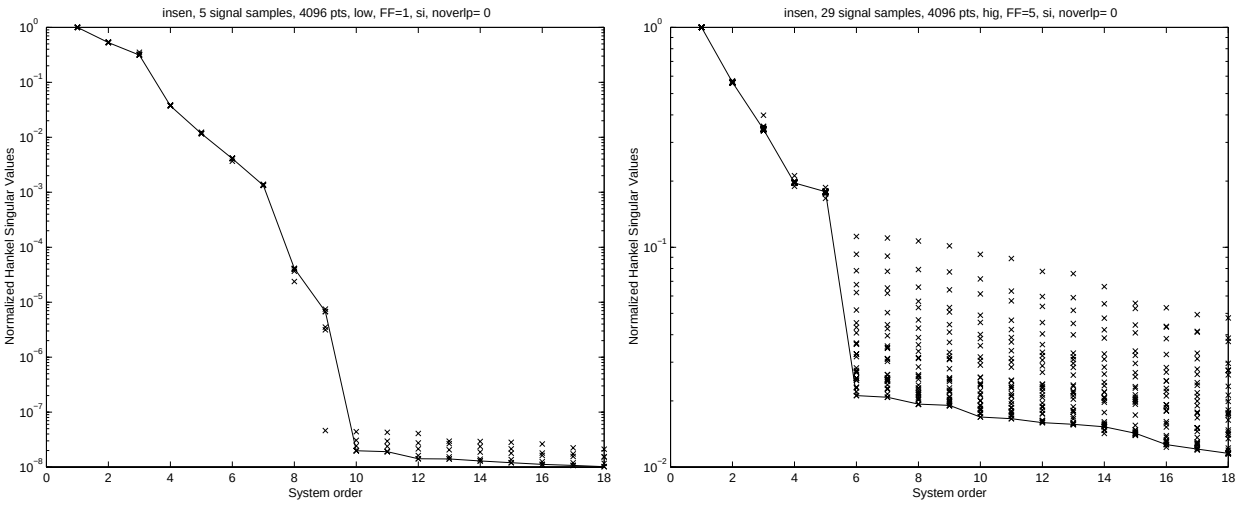

Figure 43: Singular values to determine order of input sensitivity from simulated data, low noise $\sigma = 10^{-8}$ (left), high noise $\sigma = .03$ (right).

lines denote the true frequency response while the solid lines denote the identified frequency responses. It is clear from these figures that identification results based on low noise data give a much more accurate model. The gains of the difference between true and identified frequency response for the low noise case is about one percent of the true frequency response (analogous to one percent multiplicative error for each channel) over all frequency. On the other hand, for the high noise case, the match at the low frequencies are poor while the match at the higher frequencies for the diagonal channels are excellent. These appear to be the result of the input sensitivity which attenuates the lower frequency signals at the input, causing a poor signal-to-noise ratio and the characteristic loop gain rolloff which drives the input sensitivity to identity, causing a good signal-to-noise ratio. Clearly, inspite of a significantly longer data record, using data with a high level of noise (comparable to measured data), resulted in a significantly less accurate model as compared to resulting model based on data with a low level of noise.

A.4.3 Identified models of $(I - PK)^{-1}P$ from simulated data

Figure 46 shows the singular values which help determine the orders of a state space model of the closed loop transfer function across plant based on simulated data containing low (left) and high (right) noise levels. Again, an upper bound order of 18 is chosen to compute these singular values. For the low noise case (left figure) 10 states stands out (true states being 9 only) while only 5 states stands out . for the high noise case where the noise floor is high. For the low noise case, it was found that 7, 8 and 9th order realizations were unstable and so a 6th order stable realization was chosen. On the other hand, a stable 7th order realization was chosen for the high noise case although it appears that only five states appear to dominate the response. In general, choosing higher order models often introduced fictitious poles and zeros and did not improve the model.

Figures 47 and 48 show the true (dash) and identified (solid) frequency responses for the 6th and 7th order models of the closed loop transfer function across plant corresponding to low and high noise cases respectively. Similar to earlier results for input sensitivity, low noise data leads to a more accurate model (inspite of using much longer data record for high noise data case). The multiplicative error is roughly 1 percent error for the low noise case whereas it is roughly 10 % error for the high noise case, in the frequency range of interest (say .1 to

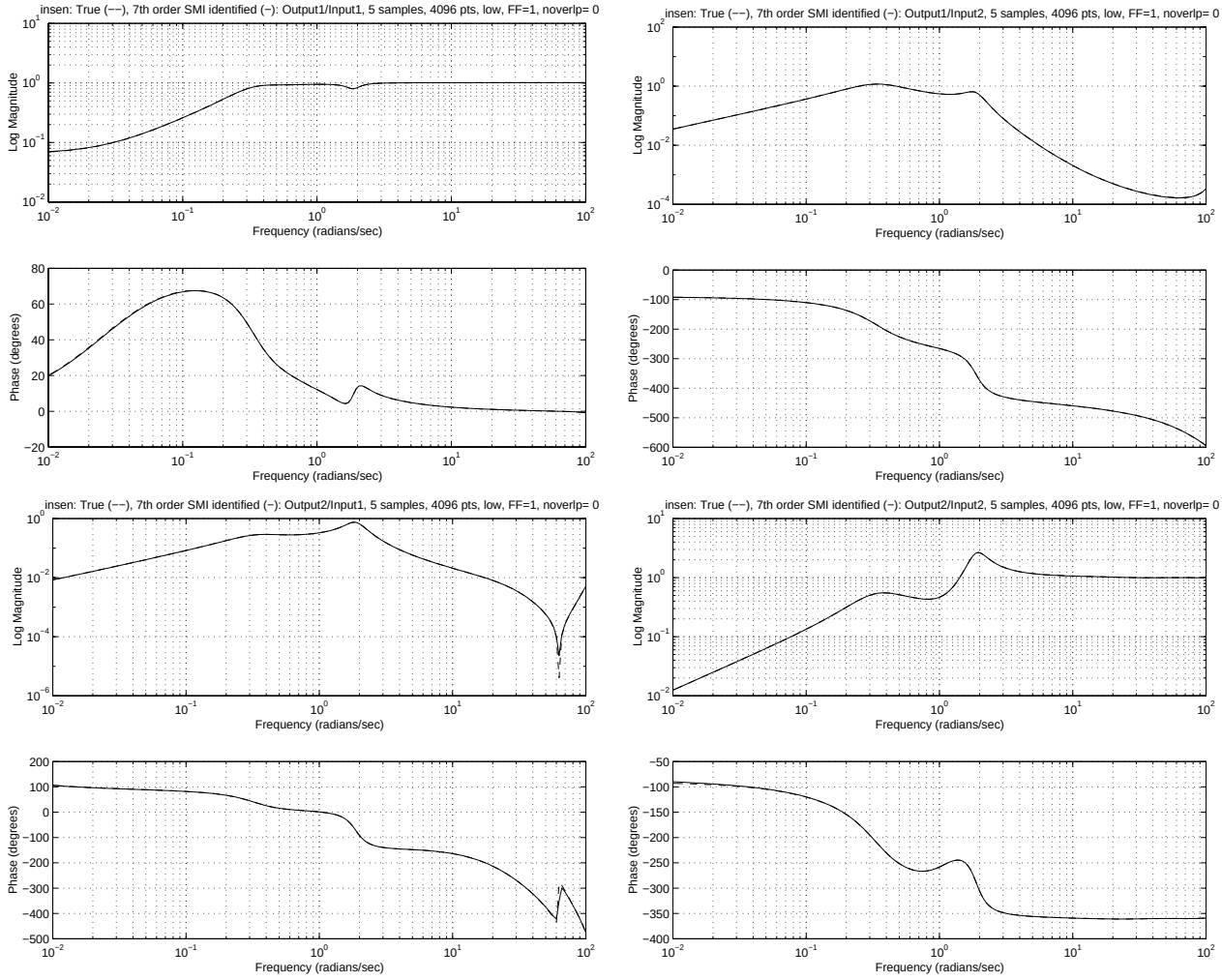

Figure 44: Input sensitivity, 20 minutes simulated data: True (dash), Identified 7th order (solid), low noise $\sigma = 10^{-8}$.

10 rad/sec).

A.4.4 Summary of simulation results

The results based on simulated data appears to validate the SMI identification methodology. Hence we show next the results of applying the identification algorithm to actual measured data. However, even in the ideal low noise simulated cases, the true order of both closed loop systems could not be determined exactly although the frequency response of the identified systems matched quite accurately ($< 1\%$). Of course this basic limitation is of concern to any identification method because internal variables or states generally do not contribute equally to the input/output data. The results demonstrate that this generic problem becomes more acute with higher levels of noise. In addition, the effects of nonlinearity can further blur the gap between dominant system states and those which appears as noise effects.

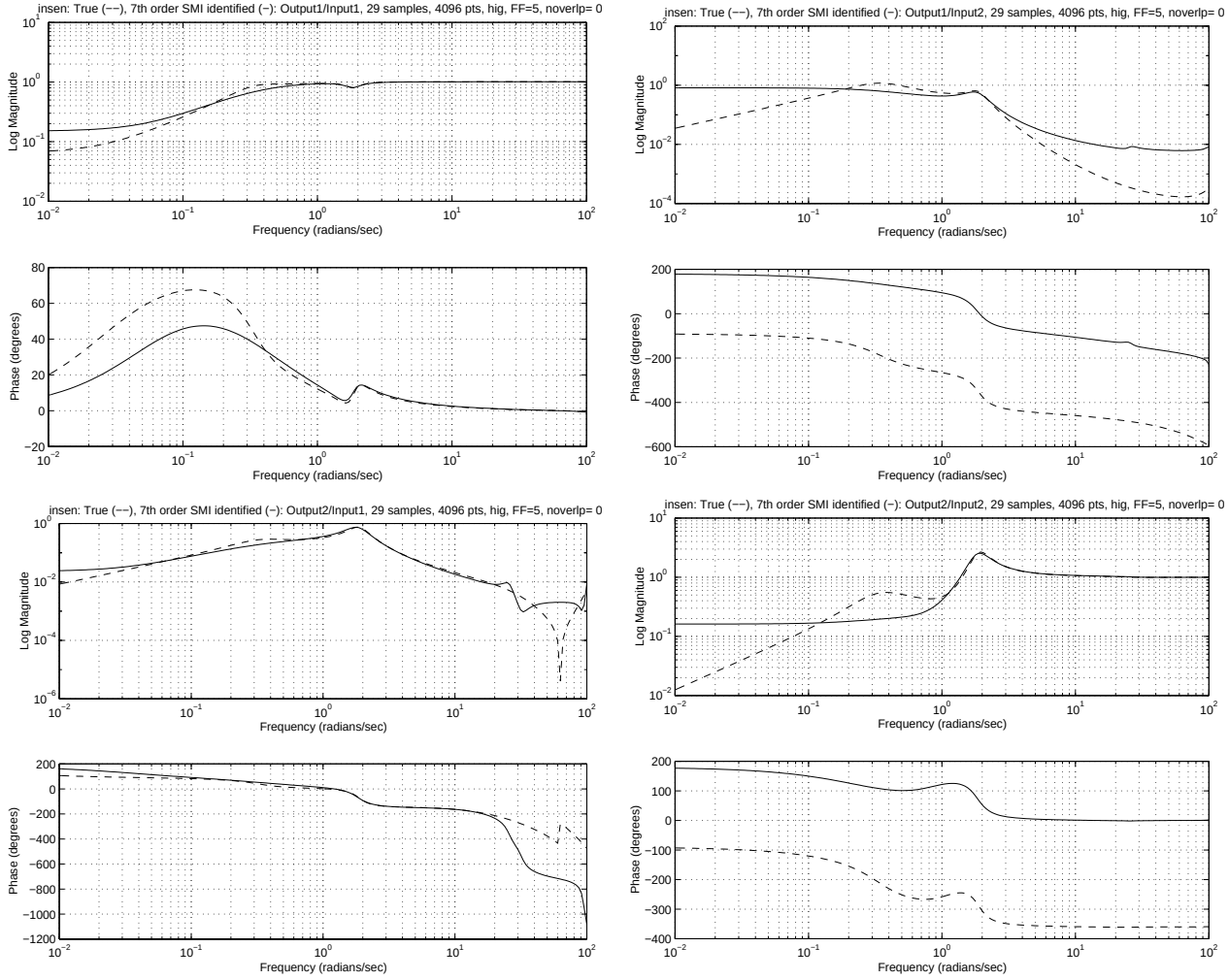

Figure 45: Input sensitivity, 100 minutes simulated data: True (dash), Identified 7th order (solid), high noise $\sigma = .03$.

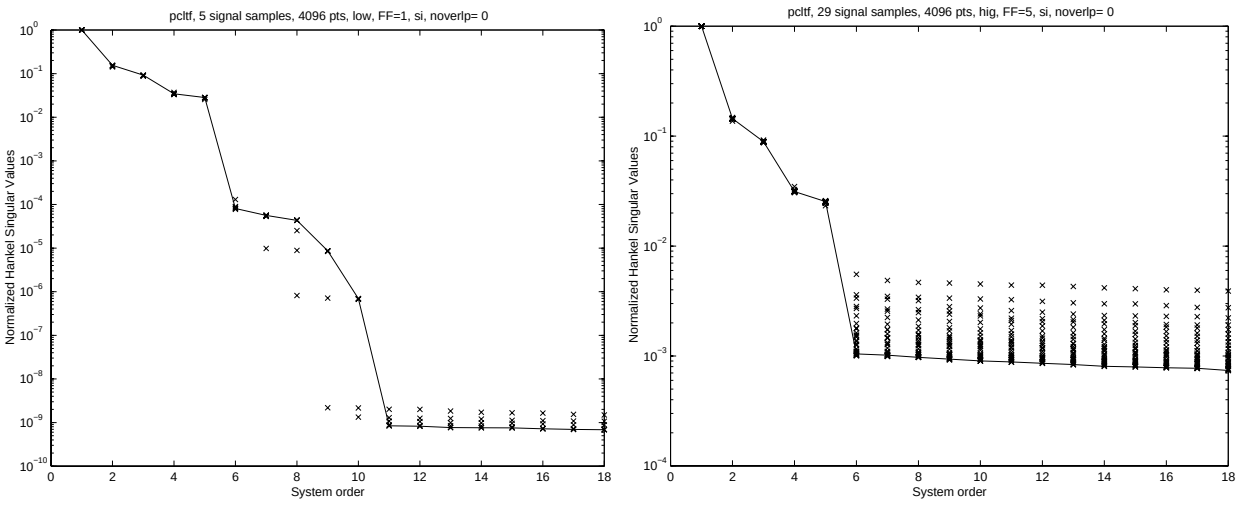

Figure 46: Singular values to determine order of closed loop transfer function across plant from simulated data, low noise $\sigma = 10^{-8}$ (left), high noise $\sigma = .03$ (right).

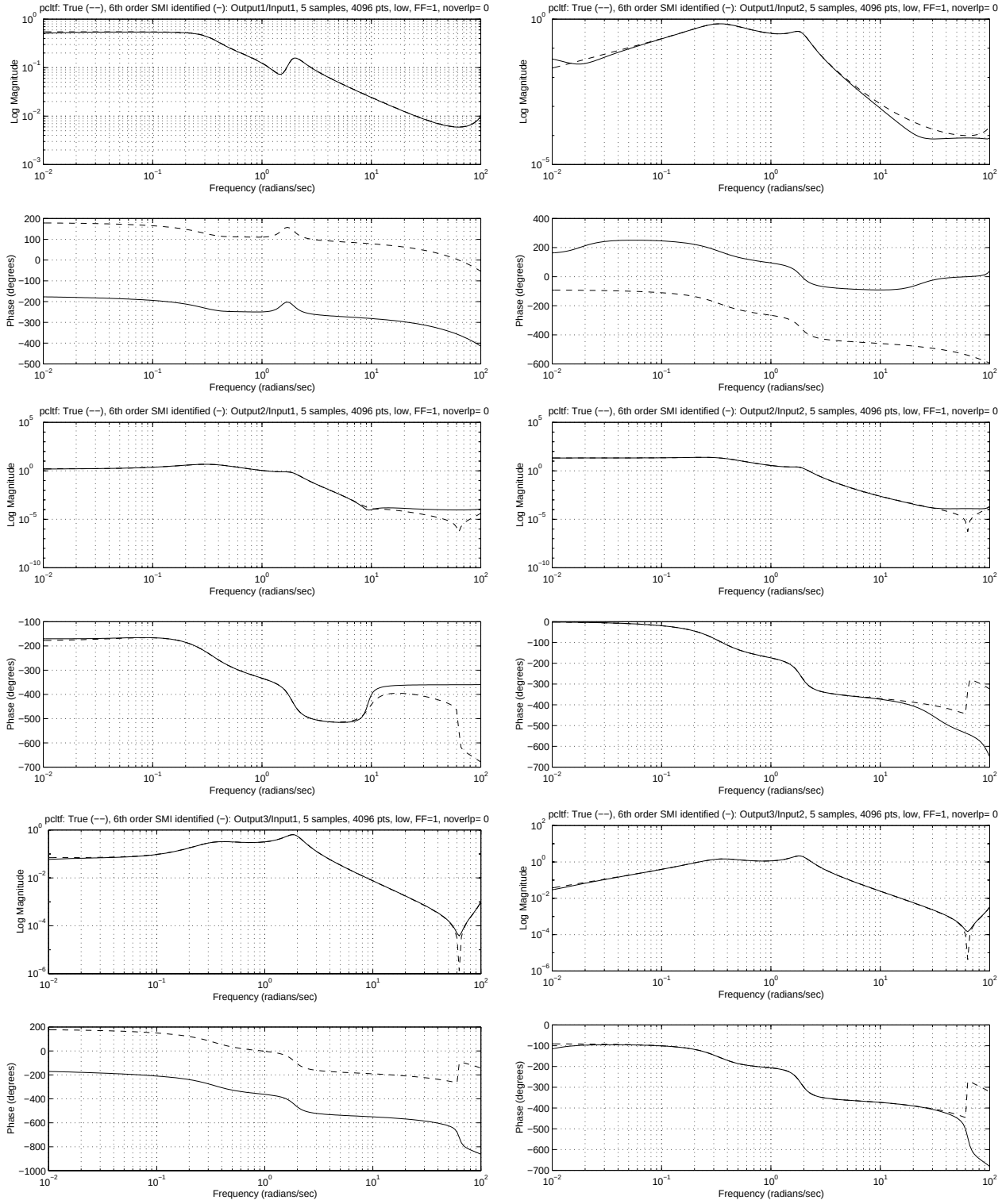

Figure 47: Closed loop transfer function across plant, 20 minutes simulated data: True (dash), Identified 6th order (solid), low noise $\sigma = 10^{-8}$.

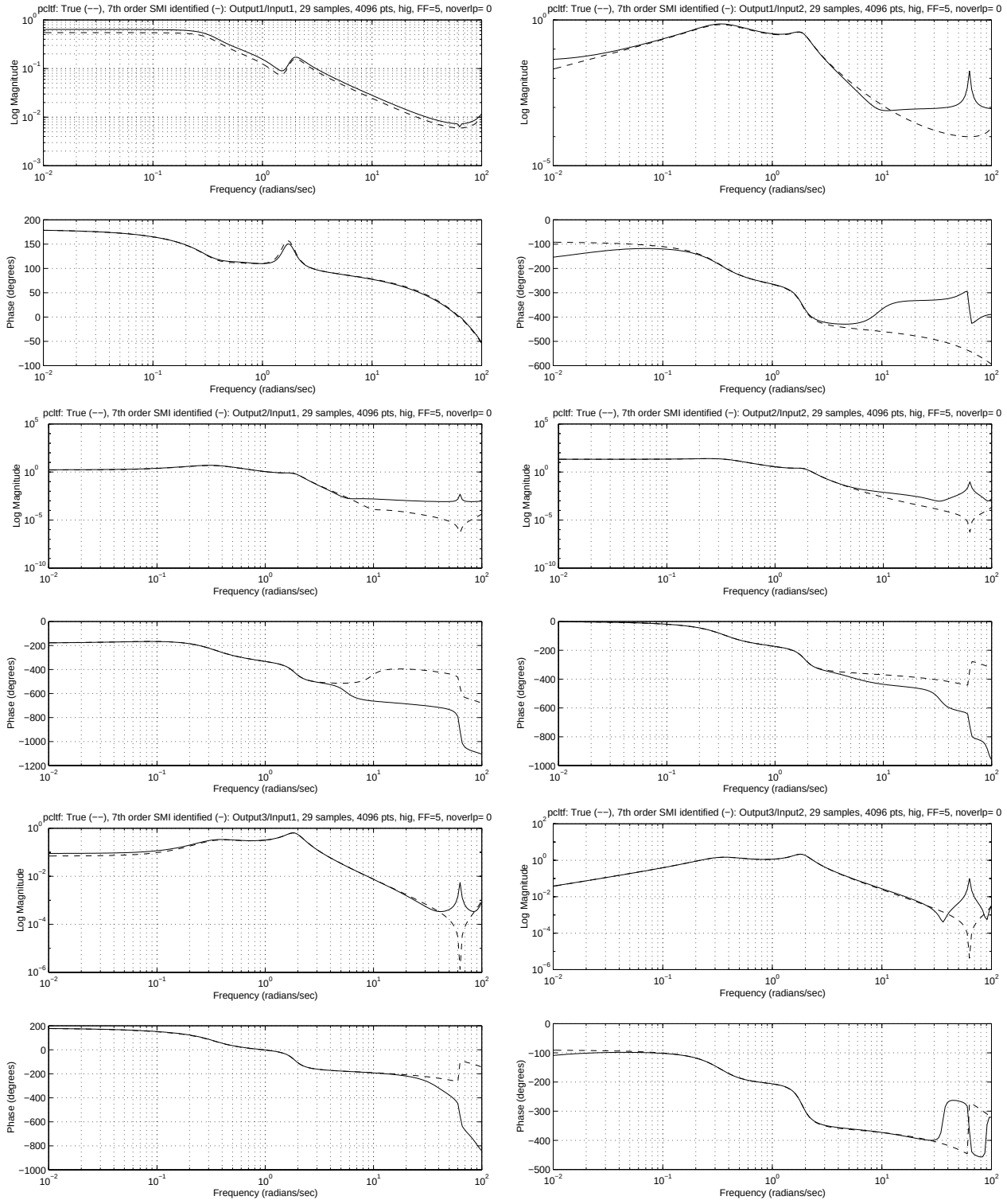

Figure 48: Closed loop transfer function across plant, 100 minutes simulated data: True (dash), Identified 7th order (solid), high noise $\sigma = .03$.

A.5 Identified models from experimental data

A.5.1 Identified model of $(I - KP)^{-1}$

Figure 49 shows the time histories of commands, total inputs and the resulting outputs from a closed loop system identification experiment. Both command signals are designed to be wideband signals which are heavily weighted for frequencies below 5 Hz. This measurement data is used to compute the singular values which are used to determine a suitable order for the input sensitivity state space model. An upper bound order of 18 (same value used in simulation) is chosen to construct the data matrix which give these singular values. To increase the number of refinements by increasing the number of samples in the calculation of these singular values, an overlap of 2048 time points are used to produce 10 samples instead of 5 resulting in slightly improved results, as shown in Figure 50. The singular values show no significant gap to indicate a natural order of the system and a 9th order realization is chosen, guided by the 9th order of the analytical input sensitivity model given earlier.

Figure 51 shows the frequency response of an identified 9th order input sensitivity model. The frequency response of this model roughly resembles the results from an analytical input sensitivity model over the frequency range of interest from .1 to 10 rad/sec. The figure show a typical dilemma in trying to decide with some confidence, which among the two approximate models is more accurate.

A.5.2 Identifed model of $(I - PK)^{-1}P$

Figure 52 shows the singular values to determine an order of a state space model of the closed loop transfer function across plant. An upper bound order of 18 is chosen to compute these singular values and an 8th order realization is chosen. Again, there are no obvious gaps in the singular value spread but these singular values drops off more rapidly than the input sensitivity case. Hence we expect a slightly better fit of the data with 8 states. It is found that a 9th order realization produced an unstable system and higher order realizations introduced unrealistic poles and zeros at unpredictable locations.

Figure 53 shows the predicted and an identified 8th order model of the closed loop transfer function across plant. Note that this identified model only roughly matches the analytical frequency response. The match appears to be better in the second input, namely, paddle angle δ_p, than for the fan motor voltage input V_m. This likely indicates a better analytical model in the dynamics associated with the paddle angle input, particularly in the prediction of the altitude z and angle of attack θ.

A.5.3 Prediction error and summary

We adopt the conventional view of an accurate model - one which accurately matches the measured output due to an arbitrary input, i.e., "the essence of a model is its prediction aspect" (page 170, [5]). To this end, Figures 54 show comparisons of magnitude spectrums of measured, analytically predicted, and corresponding prediction errors. The prediction errors for analytical and identified[5] models shown in the figures are l_2 norms over the frequency range .1 to 10 rad/sec normalized by the l_2 norms of the corresponding measured signals. Observe that the prediction errors for the identified model is less than that of the analytical

[5]The predicted response based on identified model used in the comparisons are actually two separate identified models obtained independently, input sensitivity and closed loop system across plant. However, this implies that a corresponding identified open loop plant which satisfies the closed loop equations cannot be determined exactly because it is overdetermined.

model but there is still significant discrepencies relative to the measured spectra. Note that the effects of significant but unknown disturbances and noise have not been included in the prediction by both models in the above comparisons.

In summary, the identified closed loop model appears to be more accurate than the analytical model because it better predicts the measured signals. Supported by simulation results, it was found experimentally that the orders for the identified models for both input sensitivity and closed loop across plant were unclear because of the obvious presence of significant noise levels. Overall, the identified models resembles the analytical model but appears too large when this difference is viewed as an additive model error, for robust control application.

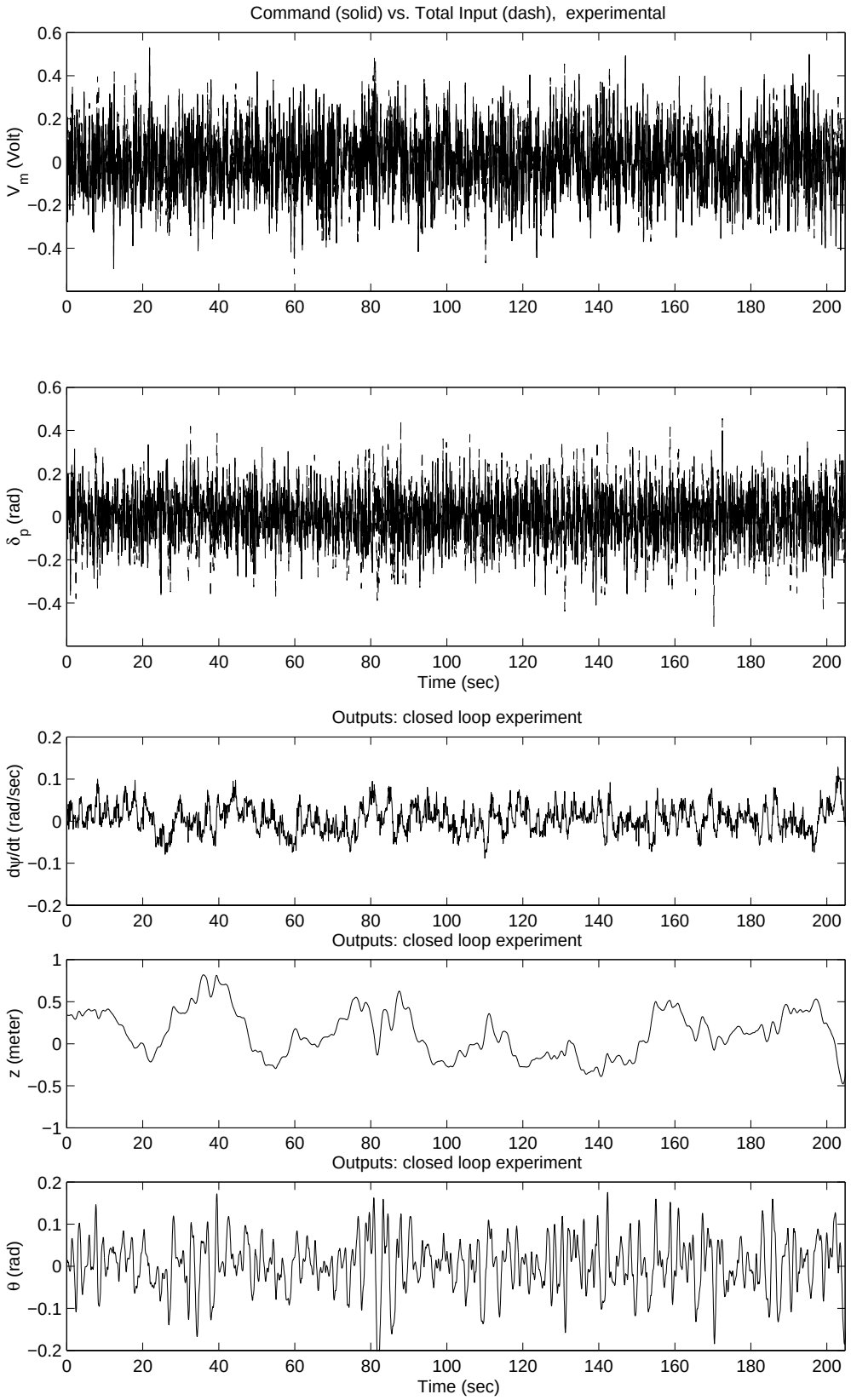

Figure 49: Closed loop measurements: command and total inputs (top), outputs (bottom).

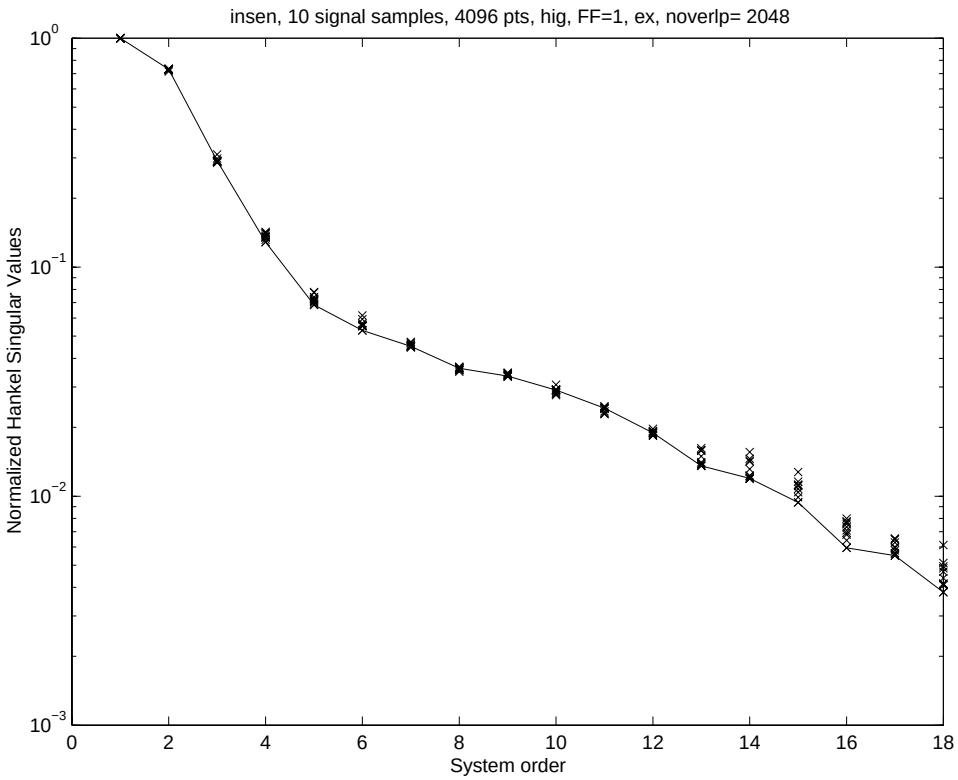

Figure 50: Singular values to determine input sensitivity order from experimental data, 10 samples each 4096 points at 20 Hz with 2048 overlap points.

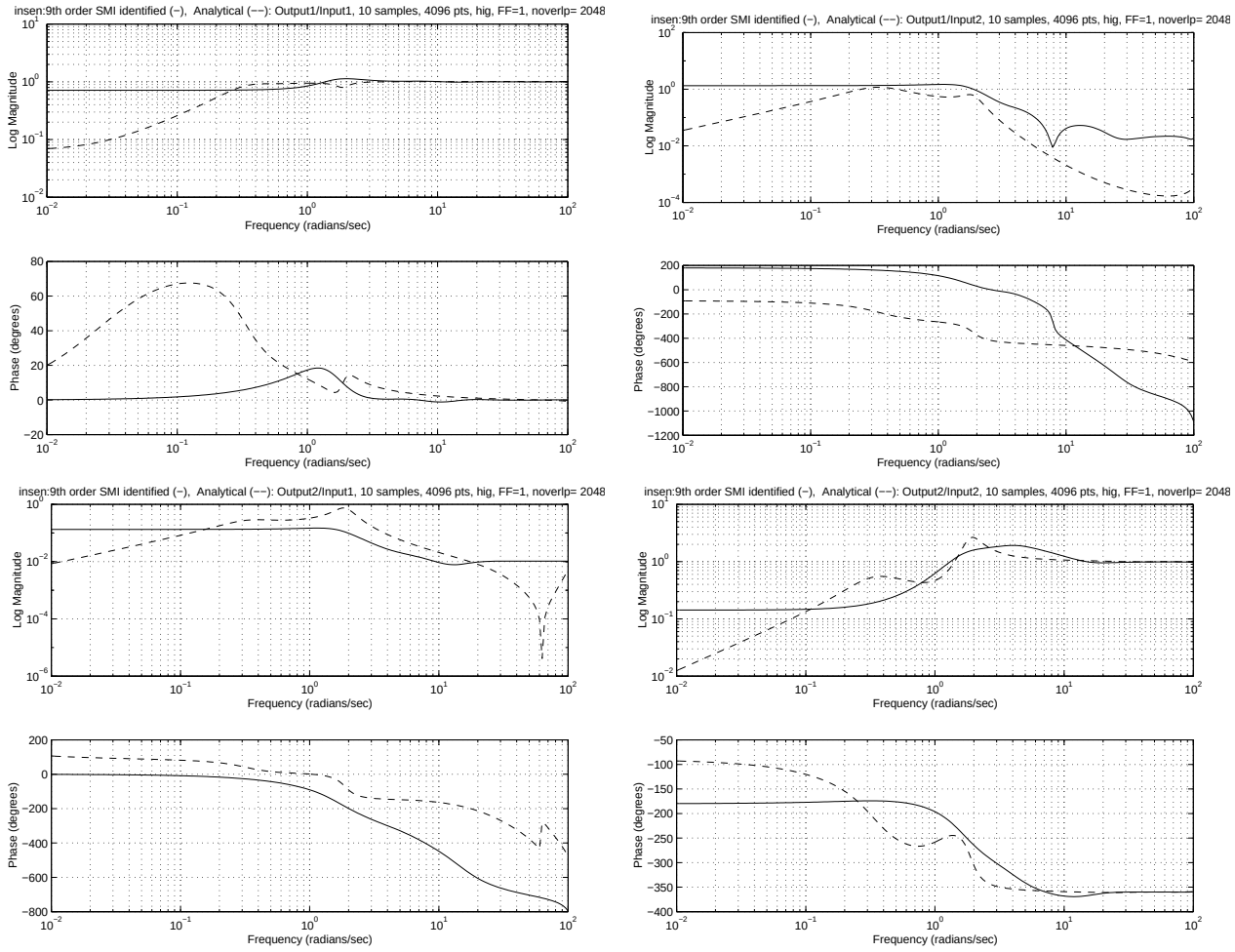

Figure 51: Input sensitivity, 20 mins closed loop experimental data: Identified 9th order (solid), analytical (dash).

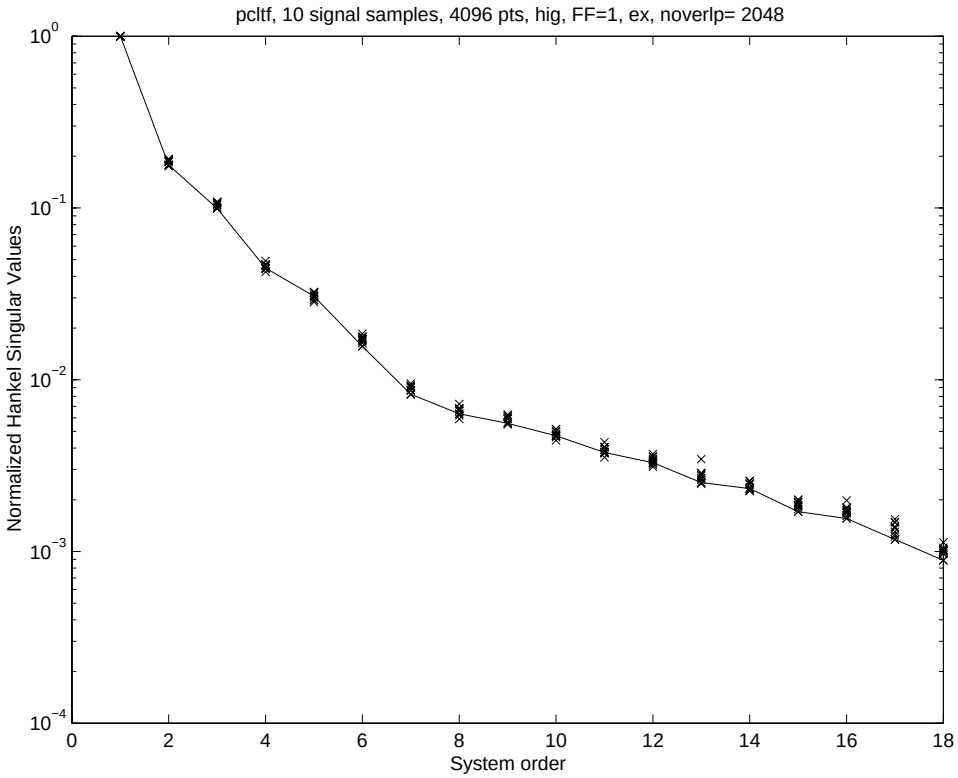

Figure 52: Singular values to determine order of closed loop transfer function across plant using experimental data, 10 samples each 4096 points at 20 Hz with 2048 overlap points.

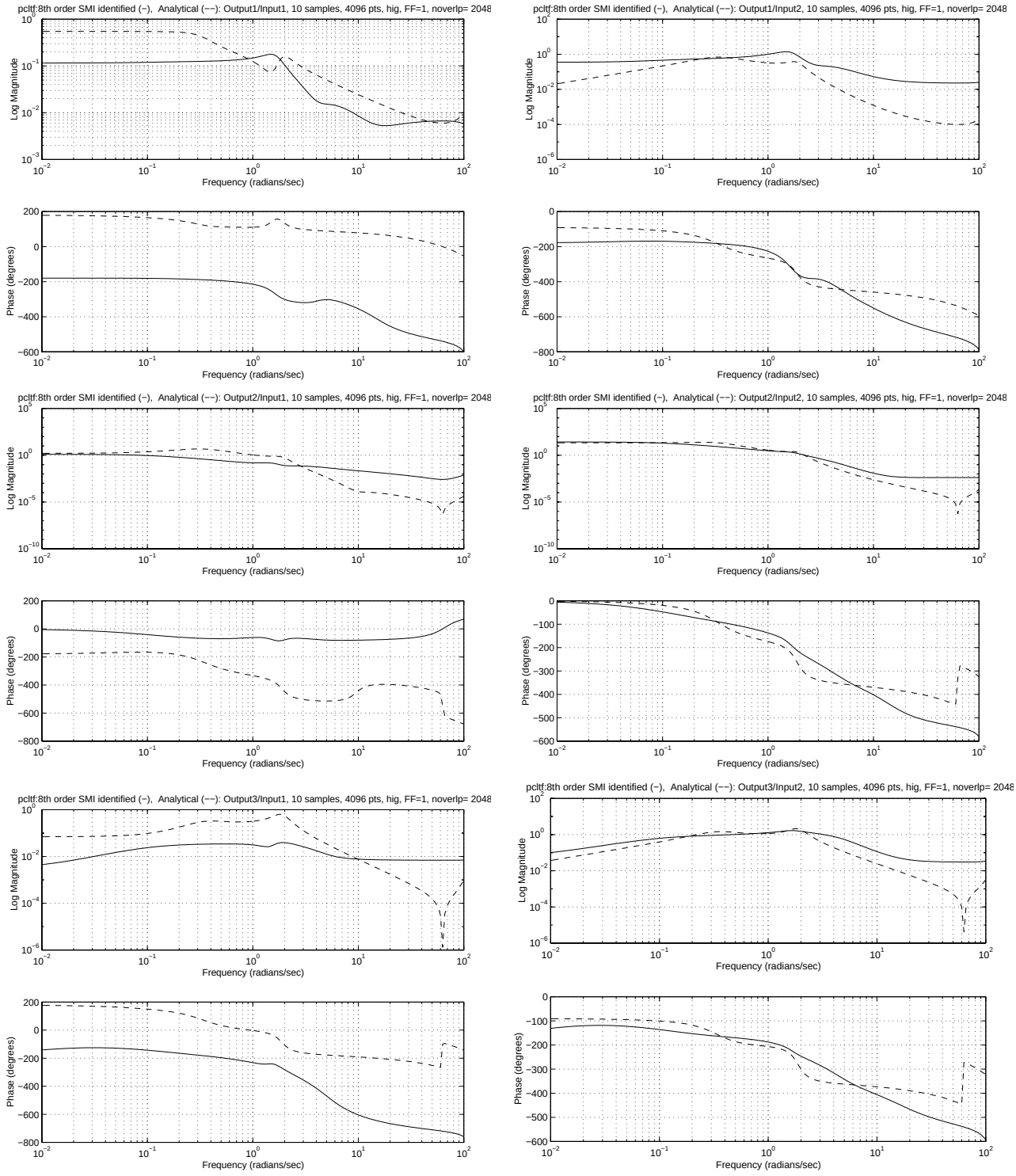

Figure 53: Closed loop transfer function across plant, 20 minutes experimental data: Identified 8th order (solid), analytical (dash).

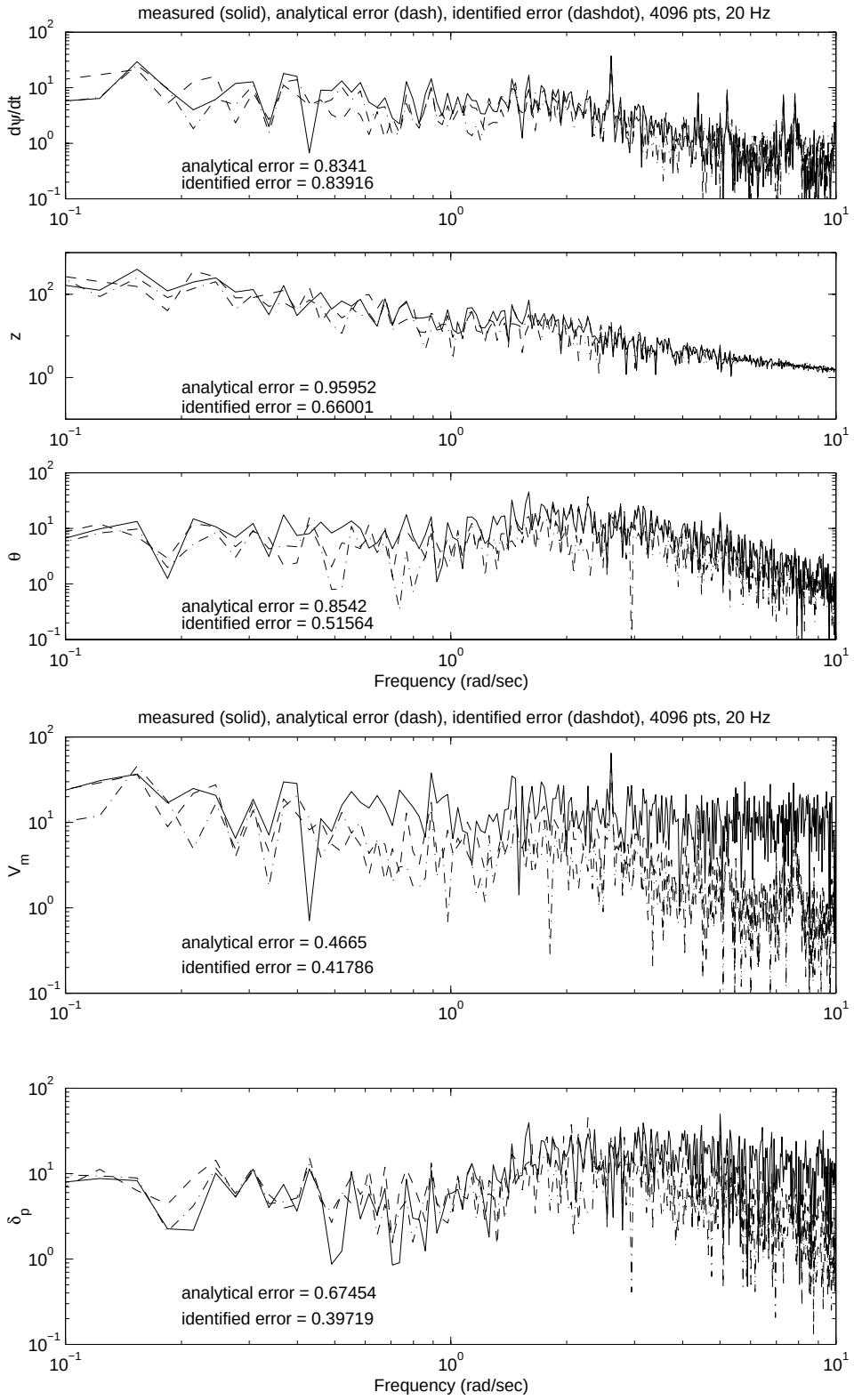

Figure 54: Comparison of measured and analytically predicted outputs and inputs

A.6 Output noise model

We consider a deterministic approach in the construction of an output noise filter from measured closed loop signals. The methodology is validated using simulated data before applying it to experimental data. Both low and high levels of simulated output noise are considered but the same command inputs are used in the simulation as in the experiments.

Figure 23 illustrates the noise identification problem for a closed loop system. The inner loop controller, K is given (actually the same PD controller is used) and signals, y, u, and commands r are measured. The signal q represents an unknown equivalent additive output noise, "equivalent" because all unknown exogenous signals are modeled as noise at the plant output. This is a modeling assumption which is obviously not physically accurate but convenient in obtaining a mathematical model of the unknown exogenous signals in the system. Figure 23b shows the output noise effect as viewed from an open loop perspective.

The goal is to obtain a suitable filter, V, such that q will be the output of V driven by a normalized discrete-time white noise, ν. For simplicity, each channel of q is assumed to be independent so that V will be diagonal. To relax this assumption, further modeling effort is needed (for example the stochastic realization approach as described in [23] and [24]). As illustrated in Figure 23c, this noise model is the preferred form for subsequent model validation and structured uncertainty norm determination and subsequently to validate the performance of an outer loop controller, C. Notice that unlike the open loop case $K = 0$, output sensitivity is needed to properly determine the spectrum of q since simply fitting each closed loop output based on $r = 0$ could lead to significant errors when the output sensitivity matrix is not diagonally dominant.

In this study, since we have no input test signal at the plant output to directly estimate the output sensitivity (so that one can effectively invert it to estimate q), we consider an approach which directly estimates the spectrum of q from frequency responses of the input sensitivity and closed loop across plant, which can be directly identified from available signals. A spectrum of q is obtained by solving the least squares problem corresponding to the overdetermined set of loop equations for inputs and outputs:

$$\begin{bmatrix} I \\ K \end{bmatrix} (I + T_{yr}K)q = \begin{pmatrix} y \\ u \end{pmatrix} - \begin{bmatrix} T_{yr} \\ T_{ur} \end{bmatrix} r \tag{32}$$

where $T_{ur} := (I - KP)^{-1}$, and $T_{yr} := (I - PK)^{-1}P$, are previously identified closed loop transfer functions obtained with independent experiments. Notice that solving for q uniquely from the output equation using an $r = 0$ experiment by inverting the output sensitivity matrix is actually a special case of the above least squares solution since $I + T_{yr}K$, the coefficient matrix of q, is actually the output sensitivity matrix. Finally, to obtain V, an ensamble average of the absolute values of the least squares solution for each signal sample are computed and then fitted with a stable discrete filter for each channel.

Due to feedback, the resulting closed loop output response due to the command input, r, and output noise, ν, could be significantly different depending on the particular controller chosen, as evident from the equations

$$\begin{pmatrix} y \\ u \end{pmatrix} = \begin{bmatrix} (I - PK)^{-1}P & (I - PK)^{-1} \\ (I - KP)^{-1} & (I - KP)^{-1}K \end{bmatrix} \begin{pmatrix} r \\ \nu \end{pmatrix}$$

In particular, the feedback will affect the signal-to-noise ratios which is a key parameter affecting the degree of success in system identification. We define the following signal-to-noise ratios at the outputs and inputs:

$$(s/n)_y := \frac{\|y\|}{\|y_\nu\|} = \frac{\|(I - PK)^{-1}Pr + (I - PK)^{-1}\nu\|}{\|(I - PK)^{-1}\nu\|} \tag{33}$$

$$(s/n)_u := \frac{\|u\|}{\|u_\nu\|} = \frac{\|(I-KP)^{-1}r + (I-KP)^{-1}K\nu\|}{\|(I-KP)^{-1}K\nu\|} \tag{34}$$

Notice that for zero mean signals, the above signal-to-noise ratios are simply the ratio of standard deviations of signals to noise. In principle, given input test signal, r, one can improve signal-to-noise ratios and hence the outcome of the closed loop system identification experiment by judiciously choosing the controller, K, such that the test signal response denoted by the first column partitioned transfer function matrix in equation A.6 is maximized and the noise response denoted by the second column partitioned transfer function matrix is minimized, subject to closed loop stability during the test.

Consider the following bounds on the signal-to-ratios:

$$\underline{\alpha}\frac{\|r\|}{\|\nu\|} - 1 \quad \leq \quad (s/n)_y \leq \quad \bar{\alpha}\frac{\|r\|}{\|\nu\|} + 1 \tag{35}$$

$$\underline{\beta}\frac{\|r\|}{\|\nu\|} - 1 \quad \leq \quad (s/n)_u \leq \quad \bar{\beta}\frac{\|r\|}{\|\nu\|} + 1 \tag{36}$$

where the lower bound factors are

$$\underline{\alpha} := \frac{\underline{\sigma}[(I-PK)^{-1}P]}{\bar{\sigma}[(I-PK)^{-1}]} \qquad \underline{\beta} := \frac{\underline{\sigma}[(I-KP)^{-1}]}{\bar{\sigma}[(I-KP)^{-1}K]}$$

and the upper bound factors are

$$\bar{\alpha} := \frac{\bar{\sigma}[(I-PK)^{-1}P]}{\underline{\sigma}[(I-PK)^{-1}]} \qquad \bar{\beta} := \frac{\bar{\sigma}[(I-KP)^{-1}]}{\underline{\sigma}[(I-KP)^{-1}K]}$$

The factor $\underline{\alpha}$ ($\bar{\alpha}$) corresponds to the ratio of the minimum (maximum) output signal gain over maximum (minimum) noise gain at output, i.e., the worst (best) signal to noise ratio at the output. Similarly, the factor $\underline{\beta}$ ($\bar{\beta}$) corresponds to the ratio of the minimum (maximum) input signal gain over maximum (minimum) noise gain at input, i.e., the worst (best) signal to noise ratio at the input. Figure 55 shows the signal-to-noise ratio lower and upper bounds $\underline{\alpha}$ and $\bar{\alpha}$ (solid) and $\underline{\beta}$, $\bar{\beta}$ (dash), which are based on the analytical plant model and a known controller. The bounds themselves are only a prediction to the extent that the plant model is an estimate of the physical system and that all unknown exogenous noise is represented by an equivalent additive noise model at the plant output. From the figure, notice that at low frequencies there is a wider range of possible variations in the signal-to-noise ratios and more so for the output channels. More importantly, note from the upper bounds of the signal-to-noise ratio predictions that at higher frequencies (say > 3 rad/sec), the best signal-to-noise ratio is less than 1, a bad sign for any sort of system identification or validation work based on measured signals at these frequencies.

A.6.1 Noise model from simulated data

To validate the methodology used to realize a discrete filter driven by discrete-time white noise, simulated low and high output noise (similar to simulated noise used in system identification study) was added internal to the feedback system consisting of PD controller and the analytical plant model. We assume that closed loop system identification has been done separately (see earlier simulation results in system identification) so that the identified input sensitivity and closed loop across plant are used, which do not match the truth model exactly. For the low noise case, the identified models (from simulated data) closely resemble

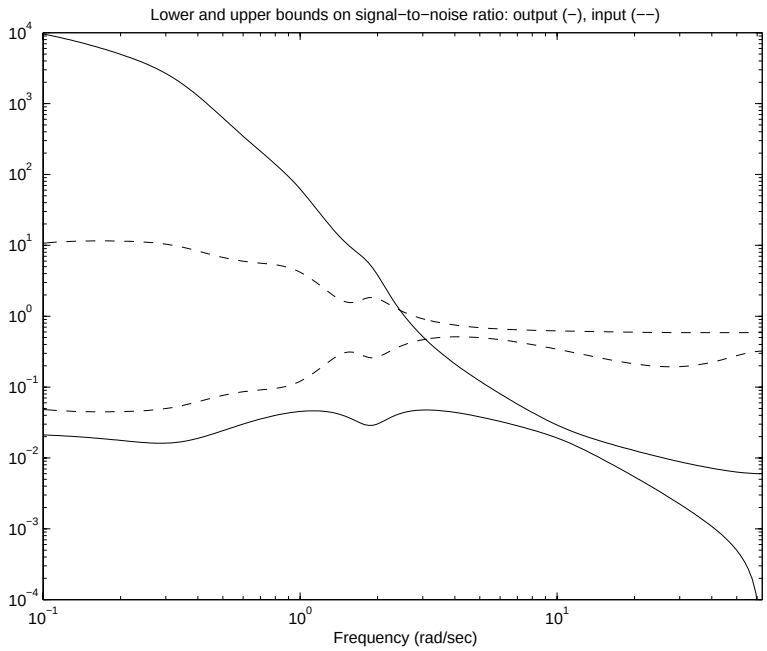

Figure 55: Lower and upper bounds of s/n ratios: $\underline{\alpha}$, $\bar{\alpha}$ on output (solid) and $\underline{\beta}$, $\bar{\beta}$ on input (dash).

the analytical closed loop system whereas in the high noise case, the identified closed loop models (from simulated data) differs substantially from the analytical model.

Figures 56 show comparisons of identified output noise for low and high noise cases respectively. In all DFT computations, rectangular windows were used and the command input was zero in the closed loop simulation. At both noise levels, the noise magnitude spectrum was accurately recovered by this procedure at nearly all frequencies except at the very low frequencies where the conditioning of the least squares problem increases to 10^3. Apparently this is a problem because the identified models were not very accurate at low frequencies which is amplified by the large condition number.

In summary, the algorithm used for estimating an output spectra appears to work reasonably well in simulation and so we apply it to actual measurement data. Using free response data ($r = 0$) also improved the recovery of the noise in the closed loop simulation. Apparently this avoids the Fourier Transform approximation error in the estimation of the effect of command input at the input and output by multiplying the identified frequency response matrices T_{yr} and T_{ur} by the DFT of r due to its time-limited signal.

A.6.2 Noise model from experimental data

An independent closed loop experiment with zero command input is carried out to capture the spectra of unknown exogenous noise in the closed loop system with the PD controller. A discrete time filter is fitted over the noise spectra for the purpose of model validation, uncertainty modeling, and designing a second controller over the PD control loop. The previously identified closed loop models are used in the least squares procedure for obtaining noise spectra as outlined earlier. Figure 24 shows the identified output noise spectra q (solid) and the corresponding stable rational filter fit for each output V (dash). To estimate the sensitivity of the least squares solution in obtaining the noise spectra, the condition number is also shown by the dash-dot line. Note the following observations:

- The condition number shows that the calculation in the noise spectra is less reliable at the lower frequencies for all three outputs. This sensitivity is with respect to both errors in the model and numerical.
- Since the identified closed loop models used almost certainly is inaccurate, the noise estimate obtained from the least squares solution of the loop equations will include both noise and model error, i.e., the estimated noise is expected to be a conservative estimate. This implies a dependence of the least squares noise on the additive model uncertainty, and is consistent with the resemblence of the noise spectra to the frequency response of the identified model.
- The noise spectrum show large disturbances at about $2.5n$ rad/sec where $n = 1, \ldots$ and most prominent in the first output, $d\psi/dt$ and less in the third output, θ, and almost none in the second channel, z. This frequency matches the rotation rate of the Ducted fan about the z-axis.

The following signal-to-noise ratios at the output and inputs are obtained:

$$\begin{aligned} (s/n)_y &= (1.429, 1.434, 2.596) \\ (s/n)_u &= (3.773, 4.563) \end{aligned}$$

certainly, very noisy signals.

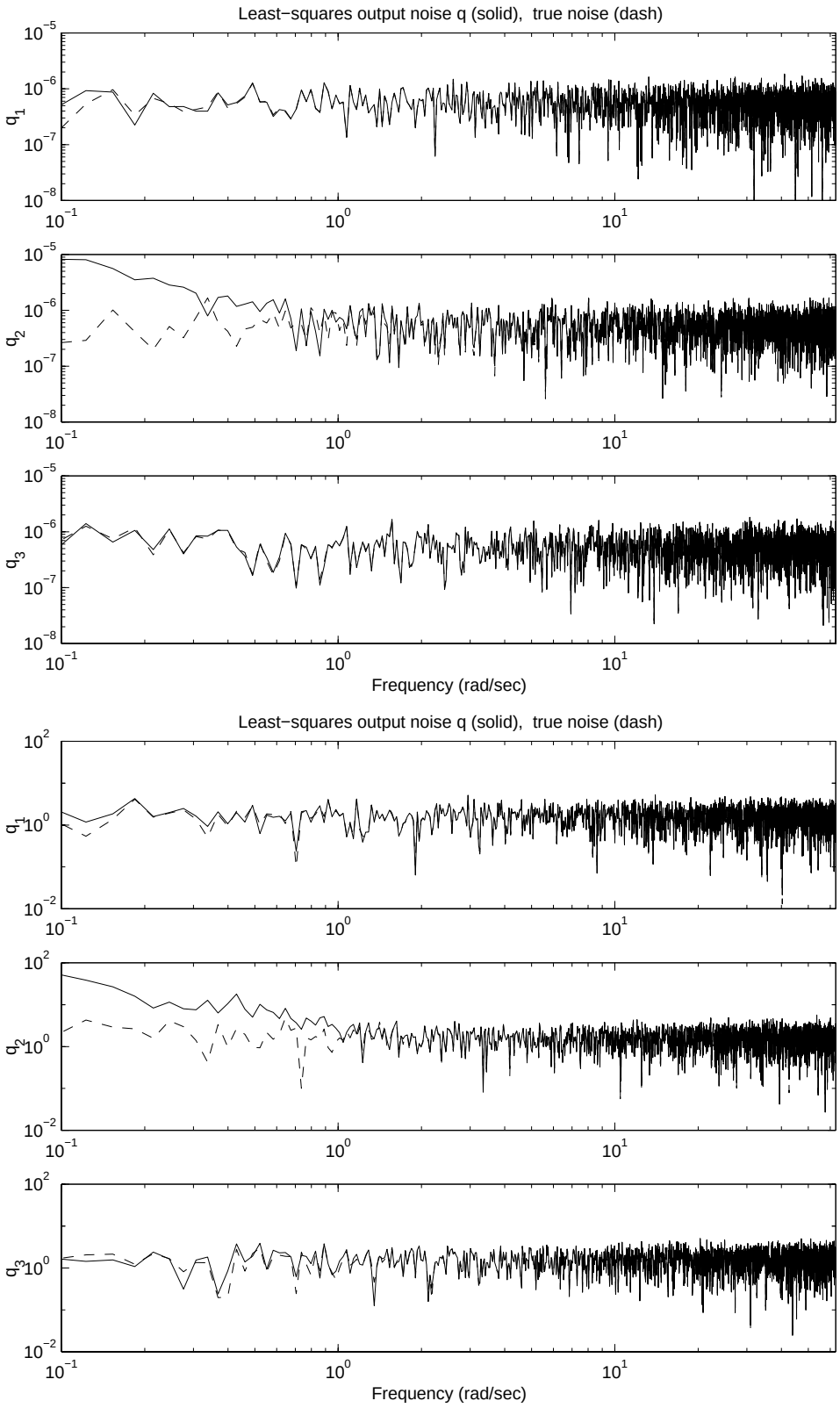

Figure 56: Identified output noise q from simulated data with low (top) and high (bottom) noise, 4096 point DFT, rectangular window.

A.7 Uncertainty models from simulated data

Due to its inherent instability (see earlier description of Ducted fan in Appendix), any substantial experiment on the Ducted fan must be tested in closed loop. For the purposes of uncertainty bound determination and performance validation, for simplicity we postulate an uncertainty structure around the closed loop system with a PD controller as described earlier. Thus, the nominal model consists of the transfer function matrix from command input r to the closed loop output of the plant y, i.e., $(I-PK)^{-1}P$. The assumed independent additive equivalent output noise is amplified by the output sensitivity and filtered/normalized by the noise filter V.

Again for simplicity, we choose unmodeled dynamics in both diagonal and unstructured forms of multiplicative uncertainties for all closed loop output channels. For this special case with no parametric uncertainties, zero disturbance allowance at input, and with only output multiplicative uncertainties, we obtain the following augmented plant:

$$\begin{pmatrix}\eta\\ y\end{pmatrix} = G\left\{\begin{array}{c}\xi\\ \binom{\epsilon}{\nu}\\ r\end{array}\right\}, \quad \text{where} \quad G(P,K,V_n) = \begin{bmatrix} 0 & [0,\ 0] & (I-PK)^{-1}P \\ I & [0, V_n] & (I-PK)^{-1}P \end{bmatrix}.$$

Since $[G_{11}, G_{12}] = 0$, the $\eta_i(\phi,\psi)$ simplifies to $\eta_i = G_{13}r$, a constant for given data. The problem of finding a smallest model validating unmodeled dynamics then reduces to:

$$\begin{aligned} \min_{\phi,\psi,\delta_1,\ldots,\delta_r,x^2} \quad & x^2 \\ \text{subject to} \quad & \|\xi_i(\phi,\psi)\|^2 - x^2|w_i|^2\|G_{13}r\|^2 \ \leq\ 0, \quad i=1,\ldots,\tau \\ & \|\phi\|^2 \ \leq\ b_o^2 \end{aligned}$$

and since $\xi_i(\phi,\psi)$ is affine and the inequalities represent ordinary norm bounds, a feasible set if it exists will be convex. For computational efficiency, we rewrite these as an optimization problem involving a linear cost function subject to a set of Linear Matrix Inequality (LMI) constraints [11]:

$$\begin{aligned} \min_{z} \quad & c^T z \\ \text{subject to} \quad & \begin{bmatrix} Q_i z - \|\xi_{o,i}\|^2 & \text{sym} \\ S_i z & I \end{bmatrix} \ >\ 0, \quad i=1,\ldots,\tau \\ & \begin{bmatrix} b_o^2 & \text{sym} \\ Mz & I \end{bmatrix} \ >\ 0 \end{aligned}$$

where $z := [\mathrm{Re}(\psi); \mathrm{Im}(\psi); \mathrm{Re}(\phi); \mathrm{Im}(\phi); x^2] \in \mathcal{R}^{2n_\psi+2n_\phi+1}$ and

$$\begin{aligned} Q_i &:= [-2\mathrm{Re}(\xi_{o,i}^H \Omega_i A),\ \alpha_i^2] \\ S_i &:= \left[\begin{bmatrix} \mathrm{Re}(\Omega_i) & -\mathrm{Im}(\Omega_i) \\ \mathrm{Im}(\Omega_i) & \mathrm{Re}(\Omega_i) \end{bmatrix}\begin{bmatrix} \mathrm{Re}(A) \\ \mathrm{Im}(A) \end{bmatrix}, 0\right] \\ M &:= \begin{bmatrix} 0_{2n_\phi \times 2n_\psi} & I_{2n_\phi} & 0_{2n_\phi \times 1} \end{bmatrix} \\ A &:= \begin{bmatrix} 0 & 0 & I_{n_\phi} & jI_{n_\phi} \\ I_{n_\psi} & jI_{n_\psi} & 0 & 0 \end{bmatrix} \\ c &:= [0_{(2n_\psi+2n_\phi)};\ 1] \\ \alpha_i^2 &:= |w_i|^2\|G_{13}r\|^2 \end{aligned}$$

The interior-point algorithm found in the MATLAB's LMI Control Toolbox [20] is used to solve for the global minimum when feasible.

A.7.1 Simulated data and case studies

Figure 57 shows the true closed loop system and output noise which is used to generate simulation data. This system consists of the unstable analytical plant model, P_{TRUE} stabilized with a PD controller, K_{PD}. The true noise, q, is simulated by a a sequence of zero mean Gaussian random number with standard deviation of $\sigma = 10^{-8}$ for low noise and $\sigma = .03$ for high noise. The command or test input r used in the simulation is chosen to be the same test input used in the experiments.

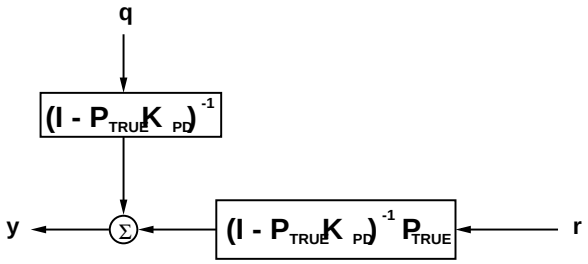

Figure 57: Truth model used for generating simulation data.

Table 5 shows the different cases considered for simulating uncertainty bound determination from data. To keep this study to a reasonable length, we consider only two forms of assumed uncertainty structure, namely, diagonal output multiplicative (denoted by "D" in Case labels) and unstructured or full output multiplicative (denoted by "F" in Case labels). These cases address, albeit in a limited sense, the effects of errors in the nominal model, uncertainty structure, noise allowances, and actual noise level in the data used for model validation. To enable us to define the correct or an incorrect uncertainty structure in this simulation study, the errors in the nominal model are simulated by perturbing an analytical truth model with specfied diagonal output multiplicative filters or with a full block output multiplicative filters, and by using identified models obtained through a system identification algorithm based on (low or high) noise corrupted signals.

Cases Sim1-1, Sim2-1, Sim3-1, Sim4-1 are meant to simulate a most ideal situation when the nominal model is a very accurate representation of the system of interest. Consequently, a very small model validating unmodeled dynamics is expected (if not zero) and serves as a necessary check of the model validation methodology.

Cases Sim1-2, Sim2-2, Sim3-2, Sim4-2 are meant to simulate the situation when the nominal model is inaccurate but has a correct uncertainty structure[6]. This is again an ideal situation since a correct uncertainty structure in a given application may not exist. Nevertheless, these cases serve as a second necessary check of the model validation methodology wherein the correct uncertainty level is expected to be recovered.

Cases Sim1-3, Sim2-3, Sim3-3, Sim4-3 are meant to simulate the situation where the correct uncertainty structure is unstructured. Clearly all cases that assume diagonal uncertainty structure (Sim*-3-D) will never recover the correct model error. Still, it does not rule out satisfying model validation conditions which involves only reproducing a particular output frequency spectra with the aid of an output noise allowance.

In Cases Sim1-4, Sim2-4, Sim3-4, Sim4-4, an identified model obtained from noisy identification data is used as a nominal model and therefore *there is no correct model uncertainty*

[6]A philosophical argument can be made to the effect that in the modeling of physical systems, a particular uncertainty structure could be viewed as a particular parameterization of the discrepency between a mathematical model one uses and an imagined "true" model which one tries to contain using an uncertainty model. In other words, a "correct" uncertainty structure may not have any deep physical significance.

Case	MV Data	Nominal Model	Uncertainty structure	Noise allowance
Sim1-1-D	Sim, low noise	True	Diagonal	True peak 2-norm
Sim1-2-D	Sim, low noise	True + Diagonal error	Diagonal	True peak 2-norm
Sim1-3-D	Sim, low noise	True + Full block error	Diagonal	True peak 2-norm
Sim1-4-D	Sim, low noise	IDed (low noise data)	Diagonal	True peak 2-norm
Sim2-1-D	Sim, low noise	True	Diagonal	True mean
Sim2-2-D	Sim, low noise	True + Diagonal error	Diagonal	True mean
Sim2-3-D	Sim, low noise	True + Full block error	Diagonal	True mean
Sim2-4-D	Sim, low noise	IDed (low noise data)	Diagonal	True mean
Sim3-1-D	Sim, high noise	True	Diagonal	True peak 2-norm
Sim3-2-D	Sim, high noise	True + Diagonal error	Diagonal	True peak 2-norm
Sim3-3-D	Sim, high noise	True + Full block error	Diagonal	True peak 2-norm
Sim3-4-D	Sim, high noise	IDed (high noise data)	Diagonal	True peak 2-norm
Sim4-1-D	Sim, high noise	True	Diagonal	.1× True mean
Sim4-2-D	Sim, high noise	True + Diagonal error	Diagonal	.1× True mean
Sim4-3-D	Sim, high noise	True + Full block error	Diagonal	.1× True mean
Sim4-4-D	Sim, high noise	IDed (high noise data)	Diagonal	.1× True mean
Sim1-1-F	Sim, low noise	True	Unstructured	True peak 2-norm
Sim1-2-F	Sim, low noise	True + Diagonal error	Unstructured	True peak 2-norm
Sim1-3-F	Sim, low noise	True + Full block error	Unstructured	True peak 2-norm
Sim1-4-F	Sim, low noise	IDed (low noise data)	Unstructured	True peak 2-norm
Sim2-1-F	Sim, low noise	True	Unstructured	True mean
Sim2-2-F	Sim, low noise	True + Diagonal error	Unstructured	True mean
Sim2-3-F	Sim, low noise	True + Full block error	Unstructured	True mean
Sim2-4-F	Sim, low noise	IDed (low noise data)	Unstructured	True mean
Sim3-1-F	Sim, high noise	True	Unstructured	True peak 2-norm
Sim3-2-F	Sim, high noise	True + Diagonal error	Unstructured	True peak 2-norm
Sim3-3-F	Sim, high noise	True + Full block error	Unstructured	True peak 2-norm
Sim3-4-F	Sim, high noise	IDed (high noise data)	Unstructured	True peak 2-norm
Sim4-1-F	Sim, high noise	True	Unstructured	.1× True mean
Sim4-2-F	Sim, high noise	True + Diagonal error	Unstructured	.1× True mean
Sim4-3-F	Sim, high noise	True + Full block error	Unstructured	.1× True mean
Sim4-4-F	Sim, high noise	IDed (high noise data)	Unstructured	.1× True mean

Table 5: Simulated cases: effects of nominal model, uncertainty structure, and noise allowance.

structure. This ambiguity is whats expected in a typical application. This contrasts sharply to the other cases where a correct uncertainty structure exists, albeit simulated, and the assumed uncertainty structure is either correct or incorrect. Still, analogous to the previous case, the existence of a model validating set cannot be ruled out, even if a "correct" model uncertainty structure is unknown. However, the identified model from simulated data closely matches the true model.

A.7.2 Perfect nominal model

Figure 58 shows diagonal uncertainty bounds for cases Sim1-1-D,. . ., Sim4-1-D which assumes perfect nominal model. This is a reference case where the recovered uncertainty bounds should be very small or ideally zero. With a low level of noise in the data, cases Sim1-1-D and Sim2-1-D show a very small level of unmodeled dynamics (circle and square dash lines). This very small level of unmodeled dynamics obtained is independent of the noise allowance levels assumed, since the circle and square dash lines overlap. However, notice that even with a perfect nominal model and the data contains only a small level of noise, the model validating unmodeled dynamics is not exactly zero. This residual is due to the fact that the output error used in model validation definition assumes

$$e_y(z) := \mathcal{Z}[y(t)] - T_{yr}(z)\mathcal{Z}[r(t)] = 0$$

under the ideal conditions: perfect model $T_{yr}(z)$, no noise or disturbance effects in $y(t)$ and r, and signals are either infinite time length or is periodic. However, since all measured time signals are of finite length even under near ideal conditions where noise effects are negligible, the following output error results

$$e_y(z) := \mathcal{Z}[y(t)h(t)] - T_{yr}(z)\mathcal{Z}[r(t)h(t)] = \mathcal{Z}[y(t)] * \mathcal{Z}[h(t)] - T_{yr}(z)\left(\mathcal{Z}[r(t)] * \mathcal{Z}[h(t)]\right) \neq 0$$

where $\mathcal{Z}[\cdot]$ denotes the z-transform operation, $*$ denotes the frequency convolution operation and $h(t)$ denotes the chosen time window (refer earlier section for a more detail discussion on the assumptions on signals and systems). Figure 59 illustrates this residual error for a perfect model with a Hanning window over a 12000 point (600 seconds) sample, which is exactly half the total length of experimental data. In this application, this residual DFT error is considered an acceptably small level of fictitious model validating unmodeled dynamics.

Figure 58 also shows what happens to the uncertainty bounds when there is a high level of noise in the data used for model validation. Using a high noise allowance level equal to the peak true, Case Sim3-1-D shows a very small uncertainty bound (diamond dot line), which is acceptable. Apparently, the remaining noise allowance is sufficient to compensate for the DFT errors. However, if only a small level of noise allowance (10% of true mean noise) is used when there is a high level of noise in the data, as in case Sim4-1-D, a large erronous level of uncertainty bound results (triangle dot line), mostly to account for the large output noise.

Assuming an unstructured uncertainty with a perfect nominal model, the computed unstructured uncertainty bounds obtained are similarly very small as shown by the circle and square dotted lines in Figure 60. The erroneous effects of using a low level of noise allowance when there is a large level of noise in the data is similar (triangle dot line).

A.7.3 Nominal model with correct uncertainty structure

Figure 61 shows the diagonal uncertainty bounds for cases Sim1-2-D, Sim2-2-D, Sim3-2-D, Sim4-2-D, whose nominal models are chosen as the analytical truth model perturbed

diagonally at the output as follows

$$P(z)_{nom} = (I + \Delta(z))P_{true}(z) \tag{37}$$

where

$$\begin{aligned}
\Delta(z) &:= W(z)\Delta_{diag} \\
W(z) &:= \text{diag}\left(.2, \quad .1736\frac{(z+.1303)}{(z-.5095)}, \quad .5208\frac{(z-.7776)}{(z+.1584)}\right) \\
\Delta_{diag} &:= I_{3\times 3}, \qquad \bar{\sigma}(\Delta_{diag}) = 1
\end{aligned}$$

This means that a correct uncertainty structure and level exists. The solid lines in Figure 61 shows the correct model error levels, a constant in the first channel and first order low and high pass filters for the second and third channels, respectively. The results show that with low noise levels in the data as in Sim1-2-D and Sim2-2-D, the correct diagonal model error levels are recovered reasonably accurately as indicated by circle and square dash lines in Figure 61. At most frequencies, the predicted uncertainty bound is slightly less than the correct levels (except at the very low frequencies where the data record length becomes a limiting factor) which do not appear to be due to the noise allowance levels (since the circle and square dash lines overlap). Figure 61 also shows that if a high level of noise is present in the data for model validation, as in cases Sim3-2-D and Sim4-2-D, apriori knowledge of the correct uncertainty structure does not help to recover the correct uncertainty bounds (compare line with diamond and triange dash lines).

As a second example of a situation where a correct uncertainty structure is known, Figure 62 shows the computed unstructured uncertainty bounds for a nominal model with a full block output model error and assuming correctly, an unstructured uncertainty at the output. For the cases with low noise in the data, Sim1-3-F and Sim2-3-F, the uncertainty bounds (circle and square lines) roughly recovers the maximum singular value of the correct unstructured model error (solid line). However, with large levels of noise in the data as in cases Sim3-3-F and Sim4-3-F, erroneous levels of uncertainty bounds result (diamond and triangle lines) independent of the level of noise allowance assumed.

A.7.4 Nominal model with incorrect uncertainty structure

Figure 63 shows the diagonal uncertainty bounds for cases Sim1-3-D, Sim2-3-D, Sim3-3-D, and Sim4-3-D, whose nominal model is the truth model perturbed at the output as follows

$$P(z)_{nom} = (I + \Delta(z))P_{true}(z)$$

where

$$\begin{aligned}
\Delta(z) &:= W(z)\Delta_{full} \\
\Delta_{full} &:= \begin{bmatrix} -0.0896 - 0.2473i & -0.0178 + 0.5314i & 0.4692 - 0.2975i \\ -0.1352 - 0.1399i & -0.3587 + 0.1471i & -0.1014 - 0.2886i \\ 0.0674 + 0.4169i & -0.1886 - 0.2629i & -0.1121 + 0.2525i \end{bmatrix}, \quad \bar{\sigma}(\Delta_{full}) = 1
\end{aligned}$$

and $W(z)$ is a diagonal filter denoting the correct uncertainty radius for each output. This is an example of a situation where the assumed uncertainty structure is incorrect and is incapable of recovering the correct uncertainty bounds. Figure 63 shows the uncertainty bounds obtained for all four cases which do not resemble the maximum singular value of the correct unstructured output model error indicated by the solid line. *Not surprisingly, due to the nonuniqueness of model validating uncertainties, all four cases satisfied model validating*

conditions in spite of the incorrect uncertainty structure assumed. Finally, note that for the two cases with low level of noise in the data (Sim1-3-D and Sim2-3-D), the uncertainty bounds are very insensitive to noise allowance (circle lines overlap square lines).

As an example of a situation where the assumed uncertainty structure is incorrect because it is overparameterized, Figure 64 show the results of Sim1-2-F,..., Sim4-2-F, where the nominal model is diagonally perturbed as given by equation 37, which is identical to cases Sim1-2-D,..., Sim4-2-D. For the case with low levels of noise in the data (Sim1-2-F and Sim2-2-F), the maximum singular value of the unstructured uncertainty (circle and square dash lines in Figure 64) roughly matches the maximum singular value of the correct diagonal model error (solid line). Of course this successful recovery is likely due to the fact that the assumed unstructured (and overparameterized) uncertainty is capable of generating the correct diagonal uncertainty bounds. Again, with high levels of noise in the data (Sim3-2-F and Sim3-2-F), erroneous uncertainty bounds result (diamond and triangle lines in Figure 64).

A.7.5 Identified nominal models

In this set of cases, identified models are used as nominal models. Cases (Sim1-4-D, Sim2-4-D) and (Sim1-4-F, Sim2-4-F) uses nominal models obtained from system identification based on signals which contain low levels of noise, hence these are more accurate identified models. The complementary cases (Sim3-4-D, Sim4-4-D) and (Sim3-4-F, Sim4-4-F) uses inaccurate identified nominal model due to the use of system identification data containing a high level of noise (compare model errors in Figures 47 and 48).

Given a 3 by 2 truth model, P_{true}, and an identified nominal model P_{id}, a correct additive uncertainty can be defined and computed unambiguously, but a multiplicative output uncertainty can only be defined by solving for Δ_{mult} from the following underdetermined matrix equation:

$$(I_{3\times 3} + \Delta)P_{id} = P_{true}$$

Notice that there is no physical preference for a least squares Δ corresponding to an output multiplicative uncertainty (let alone correct uncertainty structure). This is an example where we are only certain that the two transfer matrices are different and the correct uncertainty structure is therefore indeterminate.

Figure 65 shows the unstructured output multiplicative uncertainty bounds (circle and square dash lines) for cases Sim1-4-F and Sim2-4-F which uses a low level of noise in data. Figure 66 shows the diagonal output multiplicative uncertainty bounds (circle and square dash lines) for cases Sim1-4-D and Sim2-4-D which uses a low level of noise in data. Both diagonal and unstructured output multiplicative uncertainty bounds compares surprisingly well to the maximum singular value of the least squares output multiplicative uncertainty as shown by solid lines in Figures 65 and 66. *In spite of the unknown correct uncertainty structure for the identified models, all four cases satisfied model validation conditions and produced reasonable uncertainty levels.*

Figures 67 and 68 show the uncertainty bounds using inaccurate identified nominal models and data with high levels of noise. Clearly the uncertainty bounds (diamond and triangle dotted lines) do not resemble the maximum singular value of the least squares output multiplicative uncertainty as shown by solid lines. Again, the predicted uncertainty bounds are sensitive to the assumed noise allowance because of the high levels of noise in data.

A.7.6 Summary

Since an infinity of other uncertainty structures, parameters, noise allowance levels, and actual noise in data are possible but cannot all be considered in any simulation, the results are in no way conclusive. Nevertheless, the results suggest the following:

For all following cases with a *low level of noise in data*, all uncertainty bounds were insensitive to the noise allowances used. With accurate nominal models, the uncertainty structure was not important because the resulting uncertainty bounds required were as expected small. Namely, for the perfect nominal case, assuming diagonal uncertainty structure resulted in very small levels (circle and square lines in Figure 58) while an unstructured uncertainty structure assumption also resulted in very small levels of maximum singular value uncertainty as expected (circle and square lines in Figure 60). For the accurately identified model case, assuming unstructured uncertainty gave matching small levels of maximum singular value uncertainty levels (circle and square lines in Figure 65) while assuming diagonal uncertainty structure resulted in matching small levels of diagonal uncertainty levels (circle and square lines in Figure 66) compared to maximum singular value of the least squares unstructured output multiplicative uncertainty (solid line in Figure 66). These fictitious small levels of uncertainty bounds consists mostly of DFT errors and were mitigated by judiciously windowing reasonably long samples.

For less accurate nominal models with *correct* a priori assumptions on the uncertainty structure, the correct uncertainty levels are recovered for both diagonal (circle and square lines compared to solid line in Figure 61) and unstructured cases (circle and square lines compared to solid line in Figure 62). The underestimated uncertainty levels at most frequencies are due to the fact that the particular sample data did not reflect the worst case directional response for this multivariable system.

For less accurate nominal models with *incorrect* a priori assumptions on the uncertainty structure, the uncertainty bounds obtained were generally unpredictable. This unpredictability is of course not totally surprising since the incorrect uncertainty structure will not allow the recovery of the correct uncertainty bounds. For example, in the nominal model case with unstructured error at output, assuming diagonal uncertainty led to unrecognizable bounds (circle and square lines compared to solid line in Figure 63). However, notice from the figure that at each frequency, the maximum uncertainty component (maximum singular value of a diagonal matrix) apparently is greater than the maximum singular value of the correct full uncertainty matrix. As a second example with *incorrect* a priori assumptions on the uncertainty structure, consider the *overparameterized* uncertainty case where the correct uncertainty is diagonal but the assumed uncertainty model is assumed unstructured. The maximum singular value of the uncertainty bounds of the assumed unstructured uncertainty (circle and square lines in Figure 64) compares reasonably well, albeit an underestimation, to the correct maximum uncertainty component (maximum singular value of the true diagonal marix) indicated by solid line. This somewhat successful recovery of the correct uncertainty bound [7] was made possible because the true diagonal uncertainty structure is a subset of the corresponding unstructured uncertainty. Interestingly, note from the two previous examples that the maximum simgular value of the unstructured uncertainty was consistently smaller than that of the diagonal uncertainties, which suggests that assuming less structure in the uncertainty, and therefore intuitively more conservative, may not necessarily lead to a more conservative uncertainty model, by reducing uncertainty values with more uncertain variables.

For black-box type nominal models typical of identified models, a correct uncertainty structure is *indeterminate*, given only the identified noiminal model and possibly an imagined true model. Due to this indeterminacy, any uncertainy bound comparisons are suspect.

[7] although apples and oranges are compared since a diagonal matrix is compared to a full matrix

Nevertheless for this study, we computed and compared an equivalent output multiplicative error based on a minimum norm least squares solution to the output multiplicative uncertainty bound from data. Surprisingly, both the unstructured uncertainty bound in (circle and square lines in Figure 65) and diagonal structure uncertainty bounds (circle and square lines in Figure 66), match reasonably well with the maximum singular values of the least squares equivalent output multiplicative uncertainties (solid lines in Figure 65 and 66). In summary, incorrect or indeterminate uncertainty structure did not preclude satisfying model validation conditions but sometimes resulted in unpredictable uncertainty norm bounds.

For all cases with a *high level of noise in data*, the uncertainty bounds were unreliable and sensitive to the assumed levels of noise allowance. In the selection of noise allowance levels, a larger level is preferred over smaller levels (than true noise level in data) to avoid erroneous uncertainty bounds, unless the noise in the data is known to be extremely low. Although it is intuitively clear that any attempt to validate a model will be less reliable with higher noise levels, as shown here, the results have been further subject to a limiting feature of the model validation theory investigated which do not distinguish noise and model error effects. In fact, the validation approach is to use noise variables as a given allowance to minimize the model error uncertainty bounds necessary to satisfy model validation conditons. Hence further research is recommended whereby the noise signals in the data can be discriminated from model error effects in satisfying model validation conditions so that noise allowance will not compensate for model errors and vice versa.

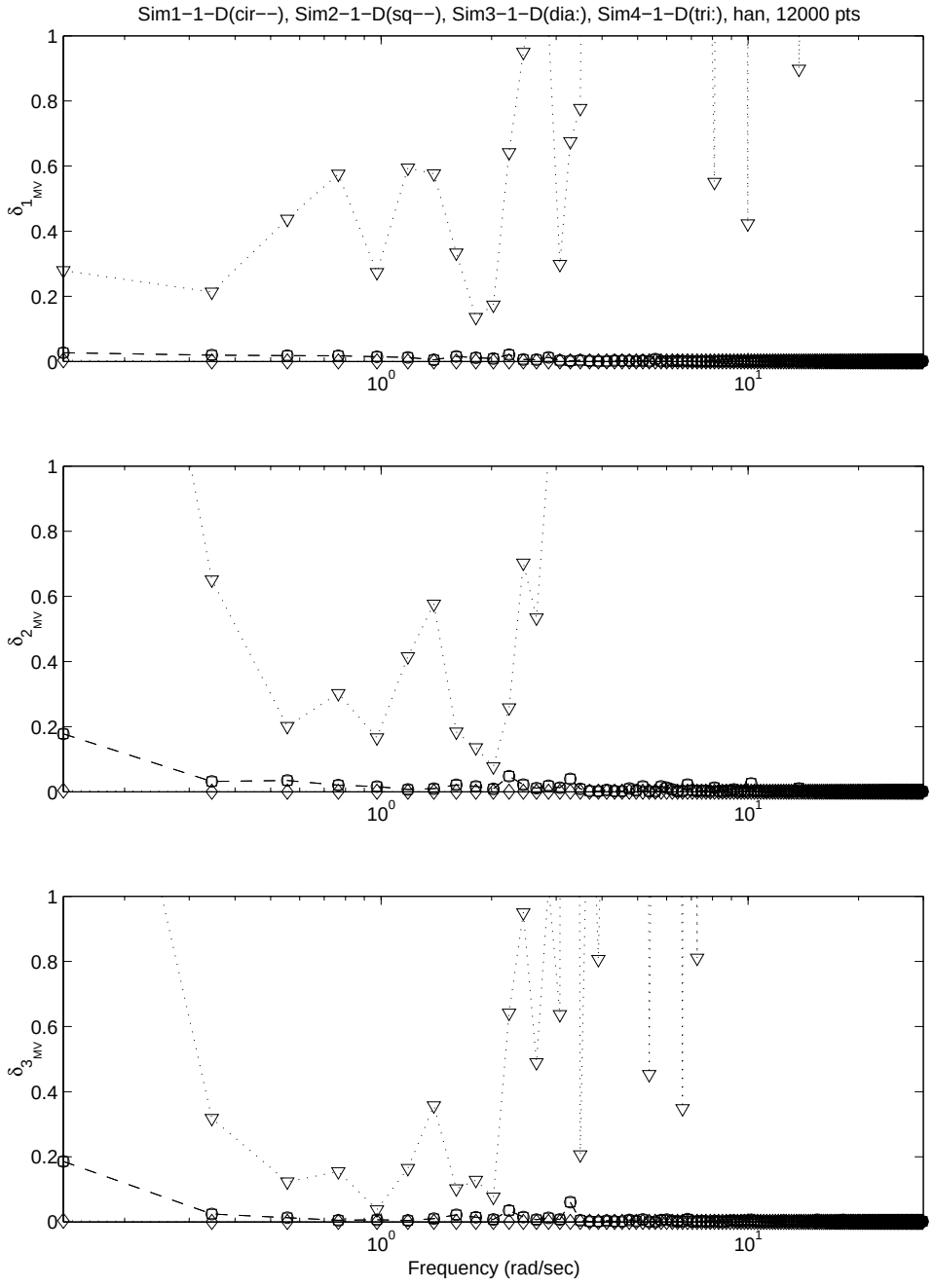

Figure 58: Diagonal uncertainty bounds for perfect nominal model: Sim1-1-D,..., Sim4-1-D.

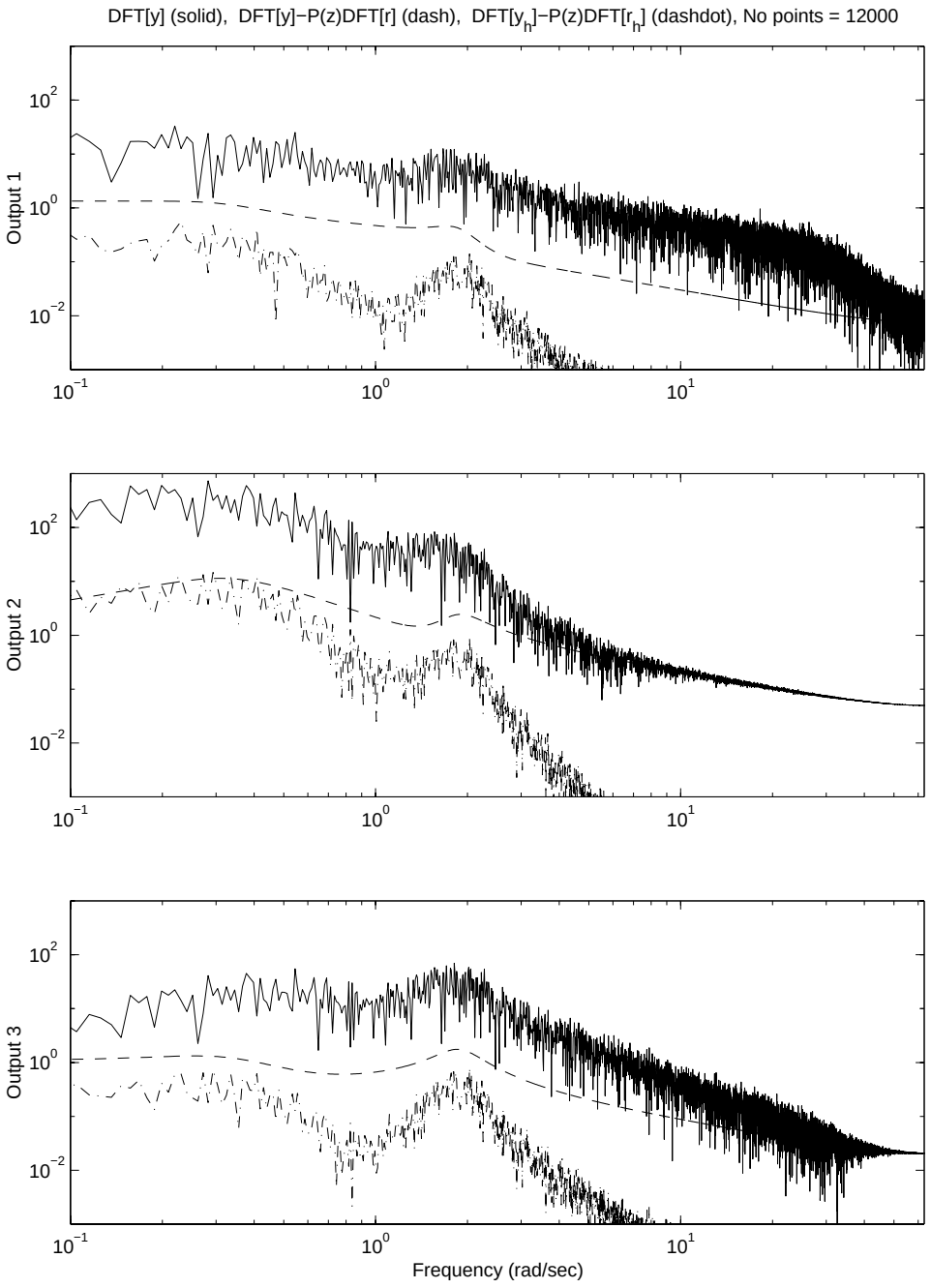

Figure 59: Errors in output spectrum due to finite record length effects and windowing, rectangular(dash), Hanning(dashdot): 12000 points DFT.

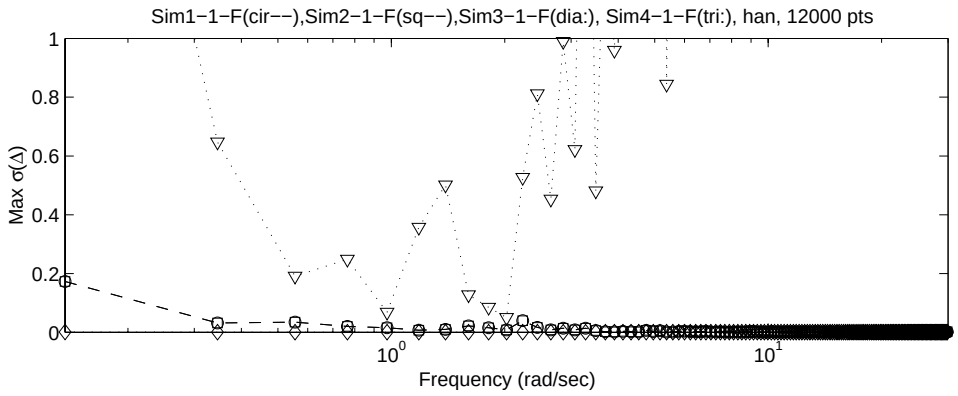

Figure 60: Unstructured uncertainty bound based on perfect nominal model, Sim1-1-F,...,Sim4-1-F.

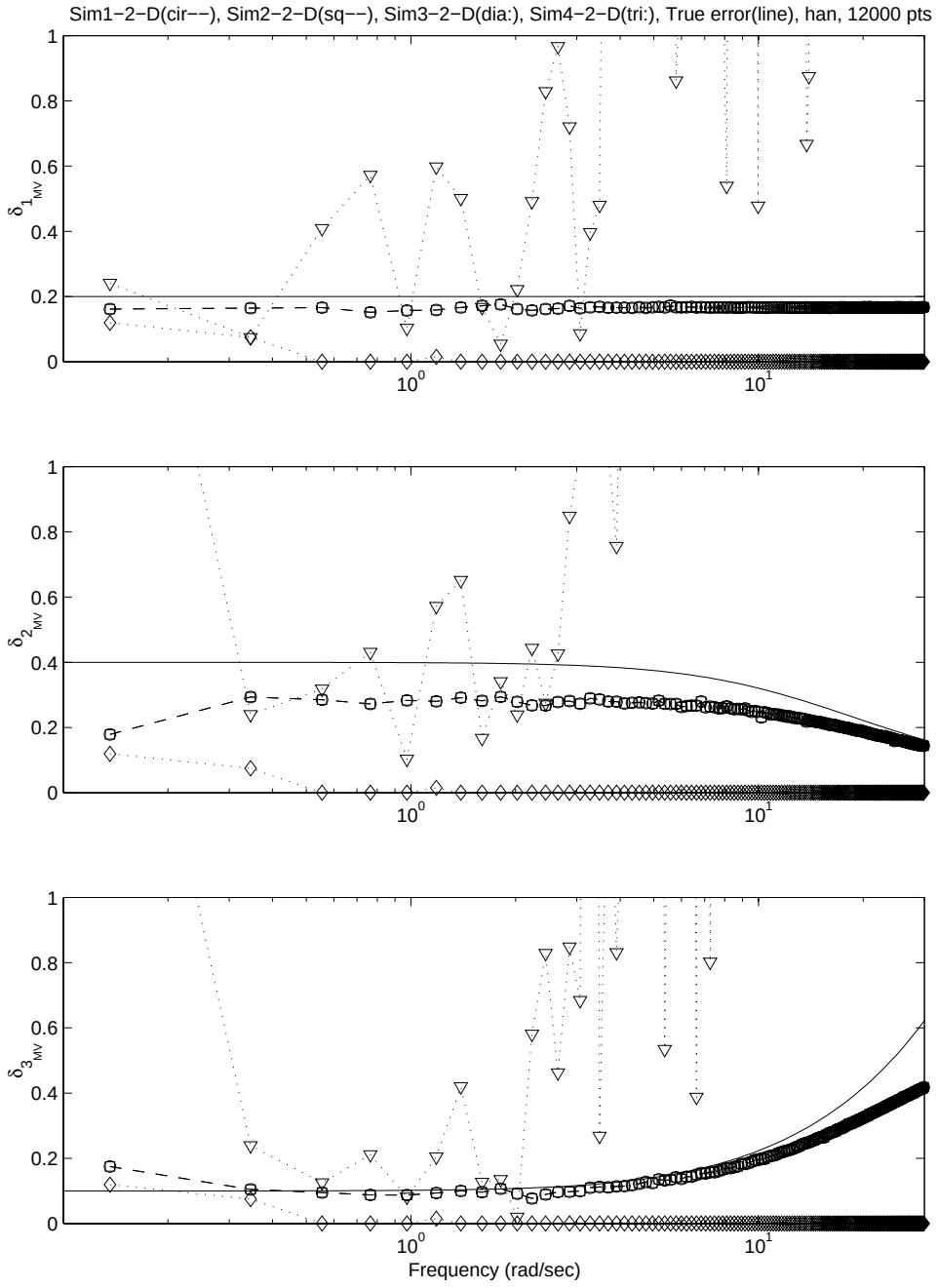

Figure 61: Diagonal uncertainty bounds for nominal model with diagonal error: Sim1-2-D,..., Sim4-2-D.

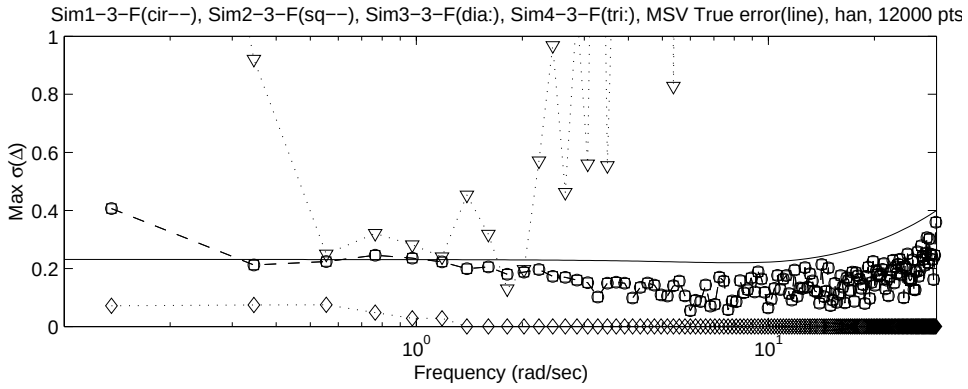

Figure 62: Unstructured uncertainty bound based on nominal model with full block error, Sim1-3-F,...,Sim4-3-F.

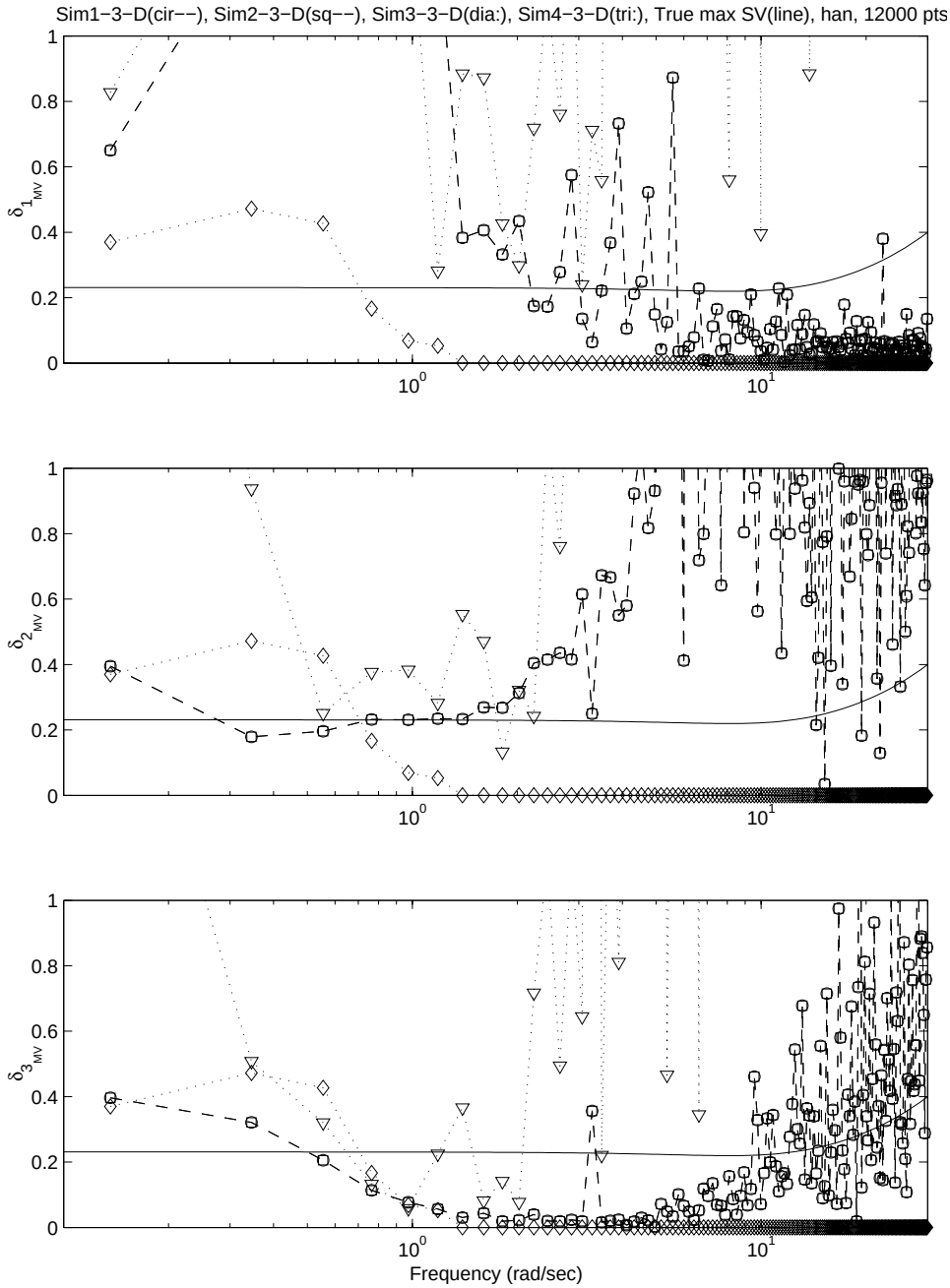

Figure 63: Diagonal uncertainty bounds for full matrix error in nominal model: Sim1-3,..., Sim4-3.

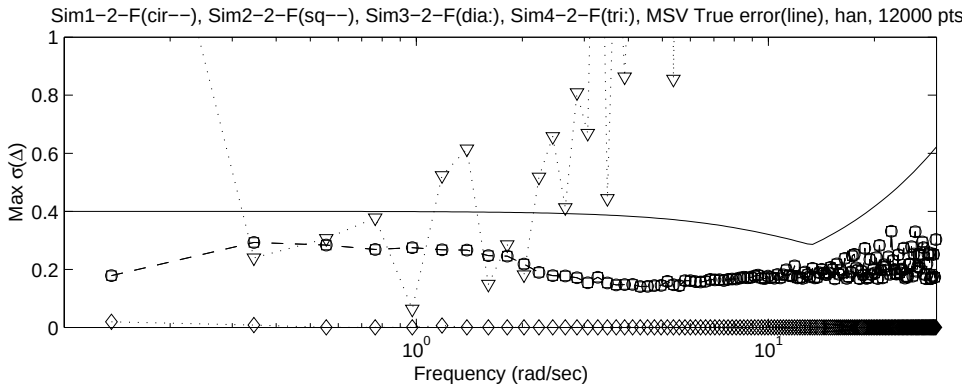

Figure 64: Unstructured uncertainty bound based on nominal model with diagonal block error, Sim1-2-F,...,Sim4-2-F.

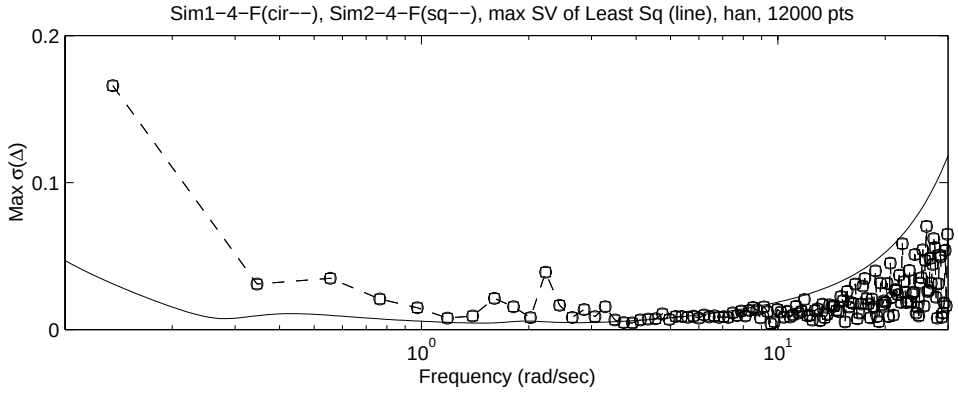

Figure 65: Unstructured uncertainty bounds for identified nominal model under low noise: Sim1-4-F and Sim2-4-F.

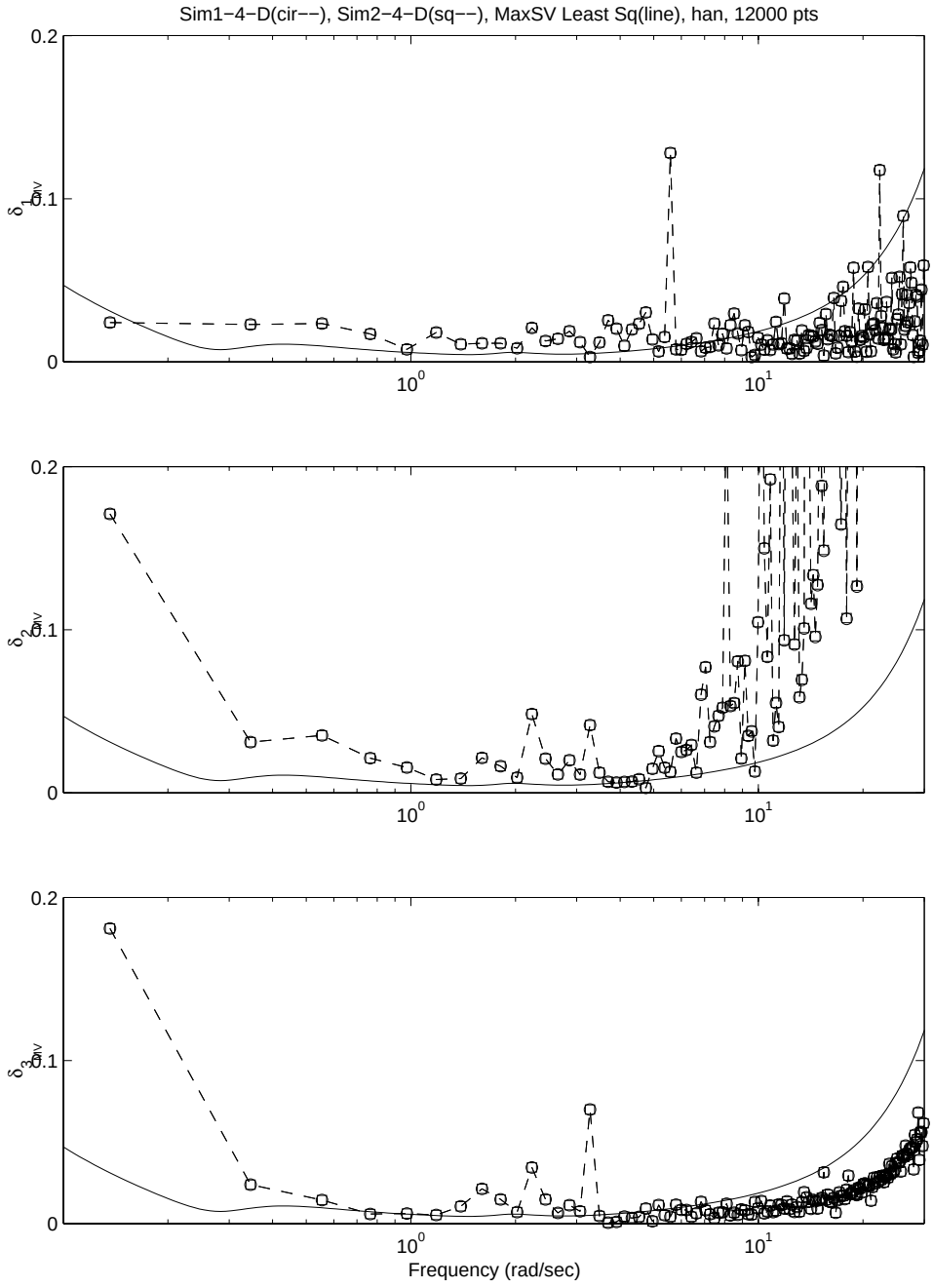

Figure 66: Diagonal uncertainty bounds for identified nominal model under low noise: Sim1-4-D and Sim2-4-D.

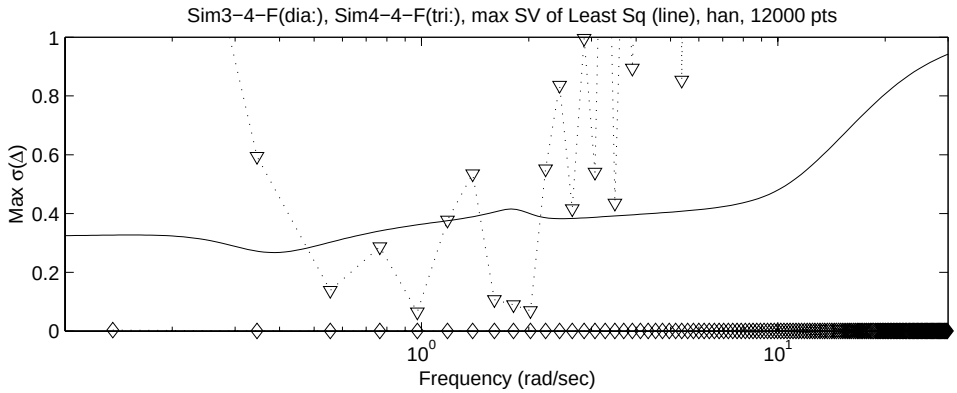

Figure 67: Unstructured uncertainty bounds for identified nominal model under high noise: Sim3-4-F and Sim4-4-F.

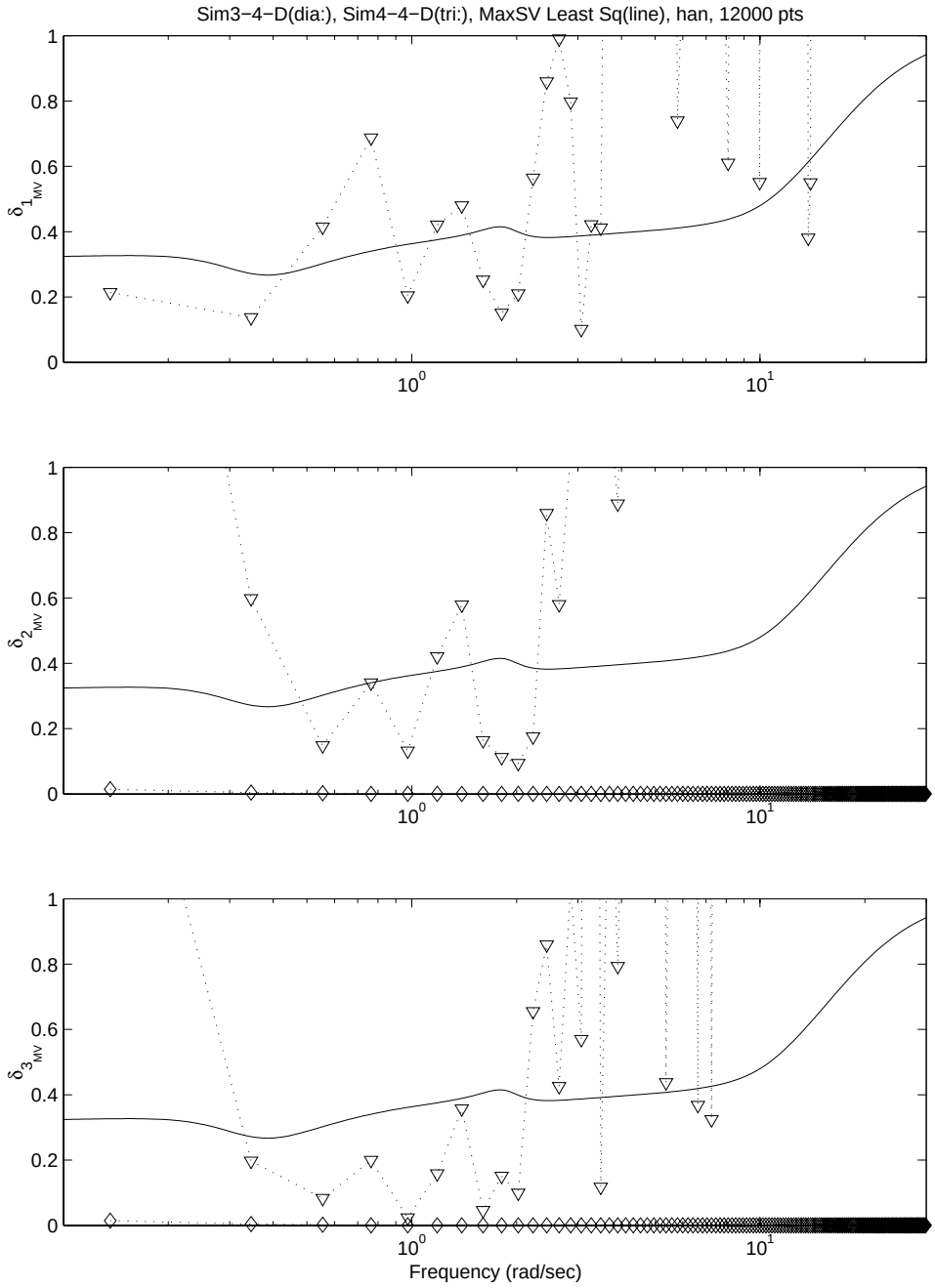

Figure 68: Diagonal uncertainty bounds for identified nominal model under high noise: Sim3-4-D and Sim4-4-D.

References

[1] Skogestad, S., and Postlethwaite, Ian, *Multivariable Feedback Control: Analysis and Design*, New York: John Wiley & Sons, 1997, Chapter 8.

[2] Zhou, K., *Essentials of Robust Control*, New Jersey: Prentice Hall, Inc., 1998.

[3] G. Balas, J.C. Doyle, K. Glover, A. Packard, and R. Smith, *μ-Analysis and Synthesis Toolbox*, User's Guide, Version 3 (online), October 1998, `http://www.mathworks.com`.

[4] Lathi, B. P., *Signal Analysis and Linear Systems*, Berkeley Press, 1995.

[5] Ljung, L., *System Identification: Theory for the user*, 2nd edition, Prentice Hall, 1999, p. 32.

[6] Lim, K.B., and Giesy, D. P., "Parameterization of Model Validating Sets for Uncertainty Bound Optimization", *Journal of Guidance, Control, and Dynamics*, vol. 23, no. 2, March-April, 2000, pp. 222-230.

[7] Smith, R.S., Doyle, J.C., "Model Validation: A connection between robust control and identification," *IEEE Transactions on Automatic Control*, vol 37, No 7, July 1992, pp.942-952.

[8] Smith, R.S., Dullerud, G., Rangan, S., and Poolla, K., "Model validation for dynamically uncertain systems," *Mathematical modeling of systems*, 1997, vol. 3, no. 1, pp. 43-58.

[9] Poolla, K., Khargonekar, P.P., Tikku, A., Krause, J., and Nagpal, K., "A time-domain approach to model validation," *IEEE Transactions on Automatic Control*, v.39, n.5, pp. 951-9, 1994.

[10] Callafon, R.A. de, and Hof, Paul M.J. van den, "Closed-loop model validation using coprime factor uncertainty models," SYSID 2000: *Symposium on System Identification*, Santa Barbara, California, June 21-23, 2000.

[11] Boyd, S., Ghaoui, L. E., Feron, E., and Balakrishnan, V., *Linear Matrix Inequalites in System and Control Theory*, SIAM Studies in Applied Mathematics, Vol. 15., 1994, Chapter 2.

[12] Astrom, K.J., and Soderstrom, T., "System Identification: A survey," *Automatica*, v.7, pp.123-62, 1971.

[13] Soderstrom, T., and Stoica, P., *System Identification*, Hempstead, Prentice Hall International, 1989.

[14] Juang, J-N., *Applied System Identification*, Prentice Hall, 1994.

[15] SYSID 2000: *Symposium on System Identification*, Santa Barbara, California, June 21-23, 2000.

[16] Newland, D.E., *Random vibrations and spectral analysis*, Longman Inc., New York, 1981.

[17] Scheid, R.E., Bayard, D.S., and Yam, Y., "A linear programming approach to characterizing norm bounded uncertainty from experimental data," *1991 American Control Conference*, pp. 1956-8.

[18] P.G. Maghami, S. Gupta, K.B. Elliott, S.M. Joshi and J.E. Walz, "Experimental Validation of an Integrated Controls-Structures Design Methodology for a Class of Flexible Space Structures," *NASA TP-3462*, November 1994.

[19] Lim, K.B., and Gawronski, W., "Hankel singular values of flexible structures in discrete time," *Journal of Guidance, Control, and Dynamics*, v. 19, n. 6, 1996, pp. 1370-77.

[20] P. Gahinet, A. Nemirovski, A. Laub, and M. Chilali, *LMI Control Toolbox*, The MathWorks, Inc., Natick, MA, 1995. `http://www.mathworks.com`

[21] T. Coleman, M. A. Branch, and A. Grace, *Optimization Toolbox*, User's Guide, Version 2 (online), Jannuary 1999. `http://www.mathworks.com`

[22] Milam, M.B., and Murray, R.M., " A Testbed for Nonlinear Flight Control Techniques: The Caltech Ducted Fan," *1999 Conference on Control Applications*, 22-27 August 1999. `http://www.cds.caltech.edu/ milam/research/res.htm`

[23] Akaike, H., "Markovian representation of stochastic processes by canonical variables," *SIAM Journal of Control*, 1975, v.13, n.1, pp. 162-173.

[24] Astrom, K. J., and Wittenmark, B., *Computer controlled systems: Theory and Design*, Englewood Cliff, NJ: Prentice Hall, 1990, Chapter 6.

[25] Verhaegen, M., and Dewilde, P., "Subspace model identification: Part 1. The output-error state-space model identification class of algorithms," *International Journal of Control*, 1992, v.56, n.5, pp. 1187-1210.

[26] Verhaegen, M., "Subspace model identification: Part 3. Analysis of the ordinary output-error state-space model identification algorithm," *International Journal of Control*, 1993, v.58, n.3, pp. 555-586.

[27] Haverkamp, B., and Verhaegen, M., *SMI Toolbox: State Space Model Identification Software for Multivariable Dynamical Systems*, Version 1.0, 1998. `http://lcewww.et.tudelft.ml/ haver/smi.html`

REPORT DOCUMENTATION PAGE

Form Approved

1. AGENCY USE ONLY (*Leave blank*)	2. REPORT DATE	3. REPORT TYPE AND DATES COVERED
	August 2003	Technical Memorandum

4. TITLE AND SUBTITLE
Structured Uncertainty Bound Determination From Data for Control and Performance Validation

5. FUNDING NUMBERS
706-21-71-01

6. AUTHOR(S)
Kyong B. Lim

7. PERFORMING ORGANIZATION NAME(S) AND ADDRESS(ES)
NASA Langley Research Center
Hampton, VA 23681-2199

8. PERFORMING ORGANIZATION REPORT NUMBER
L-18156

9. SPONSORING/MONITORING AGENCY NAME(S) AND ADDRESS(ES)
National Aeronautics and Space Administration
Washington, DC 20546-0001

10. SPONSORING/MONITORING AGENCY REPORT NUMBER
NASA/TM-2003-212441

11. SUPPLEMENTARY NOTES

12a. DISTRIBUTION/AVAILABILITY STATEMENT
Unclassified-Unlimited
Subject Category 18 Distribution: Standard
Availability: NASA CASI (301) 621-0390

12b. DISTRIBUTION CODE

13. ABSTRACT *(Maximum 200 words)*

This report attempts to document the broad scope of issues that must be satisfactorily resolved before one can expect to methodically obtain, with a reasonable confidence, a near-optimal robust closed loop performance in physical applications. These include elements of signal processing, noise identification, system identification, model validation, and uncertainty modeling. Based on a recently developed methodology involving a parameterization of all model validating uncertainty sets for a given LFT structure and noise allowance, a new software, Uncertainty Bound Identification (UBID) toolbox, which conveniently executes model validation tests and determine uncertainty bounds from data, has been designed and is currently available. This toolbox also serves to benchmark the current state-of-the-art in uncertainty bound determination and in turn facilitate benchmarking of robust control technology. To help clarify the methodology and use of the new software, two tutorial examples are provided. The first involves the uncertainty characterization of a flexible structure dynamics, and the second example involves a closed loop performance validation of a ducted fan based on an uncertainty bound from data. These examples, along with other simulation and experimental results, also help describe the many factors and assumptions that determine the degree of success in applying robust control theory to practical problems.

14. SUBJECT TERMS
Robust control/ Uncertainty structure; Uncertainty bound/ Model validation; Performance validation; Uncertainty modeling toolbox

15. NUMBER OF PAGES
136

16. PRICE CODE

17. SECURITY CLASSIFICATION OF REPORT	18. SECURITY CLASSIFICATION OF THIS PAGE	19. SECURITY CLASSIFICATION OF ABSTRACT	20. LIMITATION OF ABSTRACT
Unclassified	Unclassified	Unclassified	UL